ELECTROMIGRATION DAMAGE IN LEAD-FREE SOLDER JOINTS PREPARED USING METALLIC NANOPARTICLE DOPED FLUX

MUHAMMAD NASIR

FACULTY OF ENGINEERING
UNIVERSITY OF MALAYA
KUALA LUMPUR

2017

ELECTROMIGRATION DAMAGE IN LEAD-FREE SOLDER JOINTS PREPARED USING METALLIC NANOPARTICLE DOPED FLUX

MUHAMMAD NASIR

THESIS SUBMITTED IN FULFILMENT OF THE REQUIREMENTS FOR THE DEGREE OF DOCTOR OF PHILOSOPHY

FACULTY OF ENGINEERING
UNIVERSITY OF MALAYA
KUALA LUMPUR

2017

UNIVERSITY OF MALAYA
ORIGINAL LITERARY WORK DECLARATION

Name of Candidate: Muhammad Nasir

Matric No: KHA130142

Name of Degree: Doctor of Philosophy

Title of Thesis ("this Work"):

Electromigration Damage in Lead-Free Solder Joints Prepared Using Metallic Nanoparticle Doped Flux

Field of Study: Materials Engineering

I do solemnly and sincerely declare that:

(1) I am the sole author/writer of this Work;
(2) This Work is original;
(3) Any use of any work in which copyright exists was done by way of fair dealing and for permitted purposes and any excerpt or extract from, or reference to or reproduction of any copyright work has been disclosed expressly and sufficiently and the title of the Work and its authorship have been acknowledged in this Work;
(4) I do not have any actual knowledge nor do I ought reasonably to know that the making of this work constitutes an infringement of any copyright work;
(5) I hereby assign all and every right in the copyright to this Work to the University of Malaya ("UM"), who henceforth shall be owner of the copyright in this Work and that any reproduction or use in any form or by any means whatsoever is prohibited without the written consent of UM having been first had and obtained;
(6) I am fully aware that if in the course of making this Work I have infringed any copyright whether intentionally or otherwise, I may be subject to legal action or any other action as may be determined by UM.

Candidate's Signature Date:

Subscribed and solemnly declared before,

Witness's Signature Date:

Name:

Designation:

ELECTROMIGRATION DAMAGE IN LEAD-FREE SOLDER JOINTS PREPARED USING METALLIC NANOPARTICLE DOPED FLUX

ABSTRACT

Miniaturization of microelectronic devices and the associated increase in current density during operation raise concerns over electromigration (EM) damage in solder joints. This thesis focuses on the effects of Ni and Co nanoparticle (NP) doped flux on the microstructure, mechanical and electrical properties of the solder joints under EM. The EM tests were conducted on undoped SAC305 and NP-doped SAC305 solder joints. During EM, the electrical resistance was recorded for doped and undoped solder joints. After EM tests, the microstructure and mechanical properties were investigated. The microstructural and elemental analysis of the samples was conducted by field emission scanning electron microscopy (FESEM) and energy dispersive X-ray spectroscopy (EDX). Crystallographic information on the samples was obtained by electron backscatter diffraction (EBSD). The mechanical properties of the samples were determined by a micro-tensile testing. To investigate the effects of EM on the microstructure, EM tests were run in an oil bath at a temperature of 80° C for a maximum time of 1128 h. A constant DC current was applied to achieve a current density of 1×10^4 A/cm^2. To investigate EM effects on the mechanical and electrical properties, tests were performed for 192 h with a constant current density of 3×10^3 A/cm^2 at 160° C. Results showed that Ni and Co atoms enter into the lattice of Cu_6Sn_5 leading to the formation of $(Cu, Ni)_6Sn_5$ and $(Cu, Co)_6Sn_5$ at interfaces and in the matrix of the solder. Ni and Co thermodynamically stabilized the interfacial intermetallic compound (IMC) layers both at the anode and cathode sides. In the solder matrix, Ni and Co reduced the size of β-Sn grains and the thickness of IMC particles present in the eutectic region significantly. After EM testing, Ni and Co-NP doped flux substantially reduced the formation of cracks and voids at the cathode interface and improved the structural properties of the solder joint.

The average IMC growth rates at the anode side of the Ni and Co-containing solder joints were about five and seven-times lower compared with that of the undoped samples. EBSD results revealed that Co and Ni NP-doped flux reduced the growth of interfacial IMC grains before and after EM. Ni and Co-doped IMC layers acted as a diffusion barrier for Cu atoms moving from the cathode to the anode side. No significant change in electrical resistance occurred in Co- and Ni-doped solder during EM tests carried out for a duration of 700 h. The electrical resistance of undoped solder joints increased during EM, and the samples failed before 500 h. Ni and Co-NP significantly improved the mechanical strength of as reflowed solder and reduced the degradation of strength after EM. The strength of undoped solder was degraded by 63% after EM, while Ni and Co-NP doped solder joints suffered a strength degradation of only 23.5% and 11.3%. After EM, Ni and Co-NP also improved ductility and fracture path of the solder. Overall, this report suggests that by adding Ni and Co-NP doped flux the reliability of the SAC305 solder joints under EM can be increased significantly.

Keywords: Electromigration, Metallic nanoparticle, SAC305, Properties of solder, Doped flux.

ELECTROMIGRATION DAMAGE IN LEAD-FREE SOLDER JOINTS PREPARED USING METALLIC NANOPARTICLE DOPED FLUX

ABSTRAK

Pengecilan alat mikroelektronik serta kesan peningkatan ketumpatan arus berkaitan dalam operasi tersebut menimbulkan kebimbangan mengenai kerosakan elektromigrasi (EM) di bahagian sendi pateri. Tesis ini memberi tumpuan kepada kesan Ni dan Co nanopartikel (NP) fluks didopkan pada mikrostruktur, sifat mekanik dan elektrik sendi pateri di bawah EM. Ujian EM telah dijalankan pada un-didopkan SAC305 dan NP-didopkan SAC305 sendi pateri. Semasa EM, rintangan elektrik dicatatkan bagi sendi pateri didopkan dan un-didopkan. Selepas ujian EM, mikrostruktur dan sifat mekanik telah disiasat. Analisis mikrostruktur dan unsur sampel telah dijalankan oleh pelepasan bidang imbasan mikroskop elektron (FESEM) dan serakan tenaga X-ray spektroskopi (EDX). Maklumat Crystallographic ke atas sampel telah diperolehi oleh elektron backscatter pembelauan (EBSD). Sifat-sifat mekanikal sampel ditentukan oleh ujian mesin mikro tegangan. Untuk menyiasat kesan EM pada mikrostruktur, ujian EM telah dijalankan dengan diletakkan dalam minyak pada suhu 80 ° C untuk jangka masa yang maksimum 1128 h. Arus terus berterusan telah digunakan untuk mencapai ketumpatan arus 1×10^4 A/cm^2. Untuk menyiasat kesan EM pada sifat-sifat mekanikal dan elektrik, ujian telah dijalankan untuk 192 h dengan ketumpatan arus malar 3×10^3 A/cm^2 pada 160 ° C. Hasil kajian menunjukkan bahawa atom Ni dan Co masuk ke dalam kekisi Cu_6Sn_5 yang membawa kepada pembentukan $(Cu, Ni)_6Sn_5$ dan $(Cu, Co)_6Sn_5$ di antara muka dan dalam matriks pateri. Ni dan Co secara termodinamik menstabilkan lapisan sebatian antara logam (IMC) pada kedua-dua bahagian anod dan katod. Dalam solder matriks, Ni dan Co mengurangkan ketebalan butir β-Sn dan ketebalan zarah IMC yang hadir di kawasan eutektik dengan ketara. Selepas ujian EM, Ni dan Co-NP fluks didopkan berkurangan pembentukan retak dan lompang di antara muka katod dan meningkatkan sifat-sifat struktur sendi pateri. Purata kadar pertumbuhan IMC di sebelah anod sendi pateri Ni dan Co yang mengandungi kira-kira lima hingga tujuh kali lebih rendah berbanding dengan sampel un-didopkan. Keputusan EBSD mendedahkan bahawa fluks Co dan Ni NP-didopkan mengurangkan pertumbuhan butir IMC sebelum dan selepas EM. Ni dan Co-didopkan lapisan IMC bertindak sebagai penghalang resapan bagi atom Cu bergerak dari katod ke bahagian anod. Tiada perubahan ketara dalam rintangan elektrik berlaku di Co- dan Ni-didopkan pateri semasa ujian EM dijalankan untuk tempoh 700 h. Rintangan elektrik sendi pateri un-didopkan meningkat dalam EM dan sampel gagal sebelum 500 h. Ni dan Co-NP secara ketara meningkatkan kekuatan mekanikal pateri sebagai reflowed dan mengurangkan kemerosotan kekuatan selepas EM. Kekuatan pateri un-didopkan telah merosot sebanyak 63% selepas EM, manakala Ni dan Co-NP sendi pateri didopkan mengalami kemerosotan kekuatan hanya 23.5% dan 11.3%. Selepas EM, Ni dan Co-NP juga bertambah baik kemuluran dan laluan pateri. Secara keseluruhan laporan ini menunjukkan bahawa dengan menambah Ni dan Co-NP fluks didopkan kebolehpercayaan SAC305 sendi pateri bawah EM boleh meningkat dengan ketara.

Keywords: Elektromigrasi, Nanopartikel logam, SAC305, Ciri-ciri pateri, Fluks didopkan.

ACKNOWLEDGEMENTS

First and foremost, I would like to thank Almighty Allah SWT to be most gracious and merciful. I would also like to express my deepest appreciation, sincere thanks, and gratitude to my honorable supervisors, Prof. Dr. A.S.M.A. Haseeb Department of Mechanical Engineering, University of Malaya. I deeply appreciate his contributions, valuable guidance, advice, and support throughout my Ph.D. degree in the University of Malaya.

I gratefully acknowledge the financial support from High Impact Research grant (UM.C/HIR/MOHE/ENG/26, Grant No. D000026-16001) and University of Malaya Research Grant (UMRG, Grant No. RP021-2012D) and Post Graduate Research Grant University of Malaya (Project No. PG146-2016A) throughout my Ph.D. degree.

Special thanks to Dr. Abu Zayed Mohammad Saliqur Rahman for his advice and guidance in my Ph.D. work. Special thanks to Mr. Mohd Zulhizan Bin Zakaria and Miss. Nurshaiba Binti MD. Nasir of infra Analysis Laboratory, University of Malaya, Mr. Nazarul Zaman bin Mohd Nazir of FESEM lab, Faculty of Engineering, University of Malaya, Quasi-S Sdn. Bhd. for SEM, FESEM and EDX analysis, and Miss. Ooi Mei Hong of Hi-Tech Instruments Sdn Bhd. for helping to perform the EBSD analysis. Without their efforts and patience, it would not be possible to finish my large number of samples in time.

Finally, I gratefully acknowledge to my all friends for their input and cooperation during my period of study. I would also like to thank all the members and staff in the department of mechanical engineering, the University of Malaya for their generous help on different issues. I am very grateful to my university colleagues for providing a friendly and relaxed atmosphere for conducting research. Last but not least, I would like to thank my beloved family members especially my parents for their kind support, encouragement, and love during my period of study.

TABLE OF CONTENTS

Abstract.......... iii

Abstrak v

Acknowledgements vii

Table of Contents viii

List of Figures.......... xii

List of Tables.......... xvii

List of Symbols and Abbreviations xviii

CHAPTER 1: INTRODUCTION 1

1.1 Background 1

1.2 Objectives of the study.......... 3

1.3 Scope of the study 4

1.4 Dissertation overview 5

CHAPTER 2: LITERATURE REVIEW 6

2.1 Electronic Packaging Technology 6

2.2 Flip chip technology.......... 8

2.3 Lead-free solder joint 10

2.4 Downscaling of flip chip technology 15

2.5 Physics of electromigration.......... 17

2.6 Electromigration issues in flip chip solder joint 20

2.7 Factor affecting electromigration failures.......... 24

  2.7.1 Joule Heating effects.......... 24

  2.7.2 Current crowding effects 25

  2.7.3 Crystallographic orientation of Sn grain.......... 26

2.8 Previous methods for retardation of EM failures..31

2.8.1 Alloying method for retardation of EM failures....................................32

2.8.1.1 Ce-containing alloys 32

2.8.1.2 Ni, Co, and Sb-containing alloys...34

2.8.2 Addition of microparticle in solder joint for retardation of EM failures..36

2.8.2.1 Ni and Co microparticle...37

2.8.2.2 Sb microparticles 38

2.8.3 Addition of nanoparticle in solder joint for retardation of EM failures....41

2.8.4 Addition of carbon nanotubes in solder for retardation of EM failures....42

2.8.4.1 Effect on structural properties of solder joint 42

2.8.4.2 Effect on mechanical properties of solder joint.........................44

2.9 Overall summary...45

CHAPTER 3: METHODOLOGY 48

3.1 Solder joint preparation..49

3.2 Electromigration test...53

3.3 Structural and chemical characterization 55

3.3.1 Field emission scanning electron microscopy 57

3.3.2 Electron backscatter diffraction 57

3.4 Mechanical properties 59

3.5 Electrical test..60

CHAPTER 4: RESULTS 62

4.1 Microstructure of doped and undoped solder after reflow...................................62

4.1.1 Interfacial microstructure..62

4.1.2 Microstructure of solder matrix 64

4.1.3 Distribution of Ni and Co in solder joint 69

4.2 Interfacial microstructure after electromigration 73
  4.2.1 SAC305 solder joint....73
  4.2.2 Ni nanoparticle doped solder joint....74
  4.2.3 Co nanoparticle doped solder joint....74
  4.2.4 Comparison of thickness variation in interfacial IMC layers of doped and undoped solder....78
4.3 Crystallographic structures of doped and undoped solder....78
  4.3.1 Crystallographic structure and distribution of phases before electromigration. … 80
  4.3.2 Crystallographic structure and distribution of phases after electromigration…. 83
  4.3.3 Variation of grain size of interfacial IMC layers....84
4.4 Measurement of electrical resistance in doped and undoped solder....86
4.5 Influence of nano doped flux on mechanical strength of SAC305 solder....89
  4.5.1 Stress-strain values....89
  4.5.2 Mechanical strength....90
  4.5.3 Fracture behaviour....93

CHAPTER 5: DISCUSSION....95
5.1 Reactive dissolution of nanoparticle in SAC305 solder....95
5.2 Effect of nanoparticle on microstructure after reflow....101
  5.2.1 Effect on interfacial IMC....101
  5.2.2 Effect on solder matrix....102
5.3 Influence of nanoparticle on solder after electromigration....104
5.4 Effect of NP-doped flux on kinetics of anodic IMC formation....107
5.5 Effect of nanoparticle doping on Cu diffusion....112
5.6 Influence of Ni NP on tensile strength....114

CHAPTER 6: CONCLUSION 118

6.1 Conclusion 118

6.2 Recommendations 120

References 122

List of Publications and Papers Presented 134

Appendix 136

LIST OF FIGURES

Figure 2.1: Hierarchy of electronic packaging (Lau et al., 1998) 7

Figure 2.2: Moore’s law for Intel microprocessors (Intel, 2004) 8

Figure 2.3: Generic configuration of C4 with underfill (Zhang, Luo, & Wong, 2013) ..10

Figure 2.4: Schematic diagram describing reduction in size of solder joint (Selvaraj, 2007) 16

Figure 2.5: Schematic diagram of flip chip lead-free solder bump describing electromigration failures in Sn-based solder due to high-current density......................19

Figure 2.6: Description of EM failures in the solder joint. 21

Figure 2.7: Fracture images of tensile test after EM: (a) Optical picture of original sample, (b) fracture image without EM, (c) fracture image after EM, 5 × 10^3 A/cm^2 at 45 °C for 96 h, (d) fracture image after EM, 5 × 10^3 A/cm^2 at 145 °C for 144 h (Ren et al., 2006). 22

Figure 2.8: Tensile stress–strain curves of Sn–Ag–Cu solder joints before and after electromigration (Zhang et al., 2007). 22

Figure 2.9: Macro-fracture path after current stressing (Wang et al., 2010)..................23

Figure 2.10: Effect of the current on the shear properties of the solder joints (shear speed of 0.3 mm/s) (Wang et al., 2010)...23

Figure 2.11: A series of X-ray micrographs demonstrating the interior microstructure evolution of a solder joint under 1.1 × 10^4 A/cm^2 current stressing for t=(a) 0 h (initial), (b) 2 h, (c) 4 h, (d) 8 h, (e) 13 h, and (f) 16 h. (g) FEA simulation of the current density (Ho et al., 2016)...26

Figure 2.12: (a) and (b) Cross-sectional micrographs of the solder joints after current stressing of 4.5 10^4 A/cm^2 at 50 °C for 1862 h. (c) and (d) Zoom-in images of the cathode interface of (a) and (b) respectively. (e) and (f) Sn grain orientation for the joint in (a) and (b), respectively. (g) and (h) EBSD analysis map of Sn grain (image quality + inverse pole figure) with RD direction for the joint in (a) and (b), respectively. (i) and (j) with TD direction (Yang et al., 2015)..27

Figure 2.13: Cross-sectional microstructure of the as-soldered (a) and (d) back-scattered SEM images, (b) and (e) cross-polarized images and (c) and (f) EBSD inverse pole figure orientation image map (Huang et al., 2016). 29

Figure 2.14: Cross-sectional microstructures of the sample after EM for (a) 200 h, (b) 400 h, (c) 600 h, (d) 600 h (polished) and (e) EBSD inverse pole figure orientation image map (Huang et al., 2016). 29

Figure 2.15: Cross-sectional microstructures of the interconnects after EM for (a) 200 h, (b) 400 h, (c) 600 h, (d) 600 h (polished) and (e) EBSD inverse pole figure orientation image map (Huang et al., 2016). 30

Figure 2.16: Diffusivity ratio of Cu atoms along c and a-axis of Sn at various temperatures (Yang et al., 2015) 32

Figure 2.17: Backscattered electron microscopy images of the central region of Sn-3.9Ag-0.7Cu and Sn-3.9Ag-0.7Cu-0.5Ce joints after current stressing (Xie et al., 2014).........34

Figure 2.18: Sn-3.9Ag-0.7Cu void growth over time, showing 3D rendering (top) and cathode void top view (bottom) (Xie et al., 2014). 35

Figure 2.19: Sn-3.9Ag-0.7Cu-0.5Ce void growth over time, showing 3D rendering (top) and cathode void top view (bottom) (Xie et al., 2014). 35

Figure 2.20: Microstructures of as-reflowed solder joints: (a) SAC (b) SAC-0.45Ni, (c) SAC-0.2Co (d) SAC387-1.0Sb, (e) backscattered electron image of SAC-0.45Ni (inset illustrates the backscattered electron image of SAC-2.0Ni) (f) backscattered electron image of SAC-0.2Co. (Zhao et al., 2013). 37

Figure 2.21: Cross-sectional BS-SEM images, (a) SABI solder joint, (b) SABI+Co solder joint, (C) SABI+Ni solder joint and (d) SABI+NiCo solder joint (Kim et al., 2012).....39

Figure 2.22: The EM average failure time for SABI, SABI+Co, SABI+Ni and SABI+NiCO solder joints tested at a homologous temperature (Kim et al., 2012). 40

Figure 2.23: (a) The microstructure of Sn–Sb particles in the solder matrix without the current stressing; (b) the microstructure of Sn–Sb particles in the solder matrix after 200 h of the current stressing; (c) the cracks went through the Sn–Sb particles in the solder mat (Guo et al., 2009). 40

Figure 2.24: Formation and propagation of the pancake void at the cathode side a without current stressing; (b) current stressing after 240 h; (c) void formed between the solder matrix and the Sn–Cu IMCs (Guo et al., 2009). 41

Figure 2.25: SEM images showing the presence of Ni–MWCNTs in solder matrix after (a) Fine polishing and (b) etched (Yang et al., 2013). 42

Figure 2.26: Current density distribution in the: (a) SAC solder joint and (b) SAC/1Ni–CNT solder joint (the resistivity of Cu, Sn, Cu_6Sn_5, and CNT is 1.7 Ωcm, 11 Ωcm, 18 Ωcm and 0.01 Ωcm, respectively) (Yang et al., 2013). 43

Figure 2.27: Measured microhardness for plain solder and composite solder (Xu et al., 2014)...44

Figure 2.28: Measured shear strength for plain solder and composite solder (Xu et al., 2014)...45

Figure 3.1: Flowchart of research methodology used. 49

Figure 3.2: Schematic diagram for the preparation of line type Cu/solder/Cu sample: (a) Cu ends dipped into NP and solder disc, (b) Assembly of Cu wires and disc in an aluminum die, and (c) prepared line type Cu/solder/Cu solder joint. 52

Figure 3.3: the Mounting process of samples by using epoxy resin and hardener..........56

Figure 3.4: Illustration of sample preparation for electromigration test under high-current density (a) prepared line type Cu/solder/Cu solder joint, (b) mounted and ground sample in the epoxy resin, (c) dimensions of the ground sample and (d) cross-sectional area of the ground sample...58

Figure 3.5: A Tensile test of line type solder in a tensile testing machine with 50 N load cell. 60

Figure 3.6 Schematic diagram for the measurement of electrical resistance during the electromigration test. 61

Figure 4.1: SEM back-scattered electron images of (a) SAC305, (b) SAC305+2 wt% Ni NP, and (c) SAC305+2 wt% Co-NP solder joints. Each micrograph corresponds to one end of the solder joint..63

Figure 4.2: SEM images depicting grain structure in the matrix of (a and b) SAC305 (c and d) Ni-NP doped and (e and f) Co-NP doped solder joints.......................................66

Figure 4.3: Averaged grain areas of β-Sn grain in as reflowed SAC305, Ni-NP doped and Co-NP doped solder joints...67

Figure 4.4: FESEM images depicting the structure of IMC particles present in the eutectic region of the matrix of (a) SAC305 (b) Ni-NP doped and (c) Co-NP doped solder joints. 68

Figure 4.5: IMC particles thickness in eutectic region of matrix of doped and undoped solder 69

Figure 4.6: EDX elemental maps of the SAC305 + 2 wt% Ni NP solder joint. Elemental maps for (a) Cu and (b) Ni. 70

Figure 4.7: EDX elemental maps of the SAC305 + 2 wt% Co NP solder joint. Elemental maps for: (a) Cu and (b) Co...70

Figure 4.8: EDX spot analysis of Ni and Co NP-doped solder joint. (a) overview of Ni NP-doped solder, (b) EDX spot on magnified image of (Cu, Ni)$_6$Sn$_5$ large size particles in the matrix of Ni NP-doped solder (c) EDX analysis on figure b, (d) overview of Co NP-doped solder, (e) EDX spot on magnified image of (Cu, Co)$_6$Sn$_5$ large size particles in the matrix of Co NP-doped solder and (f) EDX analysis on figure e. 72

Figure 4.9: FESEM backscattered electron images of the SAC305 solder joint after EM test for 192, 384, 768 and 1128 h. (a), (b), (c) and (d) show cathode side, while (e), (f), (g) and (h) show anode side..75

Figure 4.10: FESEM backscattered electron images of the SAC305 + 2wt% Ni NP solder joint after EM test for 192, 384, 768 and 1128 h. (a), (b), (c) and (d) show the cathode side, while (e), (f), (g) and (h) show the anode side..76

Figure 4.11: FESEM backscattered electron images of the SAC305 + 2wt% Co NP solder joint after EM test for 192, 384, 768 and 1128 h. (a), (b), (c) and (d) show the cathode side, while (e), (f), (g) and (h) show the anode side..77

Figure 4.12: IMC thickness variation as a function of electromigration time at the cathode and anode sides of (a) SAC305, (b) Ni-NP doped and (c) Co-NP doped solder joint. ..79

Figure 4.13: EBSD orientation mapping at interfaces of as reflowed (a and b) SAC305 solder joint, (c and d) Ni-NP doped solder and (e and f) Co-NP doped solder joints.....81

Figure 4.14: Phase mapping at the interface of as reflowed (a and b) SAC305, (c and d) Ni-NP doped and (e and f) Co-NP doped solder joints..83

Figure 4.15: EBSD orientation mapping at interfaces of (a and b) SAC305, (c and d) Ni-NP doped and (e and f) Co-NP doped solder joint after the electromigration. 85

Figure 4.16: Phase mapping at the interface of (a and b) SAC305, (c and d) Ni-NP doped and (e and f) Co-NP doped solder joints after EM test of 1128 h..................................86

Figure 4.17: Variation of grain size of interfacial IMC of NP-doped and undoped SAC305 solder joint before and after the EM test. 87

Figure 4.18: Changes in electrical resistance of (a) SAC305, (b) Ni-NP doped and (c) Co-NP doped solder joints as a function of EM time..88

Figure 4.19: Stress-strain curves of the SAC305solder (a) 0 h and (b) 192 h of EM, SAC305 + 2 wt% Ni NP solder (c) 0 h and (d) 192 h of EM and SAC305 + 2 wt% Co-NP (e) 0 h and (f) 192 h of EM. 91

Figure 4.20: Tensile strength of the SAC305, SAC305 + 2wt% Ni-NP and SAC305 + 2wt% Co-NP solder joints after reflow and after electromigration for 192 h 92

Figure 4.21: Description of fracture path in (a) SAC305, (b) SAC305 + 2 wt% Ni-NP doped and (c) SAC305 + 2 wt% Co-NP doped solder joints at 0 h and 192 h EM test. .93

Figure 4.22: Description of fracture path in (a) SAC305, (b) SAC305 + 2 wt% Ni-NP doped and (c) SAC305 + 2 wt% Co-NP doped solder joints at 0 h and 192 h EM test. .94

Figure 5.1: Schematic diagram of SAC305 + NP-doped solder joint which represents the incorporation of NP into the SAC305 solder joint during the reflow process. 96

Figure 5.2: Binary Sn-Ni phase diagram from Ref. (schmetterer et al., 2007) 99

Figure 5.3: Binary phase diagram of Sn-Co from Ref. (M. Jiang et al., 2004) 100

Figure 5.4: Schematic diagrams presenting microstructure changes in the SAC305 and Ni/Co-NP- doped flux solder joints (a, b) before while (c, d) after EM test. 105

Figure 5.5: Schematic diagram illustrating the contribution of chemical and electrical forces during EM test. 108

Figure 5.6: Estimated value of constant n of equation (5.3) by using curve fitting technique (a) Ni-doped solder joint (b) Co-doped solder joint. 111

Figure 5.7: Schematic diagrams describing Cu migration in undoped SAC305 and Ni/Co NP-doped solder joint during EM. 113

LIST OF TABLES

Table 2.1: Chemical compositions of lead-free solder alloy down-selected for preliminary testing by the National Center for Manufacturing Sciences (NCMS) (Siewert, 2002)...13

Table 2.2: Criteria for down-selection of lead-free solder alloys (Siewert, 2002)..........14

Table 3.1: Electromigration parameters used during different type of EM test..............53

Table 4.1: EDX elemental compositions of IMC phases in the SAC305 and NP-doped flux solder joints...65

Table 4.2: EDX elemental compositions of IMC phases in the matrix of NP-doped flux solder joints. 73

Table 4.3: Anodic growth rate of interfacial IMC in solder joints..................................80

Table 4.4: Grain size of interfacial IMC of NP-doped and undoped solder joints..........82

Table 5.1: Diffusion coefficient of different elements in liquid Sn. 98

Table 5.2: Comparison of the estimated value of n and k with literature. 112

Table 5.3: Average tensile strength of Ni NP-doped solder joints and its correlation with literature...115

Table 5.4: Average maximum tensile strain of Ni NP-doped solder joint and its correlation with literature..116

LIST OF SYMBOLS AND ABBREVIATIONS

a : Cross-sectional

ar : Area of the interfacial IMC layers

$a_{\circ}$: Temperature coefficient of resistance for the sample

$\partial\mu$ / $\partial\mu$: Chemical potential gradient

b : Model parameter for current density

BGA : Ball Grid Array

C : Central angle

c : Concentration

CNT : Carbon nanotube

C_{Cu} : Local molar concentration of Cu in Sn

C4 : Controlled collapse chip connection

D : Diffusion coefficient of Ni

d : Thickness of anodic interfacial IMC

Df : Diffusivity

D_{Cu}^{Sn} : Diffusion coefficient of Cu in Sn

E : Activation energy

e : Charge of an electron

EDX : Energy Dispersive X-Ray

EM : Electromigration

FC : Flip Chip

FESEM : Field Emission Scanning Electron Microscopy

h : Average thickness of the interfacial IMCs layer

I : Current (Amp)

IC : Integrated Circuit

IMC : Intermetallic compound

J : Current density

j : Applied electron current density

J_{chem} : Chemical force

J_{em} : Electrical force

K : Boltzmann’s constant

k : Growth rate constant

L : Total length of the interfacial IMC layers

MTTF : Mean time to failure

n : Constant

nm : Nanometer

NP : Nanoparticle

p : Resistivity

PCB : Printed Circuit Board

ρ_{Sn} : Resistivity of Sn

Q : Activation energy

R : The radius of the whole sample

r : Electrical resistance at temperature 150 °C

R_{room} : Electrical resistance at room temperature

SAC305 : Sn-3Ag-0.5Cu

SEM : Scanning Electron Microscopy

T : Average bump temperature

t : Electromigration time

T_{app} : Applied temperature on the sample

Tm : Absolute temperature

tm : Reflow time

T_{room} : Room temperature

TMF : Travelling magnetic fields

µm : Micrometer

V : Applied voltage during EM test

x : Distance traveled by Ni during the reflow

Z^* : Effective charge number

$Z_{Cu}^{Sn\,*}$: Effective charge number of Cu in Sn

Z^*e : Effective charge assigned to the migration ion

CHAPTER 1: INTRODUCTION

1.1 Background

The recent focus of flip chip technology has been to achieve high-performance electronic devices with much smaller size and slimmer form factor. Due to miniaturization of microelectronic devices, the size of the solder joint is being down-scaled, and the operating current density in the package increased (Huang et al., 2014). Therefore, electromigration (EM) failures have become one of the main reliability issues in microelectronic packaging (Chen & Liang, 2007). During EM, atoms move along the direction of electron flow towards the anode side of the solder joint. As a result, voids, cracks or damage can be generated on the cathode side (Hsu & Chen, 2013). Hence, the increase of current density in small solder joints increases the occurrence of EM failures (Zuo et al., 2013). During EM, electrons under high-current density apply force on atoms present in the solder joint (Li et al., 2011). As Cu atoms require low activation energy compared to Sn atoms, the Cu atoms migrate rapidly during the EM (Yang et al. 2015). Migration of Cu atoms from the cathode to anode side is one of the main reasons for EM failure (Li et al., 2011). Due to rapid migration of Cu atoms from the cathode towards the anode, voids form at the cathode side of the joint. It has been found that voids created by EM weaken the cathode interface. This results in the transfer of the fracture path from the bulk to the cathode side. The formation of voids during EM reduces the strength of the solder joints and also changes the fracture mode from ductile to brittle (Ren et al., 2006). The rapid growth of IMC at the anode side reduces the strength of the solder joint because of brittleness of IMC. In order to reduce EM damage, it is important to retard Cu diffusion from the initiation points. Base on the literature review, the EM damage can be minimized by solving the following questions.

1. How to build a diffusion barrier preventing the rapid diffusion of Cu atoms away from the cathode side.

2. How to stop the rapid growth of the interfacial IMC layer at the anode side.
3. How to retard the electromigration damage in the solder joint
4. How to minimize the degradation of properties of the solder joint due to electromigration

Researchers are putting a great deal of efforts to improve the reliability of lead-free solders during EM by minor addition(s), either in the form of alloying element(s) (Zhao et al., 2013) or as micro/nano size particles (Zhang et al., 2010) or introducing under bump metallization at the solder joint interfaces (Lin et al., 2006). Reported studies on particle addition mainly use paste mixing (Ma et al., 2011; Tay, Haseeb, & Johan, 2011; Tay et al., 2013) methods. In these cases, the particles are mixed throughout the solder matrix. Alloying additions through metallurgical routes also mix the element throughout the bulk solder. Moreover, in the last few years, researchers worked on carbon nanotubes addition in the solder joint as well (Xu et al., 2014). In this technique, they used carbon nanotubes for reinforcement purposes. It was found that nanotubes built a current conduction path in the solder which increased the conductivity of current. When current has a good conduction path then it reduces Cu atom diffusion. Thus, this effort was also very useful for minimizing the EM effects. Recently, it was observed that IMC grain orientation and β-Sn grain orientation play a consequential role (Lee et al., 2011a, 2011b; Yang et al., 2015) during the EM process. According to their findings, it is important to modify the c-axis of IMC and Sn grain. These efforts were also very helpful in retarding EM failure. As the process of EM damage begins at the cathode interface of the solder joint, so it is very important to pay careful attention to the cathode interfaces in order to build a promising Cu diffusion barrier. Recently, a flux mixing technique has been developed (Haseeb, 2013) which allows the addition of nanoparticle at the solder/substrate interface and in the matrix through reactive dissolution. The characteristics of the intermetallic layers at the interface and the characteristics of β-Sn grain in the matrix play an important role in determining the reliability of the solder joints. The flux mixing technique of nanoparticle (NP) addition thus enables to modify the interfaces and matrix of the solder joint by NPs addition and to study the effects of NPs addition on the EM behavior in the solder joint. Therefore, for the prevention of rapid Cu migration at the cathode side and substantial growth of interfacial IMC layer at the anode side, the modification of the interfaces and the solder matrix by the doped flux technique was proposed in the present study.

In the past studies, researcher found that Ni and Co improved the properties of the solder joint. They added the Ni and Co into the solder joint by using different techniques such as, paste mixing technique (Haseeb & Leng, 2011; Tay et al., 2013), alloying method (Bobet, Akiba, & Darriet, 2001; Bobet, Akiba, Nakamura, & Darriet, 2000; Yano, Kataoka, Yamashita, Uchida, & Watanabe, 2007) and doped flux technique (Sujan et al., 2014; Sujan et al., 2017). They observed that Ni and Co-NP underwent reactive dissolution during reflow and entered into the solder joint and influenced the structure and properties of the solder joint through in-situ alloying. However, the effects of Ni and Co-NP on electrical, mechanical and structural properties of the SAC305 solder joint before and after EM have not been reported in the literature so far. It is, therefore, the objective of this study to investigate the effects of Ni and Co-NP addition on properties SAC305 solder joint after reflow and after EM test. The solder joints were prepared by the flux doping method. The process essentially involves the use of Ni, and Co-NP doped commercial flux at the solder substrate interface prior to the reflow.

1.2 Objectives of the study

1. Study on the effects of nanoparticle-doped flux on structural properties of the SAC305 solder joint before and after electromigration.
2. To investigate the effect of nanoparticle-doped flux on the grain size of interfacial

IMC before and after EM electromigration.

3. To study the effect of nanoparticle-doped flux on the electrical resistance of the solder joints under electromigration.
4. To determine the effect of nanoparticle-doped flux on mechanical strength and fracture behavior of the solder joint before and after electromigration.

1.3 Scope of the study

The overall aim of this study is to investigate the effect of Ni and Co-NP doped flux on microstructural, mechanical and electrical properties of the SAC305 solder joint before and after electromigration.

Before EM test, the morphology of interfacial IMC, the grain sizes of the interfacial IMC, structure, and size of the β-Sn grain in the matrix, structure, and thickness of IMC particles present in the eutectic region were investigated for as reflowed solder. After EM testing, EM damage at the cathode side, the anodic growth of interfacial IMC, rapid Cu diffusion from the cathode to anode side and reduction in cathodic IMC layer were investigated.

Microstructural properties were characterized by using several analytical techniques, including field emission scanning electron microscopy (FESEM) energy dispersive X-ray (EDX) scanning electron microscopy (SEM) electron backscattered diffraction (EBSD) and optical microscopy (OM).

To investigate the mechanical properties before and after electromigration, the micro tensile tests were conducted in a Shimadzu AGS-X Universal tensile testing machine before and after EM. To investigate the electrical properties of the doped and undoped solder joint, the electrical resistance and failure time of the solder joints were investigated and presented in this study.

1.4 Dissertation overview

This dissertation contains six chapters. Chapter 1 contains brief introduction of the thesis, including research background, electromigration issues in the solder joint, research objectives of the study and scope of the study. Chapter 2 contains comprehensive literature survey of this study and a detailed explanation of different topics related to this study. These topics include electronic packaging, flip chip packaging, lead-free solder joint, downscaling of flip chip devices, physics of electromigration, electromigration failures, root causes of electromigration, the effect of the solder modification on EM damage and an overall summary of the literature review was stated. Chapter 3 provides a methodology of this study. Chapter 3 includes information about equipment used for experiments, preparation of doped flux techniques, soldering procedure, electromigration test, tensile test and analysis of data. Chapter 4 and 5 contain the results and discussion obtained from the experiments of this study, in-depth analysis of data, comparison of data with literature, discussion and correlation of data with published data. Chapter 6 states the summary of results found in this study and recommendation for the future work.

CHAPTER 2: LITERATURE REVIEW

2.1 Electronic Packaging Technology

The demands for miniaturized electronic devices with high functionality, light in weight with low prices are increasing day by day. The functionality of the electronic device depends on the Integrated Circuit (IC). In the past, the invention of the IC has deeply changed many aspects of human life and brought into being today's trillion-dollar microelectronic trade. Electronic packaging and the IC Chip have a strong relation to each other. The IC chip will not be able to function without the electronic packaging. Electronic packaging basically helps the IC during the performance. There are four main functions of the electronic packaging (Harper, 2004).

(1) Power distribution: it provides the electrical conduction path for the electrical current to supply the power to the IC chip.
(2) Signal distribution: It provides the transportation of signals between IC chip and other components in the device.
(3) Thermal management: It dissipates the heat from the circuit.
(4) Protection: Packaging protects the IC chip from chemical and mechanical destruction.

In general, there are many layers of packaging in electronic systems, as illustrated in Figure 2.1 (Lau, Wong, Nakayama, & Prince, 1998), with distinctive sorts of interconnections for every layer. In the past, the density of IC rapidly increased in chips. The estimation by Moore's law shows that the number of transistors per integrated circuit has grown exponentially (Intel, 2004). The exponential growth in a number of transistors and chip size in each year has been maintained as shown in Figure 2.2 (Intel, 2004). The growth in the density of IC in the chip has also increased the challenges in electronic-packaging. To keep up this trend, it is important to focus on the development of the electronic packaging to provide reliable and high-density input and output (I/O) system. The strategies for accomplishing 1st level bonding (chip-to-module connections) include (a) Wire bonding, (b) flip chip bonding and (c) tape automated bonding (TAB). Tape automated bonding (TAB), and wire bonding are known as old chip on board technologies. Nowadays, the use of TAB and wire bonding is limited because of brittleness in mechanical properties of Si wafer. The usage of flip chip technology becomes more favorable and attractive because it offers an efficient technique to enable the requirements of input-output density. In recent years, flip chip technology has become the predominant technology for the chip to next level interconnects (Association, 2009).

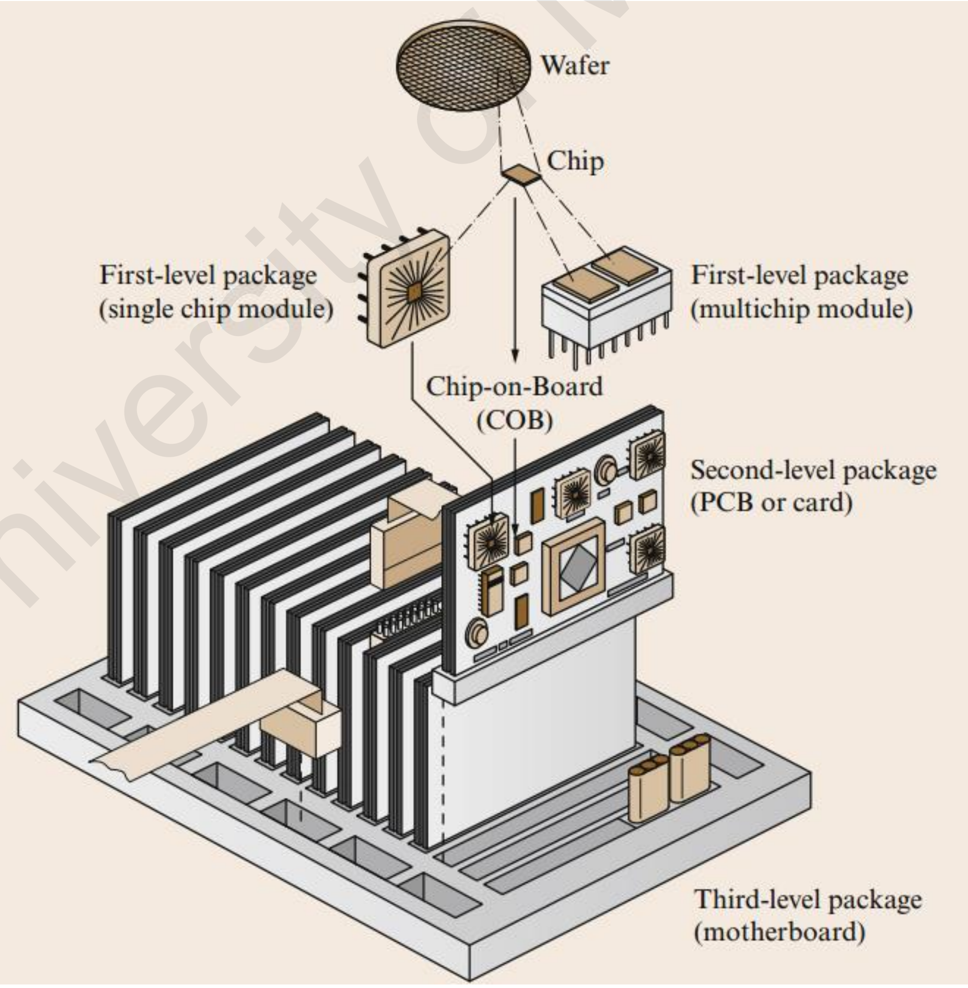

Figure 2.1: Hierarchy of electronic packaging (Lau et al., 1998).

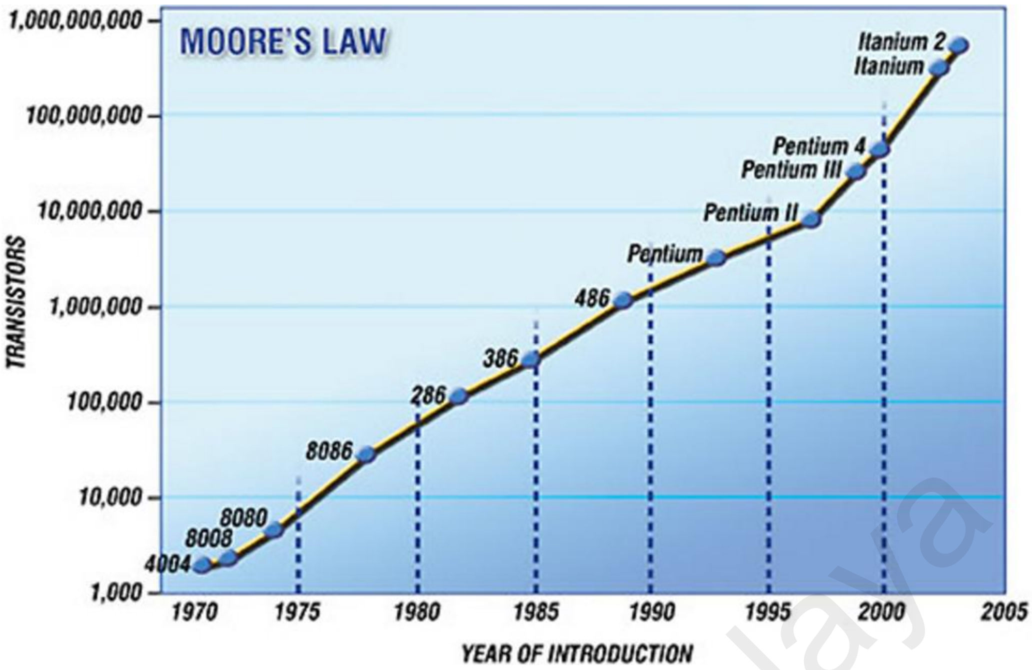

Figure 2.2: Moore's law for Intel microprocessors (Intel, 2004).

2.2 Flip chip technology

Flip chip (FC) is a semiconductor die, which is connected with the substrate circuit boards or carriers in a face-down position. Flip chip is also called controlled collapse chip connection (C4) (Oppert, Teutsch, Zakel, & Tovar, 1999). Flip chip is used for interconnecting semiconductor devices. The structure of the flip chip is shown in Figure 2.3. Normally, solder bumps are used to connect the flip chip to the substrates of the electronic devices (Oppert, Teutsch, Zakel, & Tovar, 1999). Flip chip with a solder bump provides the highest packaging density with less packaging delay in the three-chip level interconnect technologies.

The substrate is used for mounting the chip. It is also known as a chip carrier (Chung, 1995). In the beginning, the ceramic circuits and substrates were used for the flip-chip system. Ceramic has a very low coefficient of thermal expansion, and it reduces the thermal mechanical mismatching between the carrier and the chip. It also has higher thermal conductivity. Recently, flexible organic substrate and organic substrate have also been developed (Harper, 2004). Researchers found that the organic substrates more flexible, cheap and preferable to use in both flip chip packaging and flip chip on the board (Lau, 1995).

In a flip-chip structure, under bump metallization (UBM) layers are also used. These layers are metal layers and usually, are deposited between the solder bump and Al/Cu interconnects by the electrodeposition technique. The under bump metallization has three main functions at the interfaces of the solder bump (Koopman, Reiley, & Totta, 1989; Taguma, Uda, Ishida, Kobayashi, & Nakada, 1991; Totta & Sopher, 1969; Warrior, 1990). (1) It creates a Cu diffusion barrier between the Cu substrate and the flip-chip solder bump. (2) During the reflow process of the solder bump, the under bump metallization undergoes metallurgical bonding at the interfaces of the solder bump and creates an intermetallic layer (IMC) at the interfaces. The under bump, metallization is a good conductor and helps in the conduction of electrical current. (3) It also creates an oxidation barrier at the interfaces of the solder joint. The selection of UBM metal totally depends on the composition of the solder bump. Cr, Ti, and TiW are usually used for an adhesion UBM layer, and the second UBM layer is mostly made of Cu or Ni metals. The average thickness of UBM layers is 0.5 to 1.0 micron (Diehl, 1968). A gold metal has also been used as a UBM layer but as gold is an expensive metal, so mostly a thin layer of gold metal is used for a UBM. (Heinen et al., 1989). In the past, different types of UBM like TiW/Au/Cu, Ti/Ni/Au, Cr/Cr-Cu/Cu, NiV/Cu, Ti/Cu, TiW/Cu, and electroless Ni/immersion Au were also developed and applied.

In the past, lead-based solder was used in the flip chip technology (Myers, 1969). The lead-based solder bump has low surface energy and low melting temperature (Lea, 1988). But because of the restrictions on the use of lead-based solders and due to environmental concerns, researchers have developed tin-based solders such as Sn-Ag, Sn-Bi, Sn-Zn, Sn-Ag-Bi, Sn-Ag-Zn, Sn-Ag-Cu, Sn-Cu and Sn-In, etc. (Abtew & Selvaduray, 2000; Liu, Zhou, Zhang, Li, & Wu, 2010; Silva, Garcia, & Spinelli, 2016; Silva et al., 2015). After replacement of lead-based solder, now Sn-based solder joint is used in the flip chip technology.

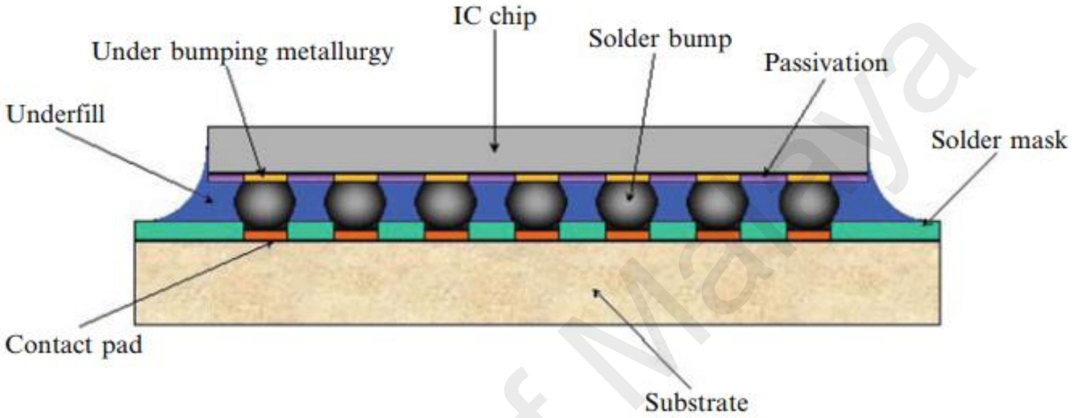

Figure 2.3: Generic configuration of C4 with underfill (Zhang, Luo, & Wong, 2013).

2.3 Lead-free solder joint

According to the environmental protection agency (EPA), both lead itself and compounds containing lead are very dangerous for the human health (Tu, Gusak, & Li, 2003; Ziegler, 1996). The lead was included in the top seventeen chemicals that pose the greatest threat to human life and society. On 1st July 2006, The European community waste electrical and electronic equipment (WEEE) banned lead-based solder joints and led to a focus on the development of lead-free solder joints (Kumar & Jung, 2013).

In chip technology, lead-based solder alloys no longer receive any interest in research. Scientists are eliminating the lead-based solders to avoid the inherent toxicity of lead in electronic industries. As a result of lead banning due to the environmental issue, lead-free solder has become a standard material for electronic joints (Lin & Lin, 2007). To replace lead-based solder, researchers used various metals (Au, Ag, Cu, Bi, In, Zn) and developed a number of lead-free solder alloys (Abtew & Selvaduray, 2000; Chen, Shen, Min, & Peng, 2009; Glazer, 1994; Igoshev & Kleiman, 2000; Lau, 1996; Mohanty & Lin, 2013; Tonapi, Gopakumar, Borgesen, & Srihari, 2002; Wu, Yu, Law, & Wang, 2004; Zeng & Tu, 2002; Zhang et al., 2010). These solder alloys have different melting temperatures and different properties.

Lead plays an important role in Sn-Pb solder. It reduces the surface energy, interfacial energy, and brittleness of the Sn-Pb solder joints (Kim, Jang, Lee, & Tu, 1999). It minimizes the Sn whisker growth and Sn pest (Lu, He, En, Wang, & Zhuang, 2009). It improves the wettability and reduces the reaction rate between the solder and under bump metallization (Kim, Jang, Lee, & Tu, 1999; Lu, He, En, Wang, & Zhuang, 2009).

The solder which contains a high concentration of lead such as 5Sn-95Pb can be used as a high-temperature solder joint due to its features of a slim two-phase region (the temperature distinction between liquidus and solidus). The melting temperature of 5Sn-95Pb solder is 308°C and its reflow temperature is 350°C which is higher than the eutectic Sn-Pb solder joint. The melting temperature of eutectic Sn-Pb is about 183°C while the reflow temperature is 200°C (Gan & Tu, 2005). As 5Sn-95Pb is a high-temperature solder and eutectic Sn-Pb is a low-temperature solder, so the combination of both solders meets the need of temperature range for the first two levels of packaging processes.

The replacement of lead-based solder joints should have at least equal or better material properties such as mechanical, electrical, thermal and structural properties than SnPb solder. Because of the good reaction ability with the many metals, formation of intermetallic compound and low temperature soldering, researchers suggested that Sn-based solder is one of the good replacement options of the SnPb solder joint (Abtew &

Selvaduray, 2000; Chen et al., 2009; Glazer, 1994; Igoshev & Kleiman, 2000; Lau, 1996; Mohanty & Lin, 2013; Tonapi et al., 2002; Wu et al., 2004; Zeng & Tu, 2002; Zhang et al., 2010).

In Table 2.1, lead-free solder alloys are listed. The selection criteria of solder alloys were done by the National Institute of Standards and Technology (NIST) (NIST). The Sn-based solder alloys include Sn-Ag, Sn-Cu, Sn-Bi, Sn-In, Sn-Zn, Sn-Sb and Sn-Ge (Zeng & Tu, 2002). In the past, the United Nations Environment Program suggested that germanium (Ge) is also dangerous for human health. It is one of the good reactive element and normally a trace amount of germanium is added to the Sn due to its high cost. Zinc shows dross due to the formation of oxides during the soldering, and it also has poor wetting properties. Indium has good wettability and good effects on physical properties of the solder alloys. But the cost of indium is high compared to other solder alloys. Bi also has excellent wettability and physical properties but as the Bi production is linked to the lead, so the use of Bi is also limited.

Table 2.1 and Table 2.2 elaborate the list of non-leaded solder alloys and also the criteria for down selection of the solder alloys by the National Center for Manufacturing Sciences (NCMS) (Siewert, 2002). In Table 2.1, lead-free solder alloys are listed. The selection criteria of solder alloys were done by the National Institute of Standards and Technology (NIST) (NIST). The Sn-based solder alloys include Sn-Ag, Sn-Cu, Sn-Bi, Sn-In, Sn-Zn, Sn-Sb and Sn-Ge (Zeng & Tu, 2002). In the past, the United Nations Environment Program suggested that germanium (Ge) is also dangerous for human health. It is one of the good reactive element and normally a trace amount of germanium is added to the Sn due to its high cost. Zinc shows dross due to the formation of oxides during the soldering, and it also has poor wetting properties. Indium has good wettability and good effects on physical properties of the solder alloys. But the cost of indium is high compared to other solder alloys. Bi also has excellent wettability and physical properties but as the Bi production is linked to the lead, so the use of Bi is also limited.

Table 2.1: Chemical compositions of lead-free solder alloy down-selected for preliminary testing by the National Center for Manufacturing Sciences (NCMS) (Siewert, 2002).

NCMS Alloy Code	Chemical Composition (% by mass)	NCMS Alloy Code	Chemical Composition (% by mass)
A1*	Sn-37Pb	EN1	Sn-5Ag-8.6In
A2	Sn-2Ag-36Pb	EN2	Sn-5.6Ag-14.4In
A3	Sn-97Pb	EN3	Sn-6.8Ag-20In
A4*	Sn-3.5Ag	EN4	Sn-3.1Ag-6.1Bi
A5	Sn-5Sb	EN5	Sn-3.5Ag-10Bi
A6*	Sn-58Bi	EN6	Sn-3.3Ag-15Bi
A7	Sn-3.5Ag-0.5Sb.1Cd	EN7	Sn-6.8Ag-30Bi
A8	Sn-75Pb	EN8	Sn-3.3Ag-11.2Bi-5.5In
		EN9	Sn-2.5Ag-11.2Bi-5.5In
B1	Sn-50Bi		
B2	Sn-52Bi	F1	Sn-2Ag-7.5Bi-0.5Cu
B3	Sn-55Bi-3Cu	F2#	Sn-2.6Ag-0.8Cu-0.5Sb
B4	Sn-48Bi-4Cu	F3	Sn-0.5Ag-4Cu
B5	Sn-2Ag—46Bi-4Cu	F4	Sn-8.8In-7.6Zn
B6	Sn-56Bi-2In	F5	Sn-20In-2.8Zn
		F6	Sn-5Bi-7Zn
C1	Sn-2Ag-1.5Sb-29Pb	F7	Sn-31.5Bi-3Zn
C2	Sn-3Ag-4Cu	F8	Sn-3.5Ag-1.5In
C3	Sn-2.5Ag-2Bi-1.5Sb	F9	Sn-2Ag-7.5Bi-0.5Cu
C4	Sn-3Ag-1Bi-1Cu-1.5Sb	F10	Sn-0.2Ag-2Cu-0.8Sb
C5	Sn-2Ag-9.8In		
		F11	Sn-2.5Ag-19.5Bi
D1	Sn-45Bi	F12	Sn-3Ag-41Bi
D2	Sn-57Bi-2In	F13	Sn-55Bi-2Cu
D3	Sn-2Ag-57Bi	F14	Sn-48Bi-2Cu
D4	Sn-57Bi-2Sb	F15	Sn-57Bi
D5	Sn-57Bi-1Sb	F16	Sn-56.7Bi-0.3Cu-1In
D6	Sn-2Ag-56Bi-1.5Sb	F17	Sn-3.4Ag-4.8Bi
D7	Sn-3Ag-55.5Bi-1.5Sb	F18	Sn-3Ag-15In
D8	Sn-3Ag-55Bi-2Sb	F19	Sn-3Ag-5Bi-10In
D9	Sn-3Ag-54Bi-2In-2Sb	F20	Sn-5Bi-10In
D10	Sn-3Ag-54Bi-2Cu-2Sb		
		F21	Sn-2.8Ag-20In
E1	Sn-3Ag-2Sb	F22	Sn-0.1Ag-1Bi-3.9Sb

Table 2.1, continued.

E2	Sn-3Ag-2Cu-2Sb	F23	Sn-0.5Ag-1.5Bi-3Sb
E3	Sn-3Ag-2Bi-2Sb	F24	Sn-55Bi-2Zn
E4	Sn-3Ag-2Bi	F25	Sn-0.5Ag-56Bi
E5	Sn-2.5Ag-2Bi	F26	Sn-4.5Ag-1.6Cu-5Sb
E6	Sn-2Bi-1.5Cu-3Sb	F27	Sn-3.5Ag-0.5Cu-1Zn
E7	Sn-2Bi-8In	F28	Sn-3Ag-10.9In-0.4Sb
E8	Sn-10Bi-10In	F29	Sn-4.7Ag-1.7Cu
E9	Sn-10Bi-20In	F30	Sn-3.2Ag-0.7Cu
E10	Sn-9Zn	F31	Sn-3.5Ag-1.3Cu

*Eutectic composition

#Composiction F2 is a proprietary composition. Castin®

Table 2.2: Criteria for down-selection of lead-free solder alloys (Siewert, 2002).

Property	Definition	Minimum Acceptance Level
Liquidus temperature	Temperature at which solder alloy is completely molten	
pasty range	The range of temperature between solidus and liquidus, Where alloy is part solid and part liquid.	<30 (°C)
Wettability	Assessed by the force required wetting a copper wire with molten solder. A large force indicates good wetting, as does short duration t0 at zero wetting force and time t2/3 to reach two-thirds of maximum wetting force.	F max > 300 µN t0 < 0.6 s t2/3 <1 s
Area of Coverage	Measures coverage of copper test piece by solder	>85 %
Drossing	Measured by amount of oxide formed in air on surface of molten solder after a fixed duration at soldering temperature	Qualitative
Thermal Mismatch	The difference in coefficient of thermal expansion that causes unacceptable thermal stress.	29ppm/°C
Creep	Stress load to failure at room temperature, in 10,000 minutes (~167 hours)	>500 psi
Yield Strength		>2000 psi
Elongation	Relative elongation of material under uniaxial tension at room temperature	>10%

Hence by comparing the advantages and disadvantages of the Sn-based solder alloys, it is found that the long list of Sn-based solder joints becomes a short list of promising replacement candidates such as Sn-3.5Ag, Sn-3.5Ag-0.7Cu, Sn-0.7Cu, and Sn-3.5Ag-4.8Bi (NEMI, 2004). Consequently, Sn-Ag-Cu and eutectic Sn-Cu and Sn-Ag were recommended as a promising replacement of the lead-based solder alloys by the National Electronics Manufacturing Initiative (NEMI) (NEMI, 2004). Researchers found that SAC solder has good mechanical properties such as high strength, better creep and fatigue resistance. To complement these properties, it is also necessary to other properties such as electrical properties, structural properties and also necessary to minimize EM failures in SAC solder joints. In the present study, the minor addition of Ni and Co elements were introduced in SAC solder joint to minimize the EM damage and to improve the electrical, mechanical and structural properties.

2.4 Downscaling of flip chip technology

Microelectronic industries are developing and producing electronic devices with more advancement in functionality, reducing cost, minimizing size and weight due to recent demand of manufacturing industries for smaller, cheaper and efficient electronic devices. These circumstances brought the continuous evolution of materials and processes. Reduction in size of the electronic device and increase in the functionality of electronic devices apparently increased the current density which has a dangerous impact on chip interconnection and packaging technology (Figure 2.4). Due to an increase of current density in electronic devices, the reliability issue has also increased (Ma et al., 2011; Tu, 2003; Yeh, Choi, Tu, Elenius, & Balkan, 2002). A number of efforts have been carried out in the past to improve the reliability of the electronic devices (Ma, Xu, Guo, & Wang, 2011). Flip chip technology has been intensively used in high-performance applications and to replace wire bond technologies because of its superior electrical performance and smaller package size (Kwon & Paik, 2002; Rungyusiri, Sa-ngiamsak, Harnsoongnoen, & Intarakul, 2009). This technology incorporates a process in which the bare chip is turned upside down, i.e., active face down, and is bonded through the input-output (I/O) to the substrate, hence called a flip chip. A solder interconnects that provides electrical connection between the chip, and the substrate is bumped on a processed silicon wafer prior to dicing for die-attach. The assembly is then reflow-soldered followed by the underfill process to provide the required encapsulation. The demand of smaller, low-cost and efficient electronic devices has increased the input and output current density while decreased the packaging size. Due to which, the size of flip chip solder and their pitch also has decreased. Reliability assessment and verification of these devices have gained tremendous importance due to their shrinking size (Tu, 2003).

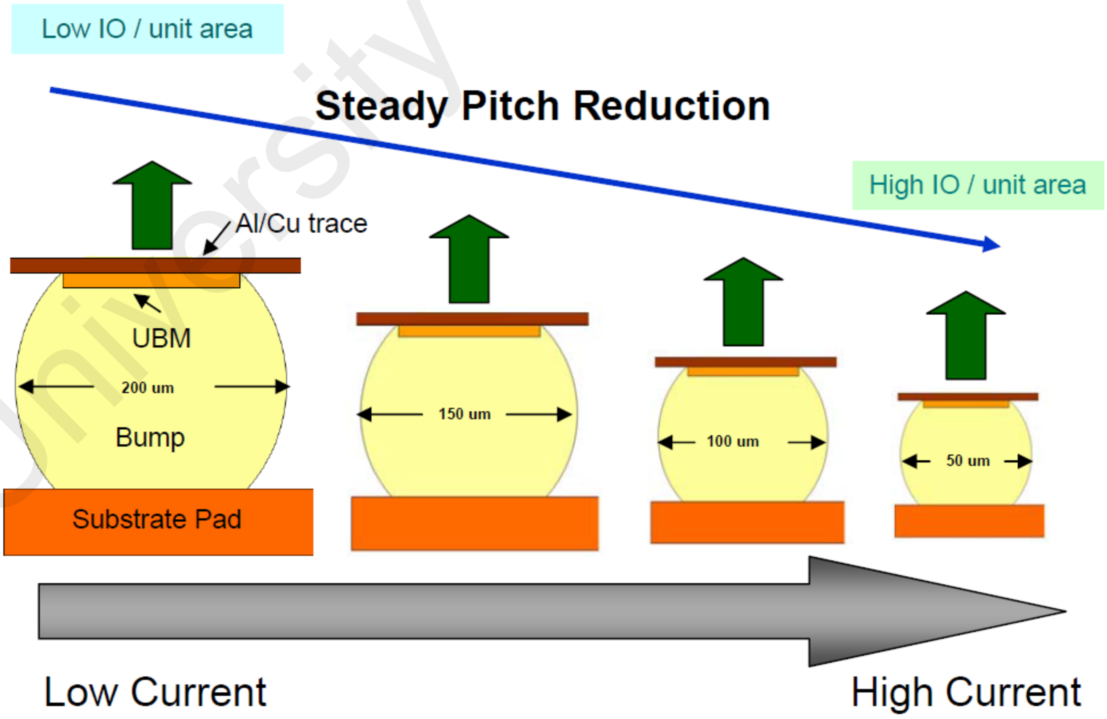

Figure 2.4: Schematic diagram describing reduction in size of solder joint (Selvaraj, 2007).

2.5 Physics of electromigration

Electromigration is a mass transportation phenomenon driven by high-current density, and it is also known as diffusion of atoms, which are driven by high-current density (Liu, Wang, Li, Li, & Chen, 2015). When a heavy electron wind passes from the substrate to the solder joint, it collides and drifts with the Cu atoms present at the cathode interface of the solder joint (Guo et al., 2015). Current wind transfers the momentum to the Cu atoms present at the cathode interface of the solder joint due to which the Cu atoms migrate from the cathode side toward the anode side (Zhao et al., 2013). The migration of Cu atoms forms vacancies at the cathode side which evolve into voids formation after a long period of EM (Ma et al., 2011; Zhao et al., 2013). In the flip chip solder joint, mostly the current enter from the corner of the solder joint (Figure 2.5). At the corner of the solder joint, the non-uniform distribution of current density occurs, which creates the current crowding effect in the solder joints (Zhang et al., 2006). This non-uniform distribution of current density also increases the Joule heating effect in the solder joint. Joule heating and current crowding play an important role in EM failure (Chen, Tong, & Tu, 2010; Guo et al., 2015). Joule heating and current crowding effects increase the electromigration process in the solder joint. The rapid migration of Cu atoms from the cathode to the anode creates a number of reliability issues in the solder joint (Kumar, Yang, Wong, Kripesh, & Chen, 2009). The electromigration issues involve the formation of voids, cracks and damage at the cathode side, reduction in thickness of interfacial IMC layer at the cathode side and rapid growth of interfacial IMC layer at anode side (Kumar, Yang, Wong, Kripesh, & Chen, 2009; Ren et al., 2006; Xu et al., 2014; Zhang, Chan, Wu, Xi, & Wu, 2008) (Figure 2.5).

In 1969, it was found that existing metal ions in an electric conductor usually subjected to two opposite forces, one is due to positive ion interaction with the electric field in the direction of the field this force is represented as (F_E). The second force (F_P) is due to momentum exchange between the charge carriers and ions. In the past, Black proposed the net force (F) equations (Lin & Basaran, 2005).

$$F = F_E \quad F_P = Z^{*}eE \tag{2.1}$$

Where,

$Z*e$ = Effective charge assigned to the migration ion,

E = Activation energy.

In 1969, Black (Lin & Basaran, 2005) proposed a mean time to failure equation (MTTF) which helps to estimate the life of the solder joint during the electromigration process. The equation is as below.

$$MTTF = A\frac{1}{J^{n}}\exp \quad \frac{Q}{kT} \tag{2.2}$$

Where,

A = Constant,

J = Current density,

b = Model parameter for current density,

Q = Activation energy, K is Boltzmann's constant,

T = Average bump temperature.

Due to increasing input current and decreasing the cross-sectional area of the solder joint, the current density has intensively increased. The relation between the cross-sectional area of the solder joint and current density can be understood by following simple equation.

$$J = \frac{I}{a} \tag{2.3}$$

Where,

J = Current density,

I = Current (Amp),

a = Cross section area.

It shows that due to a reduction in the cross-sectional area, the current density will be increased.

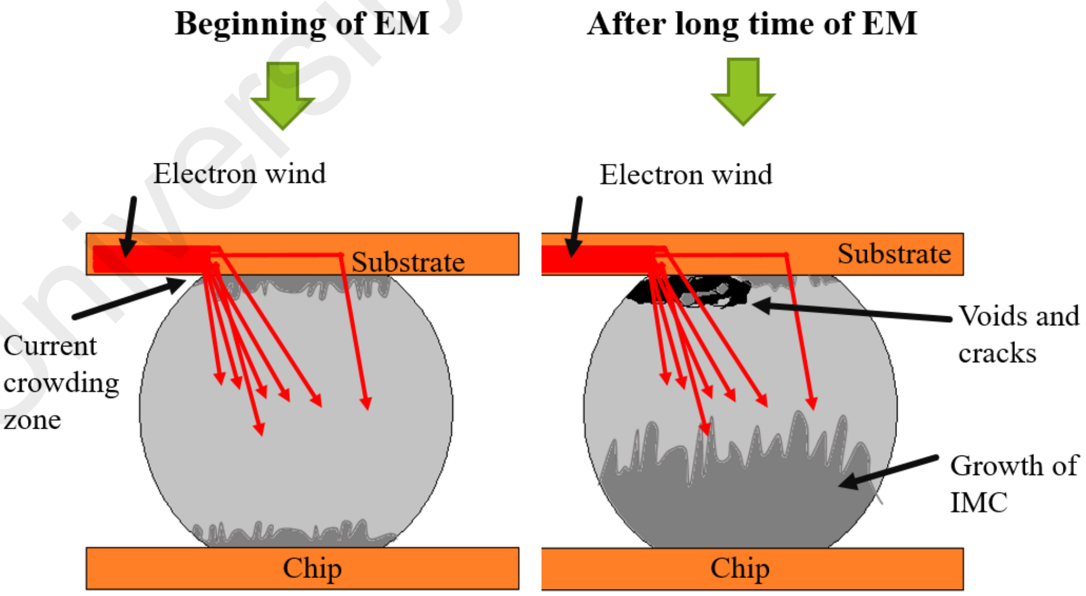

Figure 2.5: Schematic diagram of flip chip lead-free solder bump describing electromigration failures in Sn-based solder due to high-current density.

2.6 Electromigration issues in flip chip solder joint

With a high-current density, EM usually influences migration of Cu atoms from the cathode to the anode side of the solder joint. This leads to reliability concern for the solder joint. High-current density causes heavy electron wind flow through the solder joint. When high-current density enters from the substrate to the solder joint, mostly it makes drifting and collision with the atoms presents on interfaces of the solder joint. Cu atoms start to migrate in the direction of electron flow from the cathode towards the anode side (Chao et al., 2007; Ding et al., 2006; Zeng et al., 2005). Migration of atoms causes the serious electromigration failures in the solder joint. After migration of Cu atoms, they leave vacancies which lead to the formation of voids after a long time of the EM process. The diffusion of Cu atoms also depends on temperature (Ebersberger, Bauer, & Alexa, 2005). Due to the Joule heating effects present in the solder joint; rapid diffusion of Cu atoms will take place. Rapid Cu diffusion creates vacancies at the cathode side of the solder joint which lead to the formation of voids and cracks and finally separation of the joint from the cathode interfaces (Pecht, Fukuda, & Rajagopal, 2004; Rungyusiri et al., 2009; Tu, 2003; Zhao et al., 2013). These voids and cracks decrease the cross-sectional area of the solder contact, which increases the local current density and local electrical resistance. This will not only enhance the current crowding effect but also exacerbate the Joule heating effect (Tu, 2003; Zhang et al., 2010). Formation of cracks, voids, and damage are explained in Figure 2.6.

By increasing the EM time the Cu diffusion will also be increased. In the SAC305 solder joint, in the past studies, a substantial increase of IMC thickness at the anode side was observed with a corresponding decrease at the cathode side by increasing the duration of EM test (Tu, 2003). High-current density causes heavy electron wind flow through the sample. Cu atoms start to migrate in the direction of electron flow from the cathode towards the anode side because of drifting and collision of electron wind with Cu atoms.

Gradually, Cu atoms begin to form a thicker layer of IMCs such as Cu_6Sn_5 at the anode side by reacting with Sn atoms (Gan & Tu, 2005). As IMCs have brittle properties, so If IMCs layer at anode side become thicker then it will reduce the mechanical strength of the solder joint (Ren et al., 2006). On the other hand, directional migration of Cu atoms towards the anode rapidly decreases the IMC layer at the cathode interfaces, which finally lead to the separation of the solder joint from the cathode interface (Zhao et al., 2013). The change in thickness of interfacial IMCs at the cathode and anode side after EM is depicted in Figure 2.6.

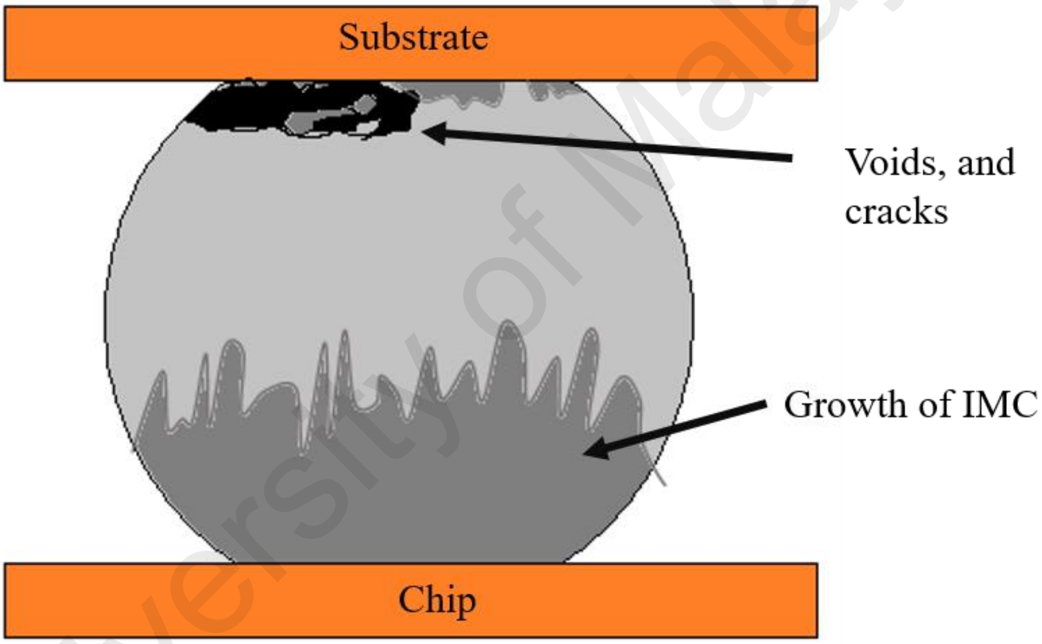

Figure 2.6: Description of EM failures in the solder joint.

The structural degradation of the interfaces can impose serious effects on mechanical performance of the solder joint. In Figure 2.7 and Figure 2.8, the effect of EM on the SAC305 solder joint can be clearly seen that the fracture migrated to the cathode interfaces. The fracture was cup and cone shaped with ductile behavior before her

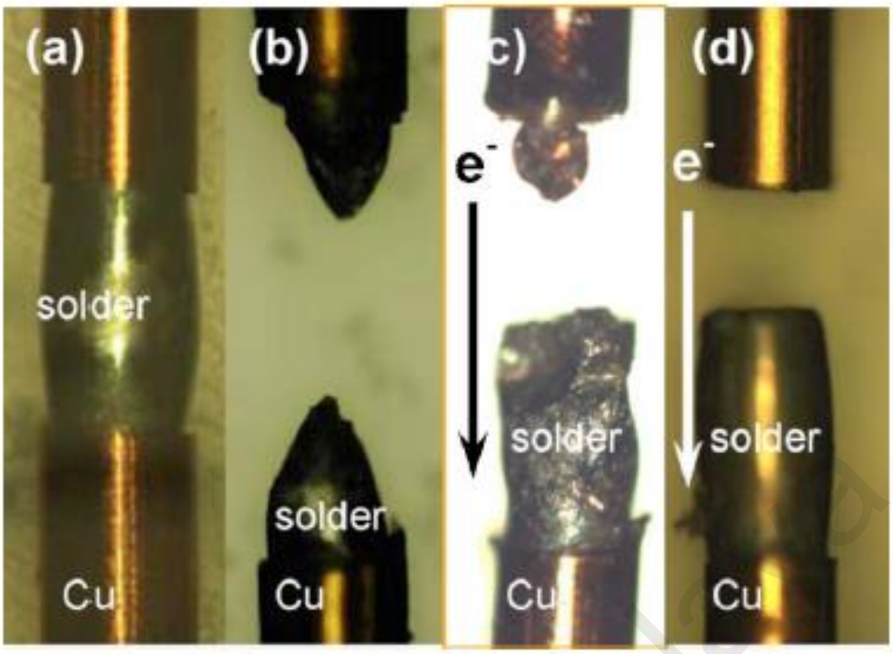

Figure 2.7: Fracture images of tensile test after EM: (a) Optical picture of original sample, (b) fracture image without EM, (c) fracture image after EM, 5 × 10^3 A/cm^2 at 45 °C for 96 h, (d) fracture image after EM, 5 × 10^3 A/cm^2 at 145 °C for 144 h (Ren et al., 2006).

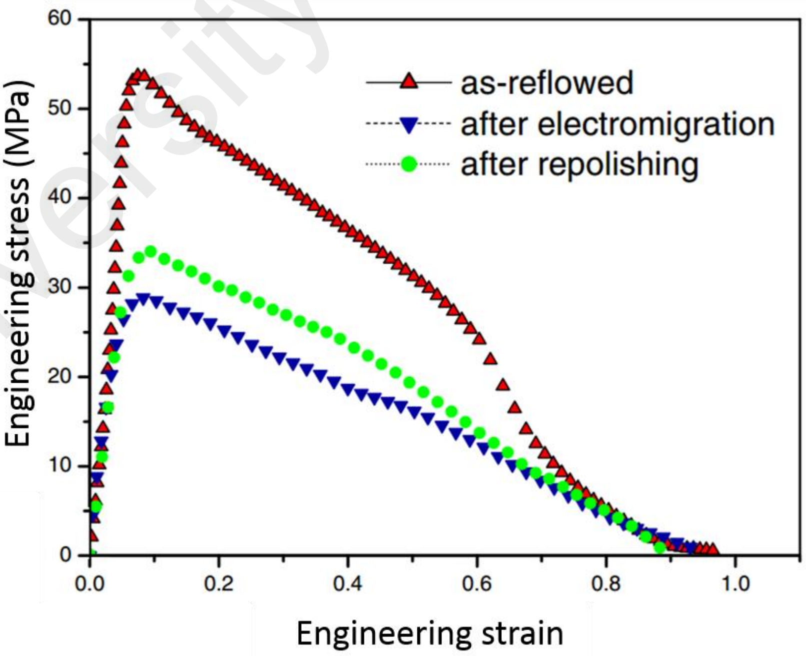

Figure 2.8: Tensile stress–strain curves of Sn–Ag–Cu solder joints before and after electromigration (Zhang et al., 2007).

Wang et al. reported that by increasing the EM time, the shear strength of the SAC solder will be decreased, and the fracture will be shifted from the solder bulk to the cathode interface with brittle behavior (Wang, Zeng, Zhu, Wang, & Shang, 2010) (Figure 2.9 and Figure 2.10). Similar results were also reported elsewhere (Zhang, Wang, & Shang, 2007).

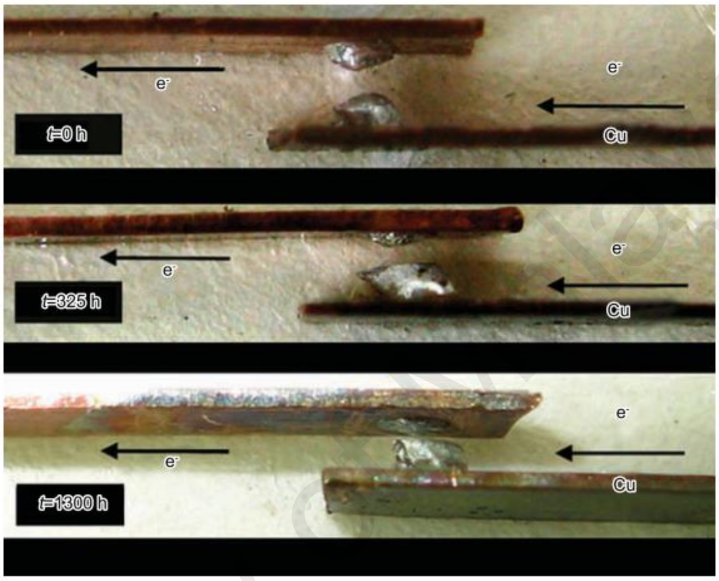

Figure 2.9: Macro-fracture path after current stressing (Wang et al., 2010).

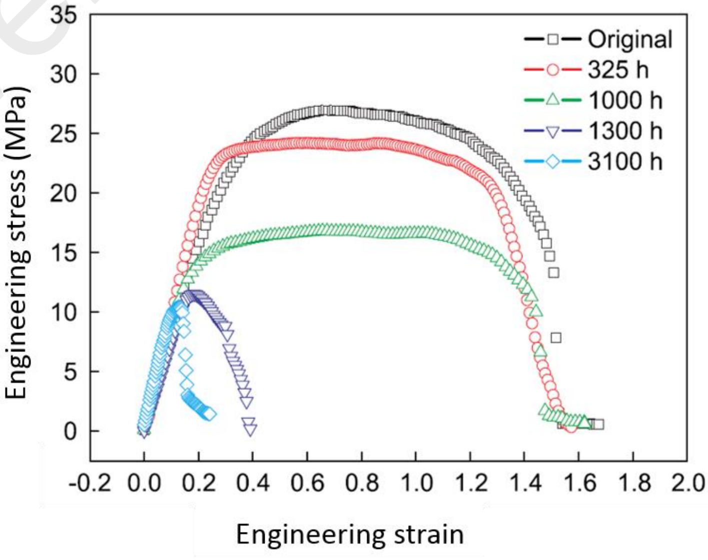

Figure 2.10: Effect of the current on the shear properties of the solder joints (shear speed of 0.3 mm/s) (Wang et al., 2010).

2.7 Factor affecting electromigration failures

The reasons for electromigration failure have been investigated in the past (Chae et al., 2006; Chao et al., 2007). It was found that Joule heating effect (Chae et al., 2007; Tu, 2003; Zhang et al., 2010), current crowding effects and grain orientation of Sn are main reasons of electromigration failures (Lee et al., 2011b; Yang et al., 2015) (Huang, Yang, Ke, Hsueh, & Kao, 2014). The details of these effects are given below in section 2.7.1, 2.7.2 and 2.7.3.

2.7.1 Joule Heating effects

A solder bump has much lower thermal conductivity than a trace (Basaran, Lin, & Ye, 2003). The actual temperature of the solder bump can thus be significantly higher than the ambient temperature of the solder bump. Due to the nature and construction of the solder bump, the bump temperature is governed by the heat dissipation of the chip and the Joule heating effect (Tu, 2003; Zhang et al., 2010). Since Joule heating is a nonlinear function of current (I), any increase in a current adversely affects the solder bump temperature (Selvaraj, 2007). It is essential to control the temperature of the solder bump to reduce the failure in the solder bump. Different elements in the solder bump can be resistive leading to an increase in overall bump resistance. This might affect the Joule heating characteristics in the solder bump. In the past, the sizes of the solder joint and traces were larger. So the occurrence of heating was very low due to a bigger size. The Joule heating effects were not so pronounced in the solder joints and traces. As recently, the size of the solder joint and traces have been diminished. The scaling down in the size of the solder joint and traces has impacted not only the solder joints but also the traces that form the interconnection. Each of the new generations of flip chip device has had to deal with higher Joule heating in a trace and smaller-sized solder joints. The Joule heating effect is not only because of reduction in the size of the solder joint and traces but also because of an increase in current density (Bauer, Fischer, Birzer, & Alexa, 2011; Dusek, Okoro, & Hunt, 2006; Huang, Zhang, Yang, & Zhao, 2015). The high-temperature in the solder joint will accelerate the electromigration process in the solder joint. So it is very important to minimize the formation of Joule heating at the solder joint and traces to minimize the EM failures.

2.7.2 Current crowding effects

When a high-current density enters into the solder joint from the substrate, it changes the direction from horizontal to vertical (Jang, Ramanathan, Tang, & Frear, 2008) as shown in (Figure 2.5). During current flow, most of the current enter from the corner of the solder joint. The distribution of current density becomes non-uniform at the cathode interface (Chen et al., 2010; Yang et al., 2015). The non-uniformity in the distribution of current density creates current crowding at the cathodic interface (Chen et al., 2010; Yang et al., 2015). The explanation of current crowding is also given in (Figure 2.5). The non-uniform distribution of current density significantly increases the current density at the corner which increases the current crowding. An effort was done to investigate and to understand the current crowding effect on the solder joint in the presence of high-current density (Ho, Yang, Lee, & Chen, 2016). A 3D simulation model was constructed to understand the effect of current crowding. Electromigration tests were run for the different time intervals. Figure 2.11a-h shows x-ray micrographs of the samples. It was found that a high amount of current enters from the corner of the solder joint in all samples. FEA simulation detected that at the corner of the solder joint, the current density significantly increases from 1.1×10^4 A/cm^2 to 3.58×10^4 A/cm^2 at the corner of the solder joint (Figure 2.11g).

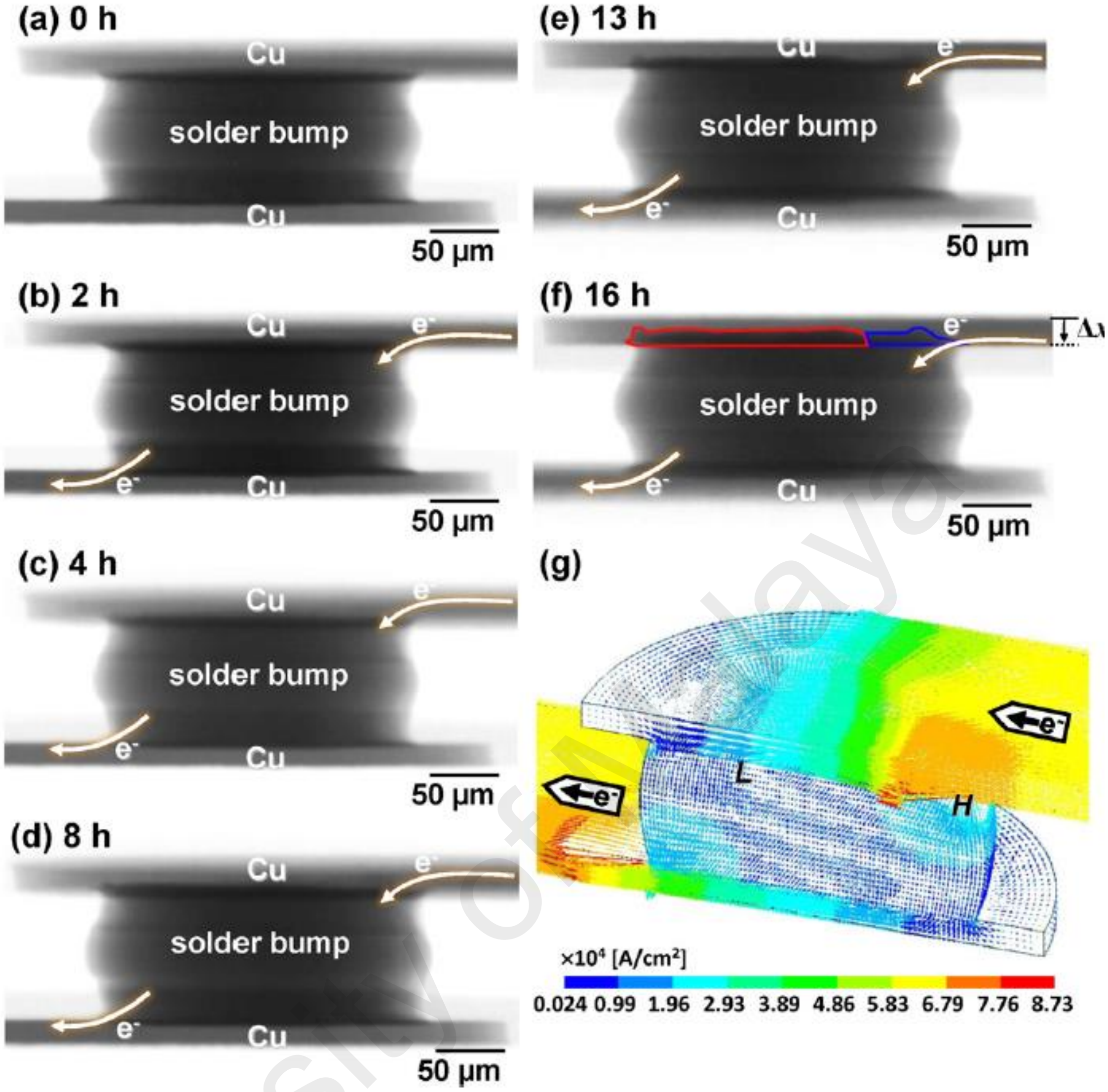

Figure 2.11: A series of X-ray micrographs demonstrating the interior microstructure evolution of a solder joint under 1.1 × 10^4 A/cm^2 current stressing for t=(a) 0 h (initial), (b) 2 h, (c) 4 h, (d) 8 h, (e) 13 h, and (f) 16 h. (g) FEA simulation of the current density (Ho et al., 2016).

2.7.3 Crystallographic orientation of Sn grain

The crystallographic orientation of Sn grain and crystallographic orientation of interfacial IMC plays an important role in the migration of Cu atoms from the cathode to the anode side of the solder joint. When the c-axis of Sn grain and interfacial IMC are parallel to the direction of current flow, the Cu diffusion will be faster (Huang et al., 2014). The vertical direction of the c-axis of the current flow has been found as an ideal

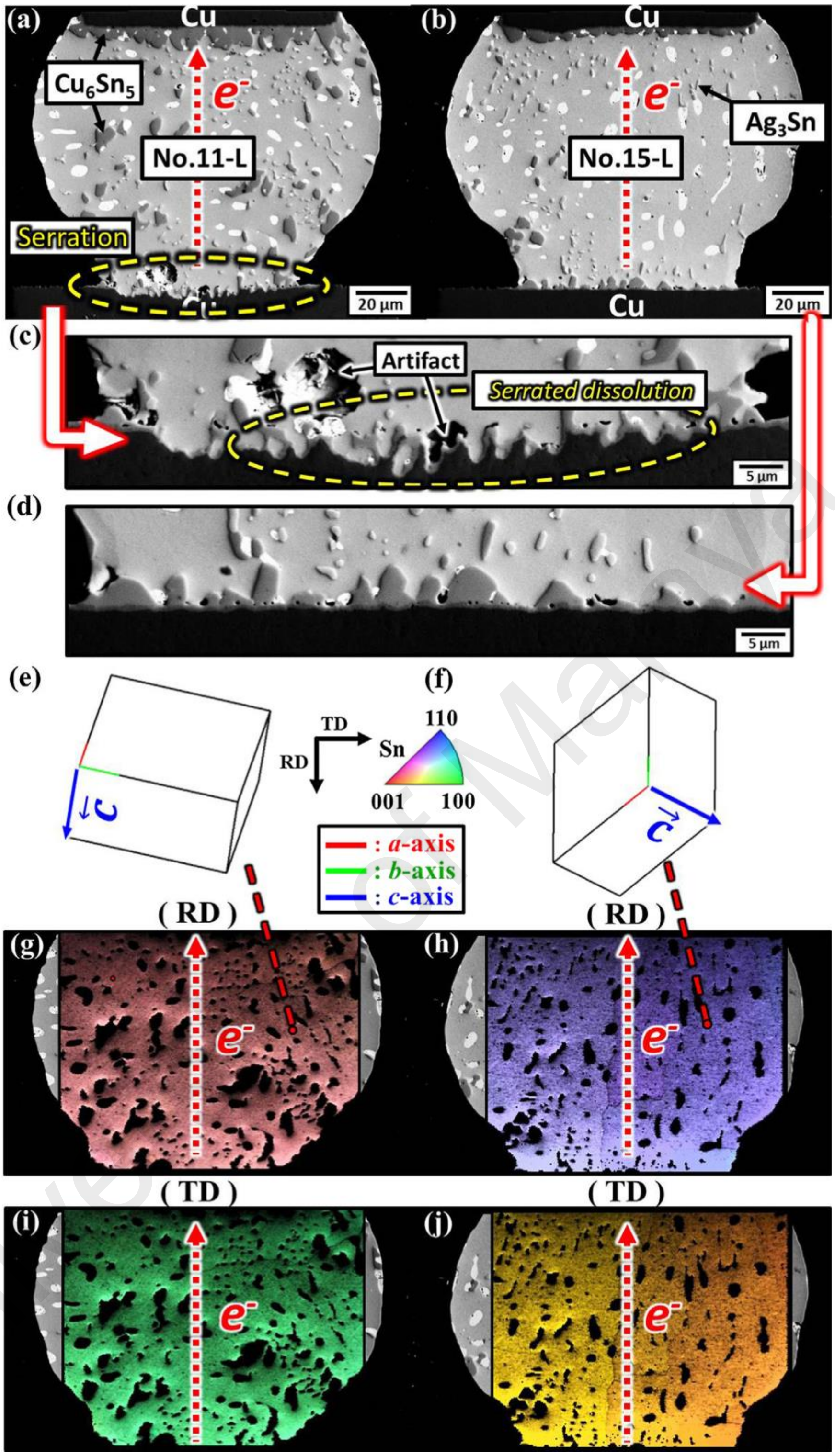

Figure 2.12: (a) and (b) Cross-sectional micrographs of the solder joints after current stressing of 4.5 10^4 A/cm^2 at 50 °C for 1862 h. (c) and (d) Zoom-in images of the cathode interface of (a) and (b) respectively. (e) and (f) Sn grain orientation for the joint in (a) and (b), respectively. (g) and (h) EBSD analysis map of Sn grain (image quality + inverse pole figure) with RD direction for the joint in (a) and (b), respectively. (i) and (j) with TD direction (Yang et al., 2015).

condition to reduce the diffusion of Cu atoms (Lee et al., 2011b; Yang et al., 2015). In early studies, it was also found that the diffusion of Cu atoms in the a-axis and b-axis of the Sn grain is 500 times slower than the c-axis.Hence the orientation of the c-axis plays a very important role in the migration of Cu atoms. Yang et al. carried out an experiment to investigate the effect of Sn grain orientation on the migration of Cu atoms. In their experiment, it was observed that the migration of Cu atom was very fast when the orientation of the c-axis of Sn grain was parallel to the direction of current flow (Figure 2.12 a). The electromigration effects on the cathode side are shown in Figure 2.12 c. The Sn grain orientation was taken by EBSD image map which is given with the rolling direction (RD) and transverse direction (TD) as shown in Figure 2.12 g and i. The migration of Cu atom was significantly controlled when the angle between the orientation of the c-axis of Sn grain and direction of current flow was bigger (Figure 2.12 b). The reduction in EM effects on cathode side are shown in Figure 2.12 d. The EBSD image map was used to take the Sn grain orientation witdirection (Figure 2.12 h and j). Hence the angle θ between the c-axis of Sn grain and direction of current flow plays a very important role in Cu migration from the cathode side to the anode side of the solder joint (Yang et al., 2015).

In another study, researchers also found that the diffusion of Cu atoms and IMC accumulation depend on the orientation of β-Sn grain in the line type solder joint (Huang, Zhao, Zhang, & Zhao, 2016). They investigated the effect of grain orientation on the migration of Cu atoms (Huang, Zhao, Zhang, & Zhao, 2016). They prepared two samples and each sample contains two big grains. Figure 2.13 a and d represent the cross-sectional image of both samples. Figure 2.13 b and e represent the cross-polarized images and (c) and (f) represent the EBSD inverse pole figure orientation image map of both samples (Huang et al., 2016). In both samples, one grain has a big θ angle and another has smaller. The θ angle is an angle between the c-axis of β-Sn grain and direction of current flow. In the first sample, the direction of current was from low to high θ angle. It was found that in the low θ angle, the Cu diffusion was very fast. It produced voids at the cathode side of the solder joint (Huang et al., 2016). While the grain with high θ angle showed very less Cu diffusion towards the anode side (Figure 2.14). Due to different grain orientation, the thick IMC layer was produced between both of the grains. In the second sample, the direction of current was from high to low θ angle. Significant reduction Cu diffusion was found due to high θ angle (Figure 2.15).

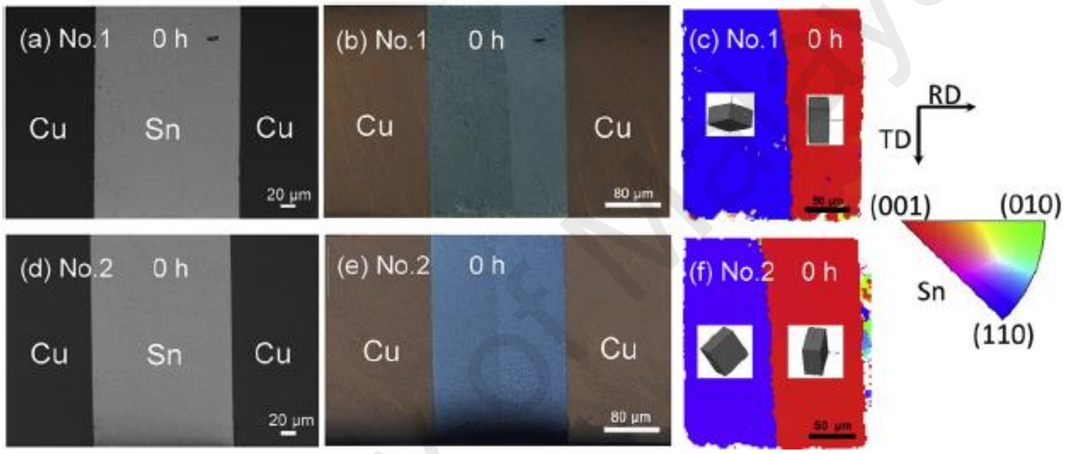

Figure 2.13: Cross-sectional microstructure of the as-soldered (a) and (d) back-scattered SEM images, (b) and (e) cross-polarized images and (c) and (f) EBSD inverse pole figure orientation image map (Huang et al., 2016).

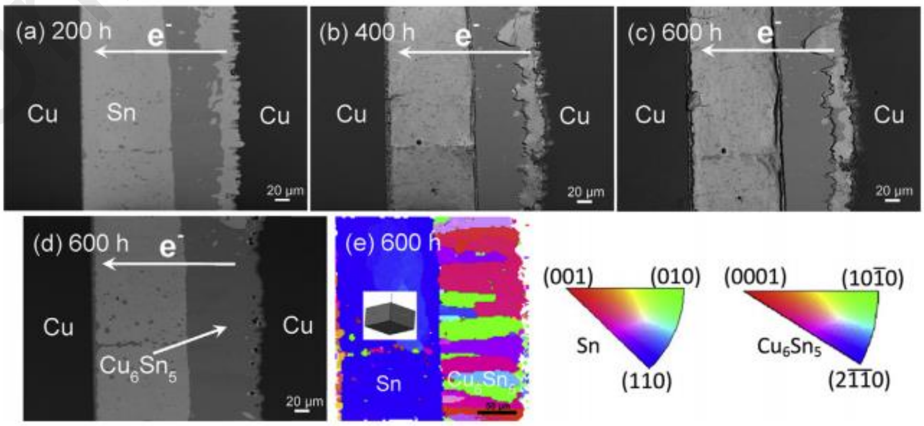

Figure 2.14: Cross-sectional microstructures of the sample after EM for (a) 200 h, (b) 400 h, (c) 600 h, (d) 600 h (polished) and (e) EBSD inverse pole figure orientation image map (Huang et al., 2016).

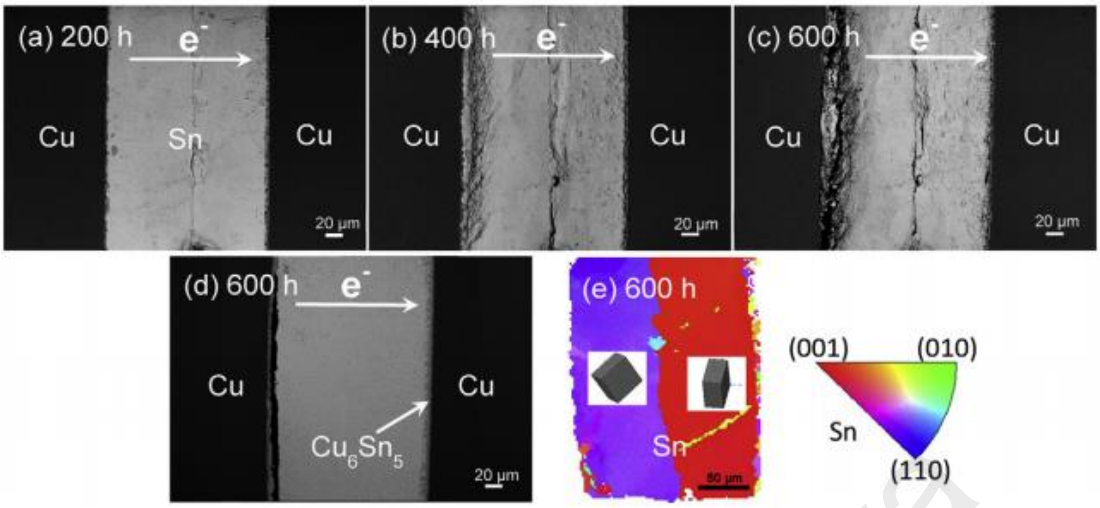

Figure 2.15: Cross-sectional microstructures of the interconnects after EM for (a) 200 h, (b) 400 h, (c) 600 h, (d) 600 h (polished) and (e) EBSD inverse pole figure orientation image map (Huang et al., 2016).

In previous studies, it was also found that the rate of diffusivity of Cu atoms is different along a different axis of the Sn grain (Huang et al., 2016). Yang at al. quantified the diffusivity of Cu atoms into Sn along a-axis and c-axis of Sn grain into the Sn2.6Ag solder joint (Yang et al., 2015). The EM test was conducted in 4 different samples. It was found that in each sample, the orientation was different and in each different orientation the EM behavior was different. Base on orientation, they quantified the diffusivity ratio of Cu by using following method (Yang et al., 2015).

$$J_{EM}^{Cu} = C_{Cu} \frac{D_{Cu}^{Sn}}{kt} z_{Cu}^{Sn\,*} e \rho_{Sn} j \qquad (2.4)$$

Where,

C_{Cu} = Local molar concentration of Cu in Sn,

D_{Cu}^{Sn} = Diffusion coefficient of Cu in Sn,

$z_{Cu}^{Sn\,*}$ = Effective charge number of Cu in Sn,

k = Boltzmann constant,

t = Absolute temperature,

e = Charge of an electron,

ρ_{Sn} = Resistivity of Sn,

j = Applied electron current density.

The term D_{Cu}^{Sn} for a-axis and c-axis was calculated as below(Dyson, Anthony, & Turnbull, 1967; T. Yang et al., 2015)

$$D_{Cu}^{a\ axis} = 2.4\times10^{3}\exp\frac{33.18(kJ\ /\ mole)}{kT}\ (cm^{2}/\ s) \tag{2.5}$$

$$D_{Cu}^{c\ axis} = 1.0\times10^{3}\exp\frac{16.8(kJ\ /\ mole)}{kT}\ (cm^{2}/\ s) \tag{2.6}$$

The ratio of Cu diffusivity is given in Figure 2.16. Hence it can be said that orientation of Sn grain plays a very important role during the electromigration process. Fine grain structure can suppress the electromigration failures in the Sn-based solder joints.

2.8 Previous methods for retardation of EM failures

In the past, due to the larger size of the solder joint and low input-output current, the EM process was slow. In recent research, EM failures are very common and known as one of the main reliability issues because of the small-sized solder joint and high input-output current. Researchers paid serious attention to the EM issues in last decade.

Researchers modified the solder joint by using different techniques to minimize the EM failures. Their solder modifications techniques include minor addition(s), either in the form of alloying element(s) (Wang et al., 2009; Zhao et al., 2013) or as micro/nano-sized particles (Arafat, Haseeb, & Johan, 2011; Guo et al., 2009; Nadia & Haseeb, 2012b; Rhee et al., 2003; Zhang et al., 2010) and addition of carbon nanotubes (Xu et al., 2014; Yang, Zhou, & Wu, 2013). The detailed of these modification techniques are given below in section 2.8.1-2.8.2.

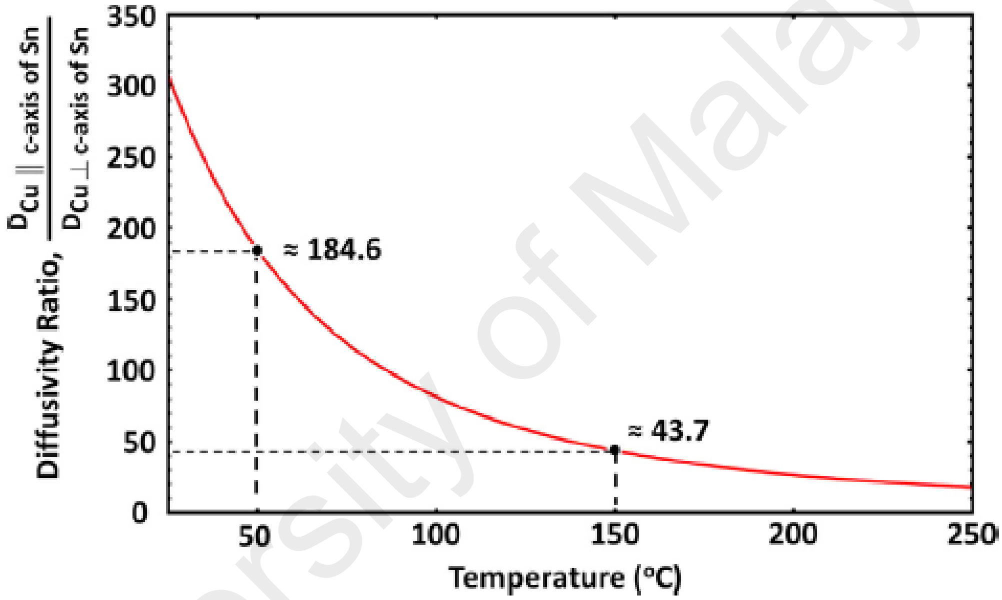

Figure 2.16: Diffusivity ratio of Cu atoms along c and a-axis of Sn at various temperatures (Yang et al., 2015).

2.8.1 Alloying method for retardation of EM failures

2.8.1.1 Ce-containing alloys

In the past, cerium (Ce)-containing Sn-3.9Ag-0.7Cu alloy was investigated under high-current density (Xie, Friedman, Mirpuri, & Chawla, 2014). It was found that after addition of Ce, the interfacial IMC layer was thinner than the interfacial IMC layer of the

SAC solder joint. Ce formed $CeSn_3$ IMC at interfaces as well as inside the solder bulk. $CeSn_3$ forms high-angle boundaries inside the solder joint which reduce the migration of atoms (Dudek & Chawla, 2009, 2010). $CeSn_3$ also has a good ability to react with Sn and block its migration towards the anode side of the solder joint. The voids were propagated in both types of the solder joints but comparing the SAC solder joint with Ce-containing solder joint; the voids were suppressed in the Ce-containing solder joint due to finer microstructure and formation of $CeSn_3$ (Xie et al., 2014). Figure 2.18 and Figure 2.19 show 3D view of voids formed in the SAC solder and Ce added SAC solders. It was detected that without the addition of Ce the number of voids significantly increased after a long time of EM process (Figure 2.18). $CeSn_3$ reduced the Cu migration due to which the size of the voids was smaller at the cathode side (Figure 2.19).

Thus the use of Ce as an alloying element into Sn-3.9Ag-0.7Cu reduced the EM effects due to the reduction of Cu migration from the cathode to the anode side. The researchers also investigated the effect of other alloying elements such as Ni, Co and Sb on the EM failures into lead-free solder joints (Zhao et al., 2013; Ma, Xu, Sun, et al., 2011; Hsu & Chen, 2013). A detailed discussion of the addition of Ni, Co, and Sb as an alloying element into lead-free solder joint and their effects on EM damage are given below in section 2.8.1.2. After addition of Ce, the formation of the voids was less and the microstructure of the solder joint was finer (Figure 2.19). The reason for the reduction in void formation is the formation of $CeSn_3$ IMC particles in the solder matrix and finer microstructure of the solder joint (Figure 2.17).

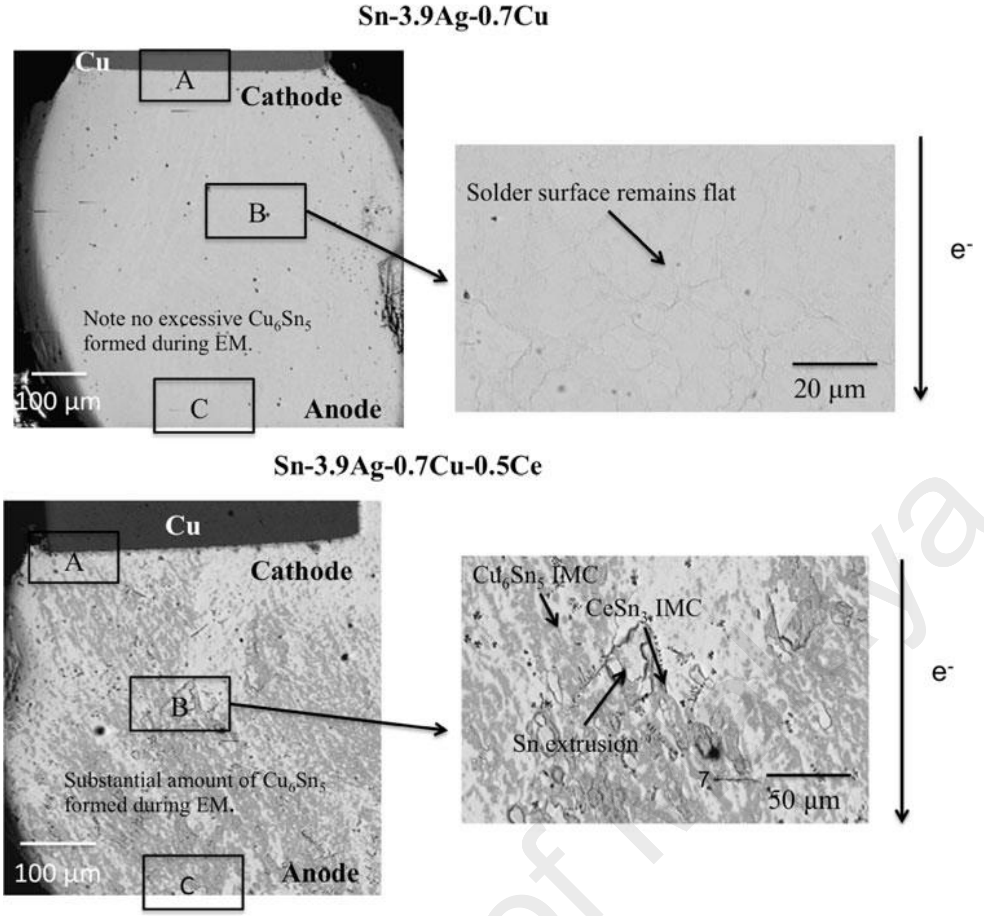

Figure 2.17: Backscattered electron microscopy images of the central region of Sn-3.9Ag-0.7Cu and Sn-3.9Ag-0.7Cu-0.5Ce joints after current stressing (Xie et al., 2014).

2.8.1.2 Ni, Co, and Sb-containing alloys

Zhao et al. used the alloying method to add Ni, Co, and Sb powder into the SAC solder paste (Zhao et al., 2013). They prepared four types of the solder joint; SAC solder, SAC + Ni, SAC + Co and SAC + Sb solder joints. After addition of Ni, Co, and Sb, the morphology of the solder joint has changed at interfaces as well as inside the solder joint (Figure 2.20).

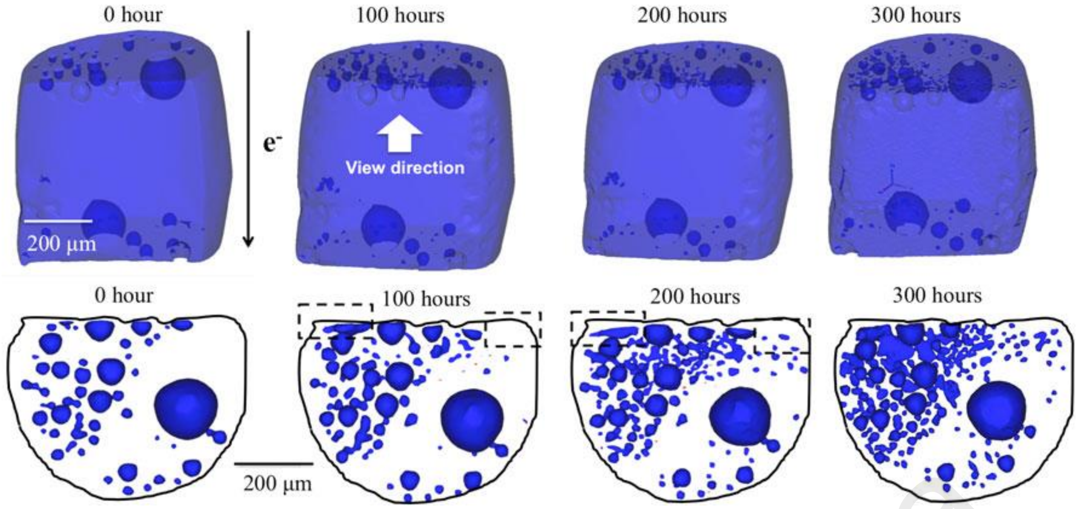

Figure 2.18: Sn-3.9Ag-0.7Cu void growth over time, showing 3D rendering (top) and cathode void top view (bottom) (Xie et al., 2014).

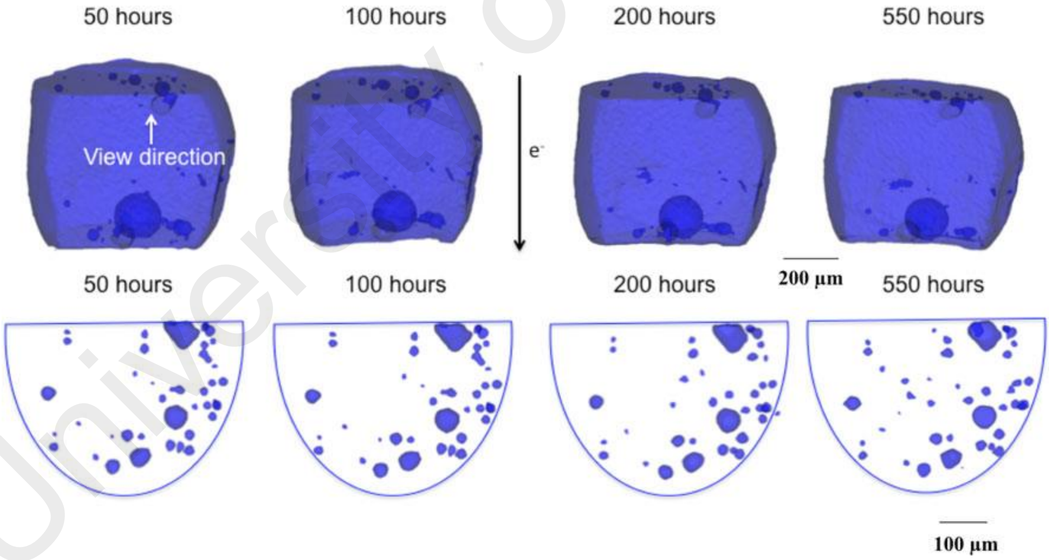

Figure 2.19: Sn-3.9Ag-0.7Cu-0.5Ce void growth over time, showing 3D rendering (top) and cathode void top view (bottom) (Xie et al., 2014).

After addition of Co and Ni, the migration of Cu atoms from the cathode side to the anode side has been significantly suppressed. Due to a reduction in migration of Cu atoms, the overall electromigration effect was suppressed. In the case of Sb alloyed solder joint, Sb made Sb-Sn IMC at interfaces and inside the solder joint. Sb-Sn IMC found to be brittle and produced cracks in the solder joint (Zhao et al., 2013). Another study was carried out to investigate the Co addition as a minor alloying element into the SAC305 solder joint (Ma, Xu, Sun, et al., 2011). They also detected that Co improved the resistance of EM in the SAC305 solder joint. Hsu et al. investigated the effect of Co in Sn–0.25 wt% Co alloy under EM (Hsu & Chen, 2013). They also detected that Co minimized the effect of EM on interfacial IMC at the anode side.

Overall, the alloying method was found to be useful to minimize the EM failures such as the formation of voids, cracks, reduction of interfacial IMC layer at the cathode side, the substantial growth of interfacial IMC at the anode side and rapid Cu migration. But researchers also found complicity in preparation of the sample. Because the alloying method needs very high-temperature to meltdown all the elements and to prepare the sample. For the simplicity of sample preparation, the researchers also introduced “microparticle addition” technique. The detail of this technique is given below in section 2.8.2.

2.8.2 Addition of microparticle in solder joint for retardation of EM failures

To minimize the EM failures, the researchers also introduced another technique of solder modification in which the microparticles are added to the lead-free solder joint during the reflow process. This technique does not require high-temperature, and the sample can be prepared by a standard reflow process (Kim et al., 2012). The researchers added a different type of microparticles such as Ni, Co, and Sb into the lead-free solder joint to minimize the effect of EM failures (Guo et al., 2009; Kim et al., 2012). The detail on microparticle addition in Sn-based solder is given below in section 2.8.2.1 and 2.8.2.2.

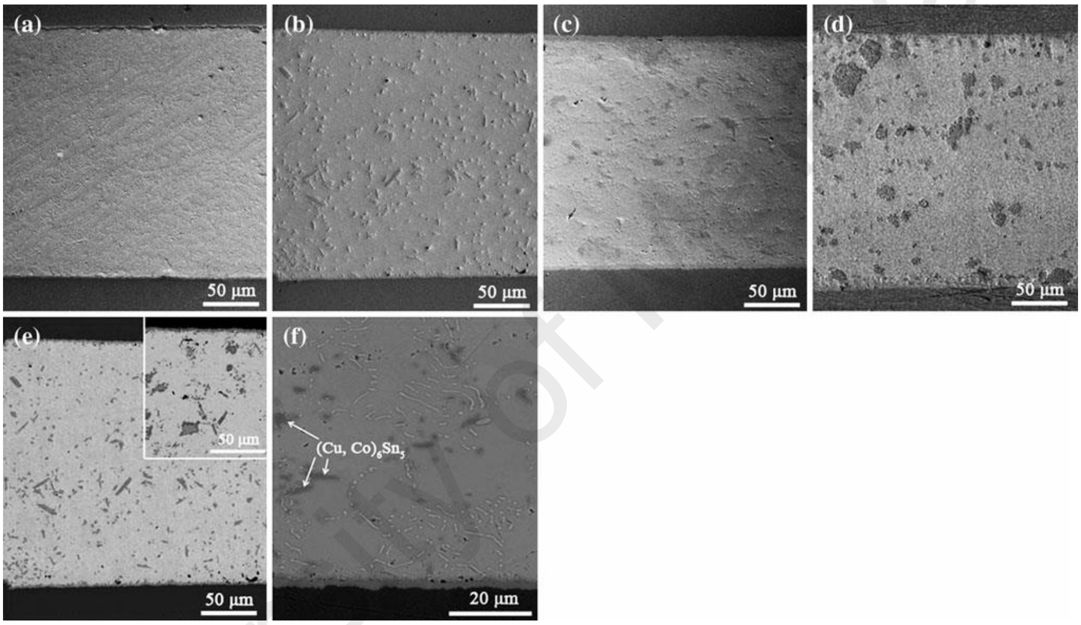

Figure 2.20: Microstructures of as-reflowed solder joints: (a) SAC (b) SAC-0.45Ni, (c) SAC-0.2Co (d) SAC387-1.0Sb, (e) backscattered electron image of SAC-0.45Ni (inset illustrates the backscattered electron image of SAC-2.0Ni) (f) backscattered electron image of SAC-0.2Co. (Zhao et al., 2013).

2.8.2.1 Ni and Co microparticle

The addition of Ni and Co microparticle through past mixing techniques were investigated in the past (Kim et al., 2012). Significant improvement was found in the microstructure and electromigration behavior of the solder joint after addition of Ni and Co microparticles. Four types of the solder joints were prepared, SABi, SABi + Ni, SABi

+ Co and SABi + NiCo (Figure 2.21). After the electromigration test, it was found that Ni and Co-containing solder joints failed after a longer period of electromigration compared with SABi solder joint (Figure 2.22). It was found that microstructures changed after addition of Ni and Co microparticles. The micrographs of as reflowed samples are given in Figure 2.21.

2.8.2.2 Sb microparticles

Guo et al., (2009) added Sb microparticle into the SAC solder using a paste mixing technique. The size of Sb microparticle was 6µm. They investigated the effect of Sb particles on electromigration failures in the SAC solder joints. After reflow, the Sn-Sb particles were formed in the solder bulk. After electromigration, the cracks were produced by the brittle properties of Sn-Sb particles. A similar result was found at the cathode interfaces after electromigration (Figure 2.23 and Figure 2.24) (Guo et al., 2009).

Microparticle addition was a useful method to minimize the electromigration damage in the lead-free solder joint. The researchers found that during the reflow process, the microparticle did not completely dissolve at the interface and solder matrix due to their bigger size. Recently, another method has been developed in which the nanoparticle are added into solder joint (Sujan, Haseeb, & Afifi, 2014). It was found that nanoparticle underwent reactive dissolution and completely dissolved into solder joint (Arafat et al., 2011; Chan, Arafat, & Haseeb, 2013; Sujan, Haseeb, & Afifi, 2014). This technique was found to be more effective than the addition of microparticle. The detail on nanoparticle addition into lead-free solder joint and their effects on EM failures are discussed below.

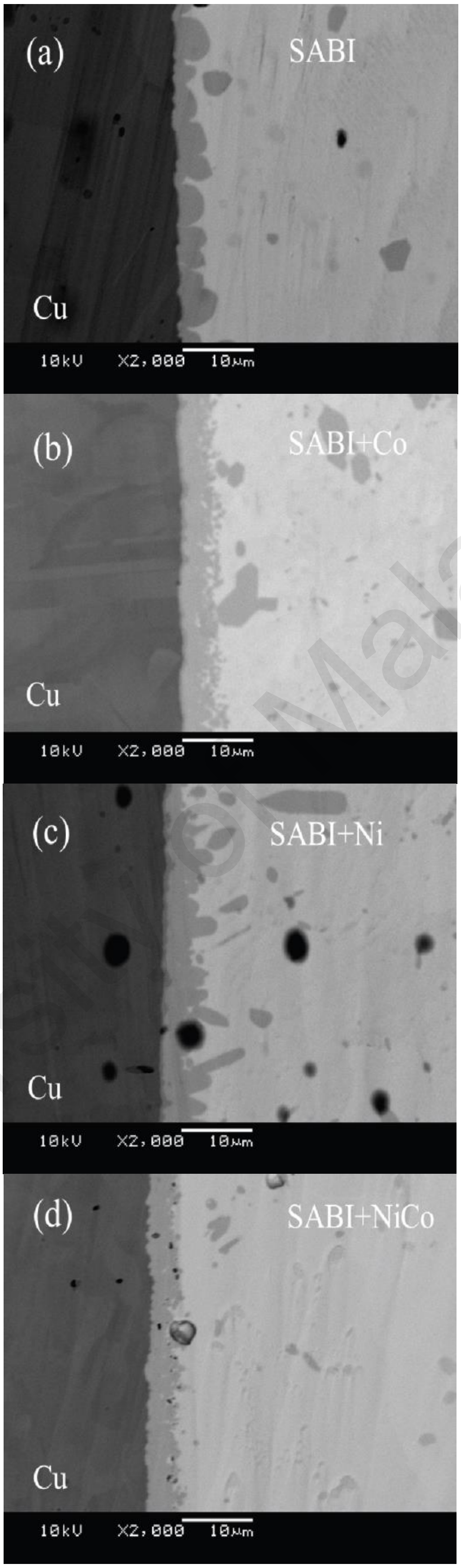

Figure 2.21: Cross-sectional BS-SEM images, (a) SABI solder joint, (b) SABI+Co solder joint, (C) SABI+Ni solder joint and (d) SABI+NiCo solder joint (Kim et al., 2012).

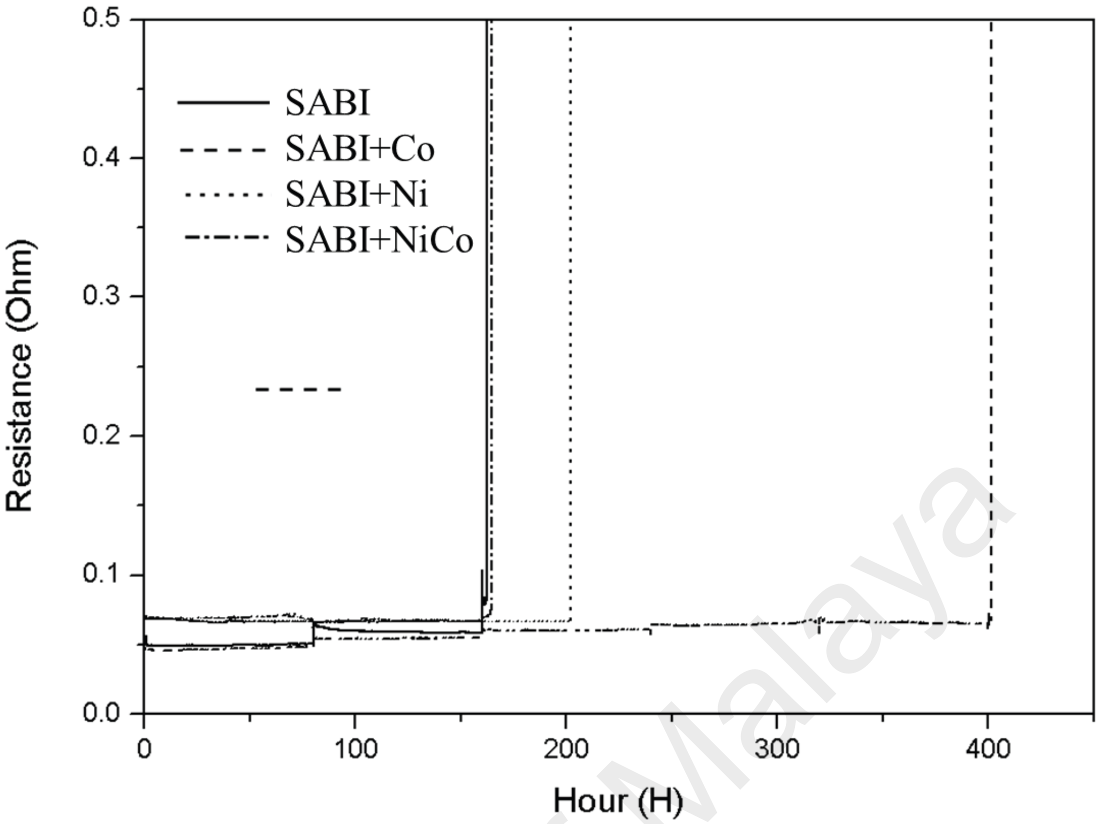

Figure 2.22: The EM average failure time for SABI, SABI+Co, SABI+Ni and SABI+NiCO solder joints tested at a homologous temperature (Kim et al., 2012).

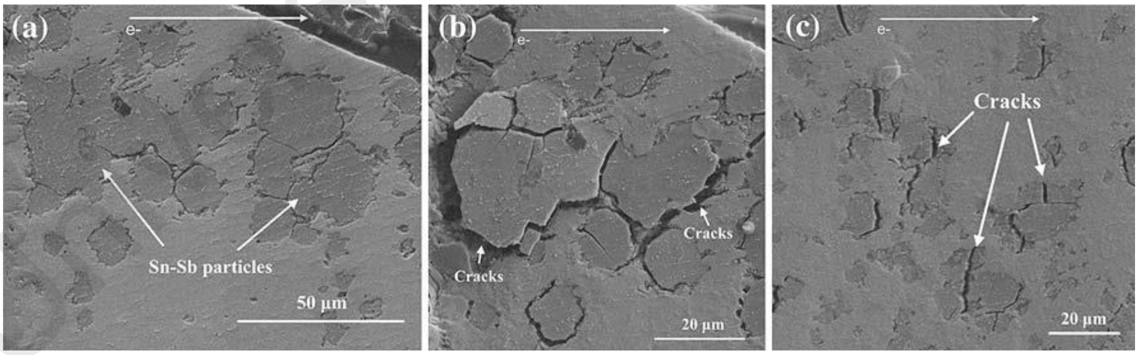

Figure 2.23: (a) The microstructure of Sn–Sb particles in the solder matrix without the current stressing; (b) the microstructure of Sn–Sb particles in the solder matrix after 200 h of the current stressing; (c) the cracks went through the Sn–Sb particles in the solder mat (Guo et al., 2009).

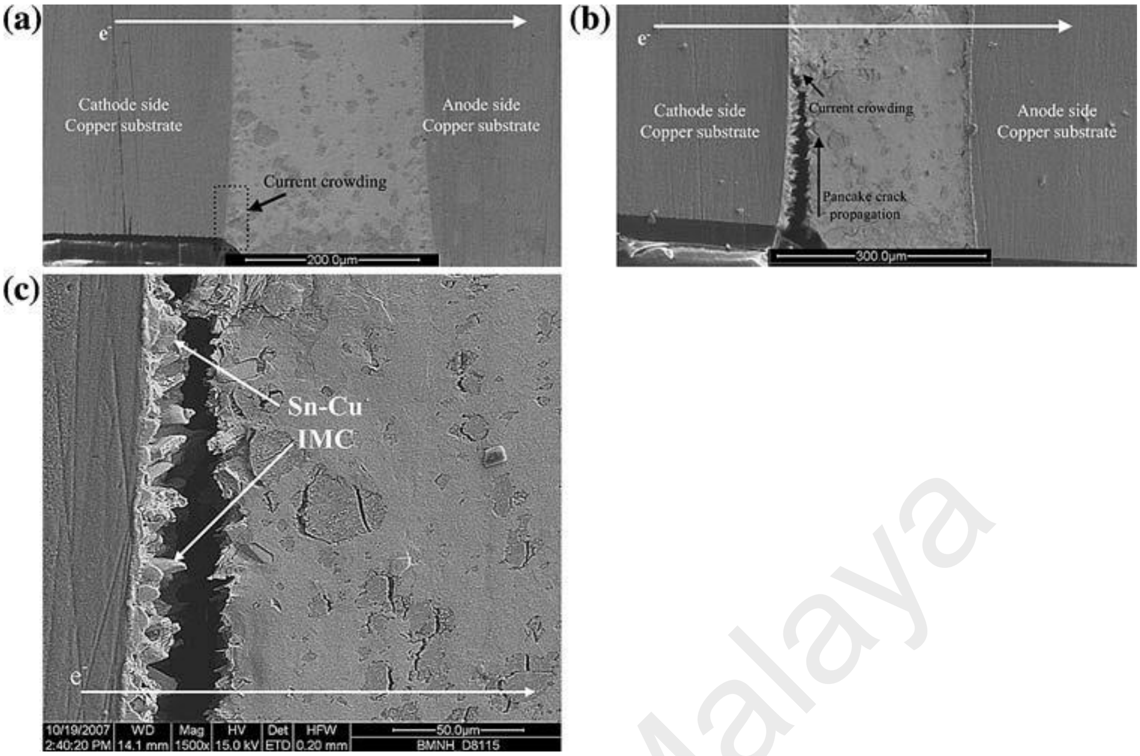

Figure 2.24: Formation and propagation of the pancake void at the cathode side a without current stressing; (b) current stressing after 240 h; (c) void formed between the solder matrix and the Sn–Cu IMCs (Guo et al., 2009).

2.8.3 Addition of nanoparticle in solder joint for retardation of EM failures

In the past, the researchers added nanoparticle into solder to investigate their effects on as reflowed solder (Haseeb & Leng, 2011; Haseeb, Leong, & Arafat, 2014; Nadia & Haseeb, 2012a; Tay et al., 2013). Most of the techniques were performed by used paste mixing technique (Arafat et al., 2011; Chan, Arafat, & Haseeb, 2013; Haseeb & Leng, 2011). These studies mainly focus on the effect of nanoparticle on Sn-solder during reflow and the heat treatment process. Very fewer studies were performed on the effect of nanoparticle on electromigration failures in the Sn-based solder joint. Khan et al. investigated the effect of Ag nanoparticle on electromigration failures of the SnBi solder joint (Khan, Lau, & Chan, 2013). During the investigation, they observed that Ag nanoparticle formed Ag containing IMC in the solder matrix which behaved as a migration barrier. By reducing in atomic migration, the Ag nanoparticle improved the microstructure and mechanical strength of the solder joint.

2.8.4 Addition of carbon nanotubes in solder for retardation of EM failures

2.8.4.1 Effect on structural properties of solder joint

In the past, Yang et al. investigated the effect of Ni-coated carbon nanotubes on Cu/SAC/Cu solder joint (Yang et al., 2013). It was found that the Ni-coated carbon nanotubes incorporated in the solder joint as a reinforcement material. It changed the morphology of interfacial IMC of the solder joint. After electromigration testing, it controlled the thickness of anodic interfacial IMC significantly (Yang et al., 2013). Nanotubes built a network inside the solder joint (Figure 2.25). Which produced electric conduction path inside the solder joint.

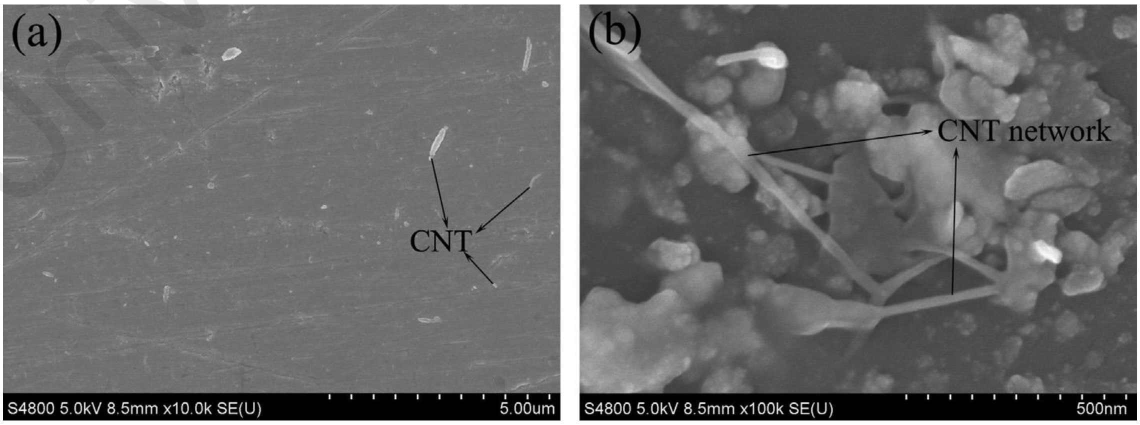

Figure 2.25: SEM images showing the presence of Ni–MWCNTs in solder matrix after (a) Fine polishing and (b) etched (Yang et al., 2013).

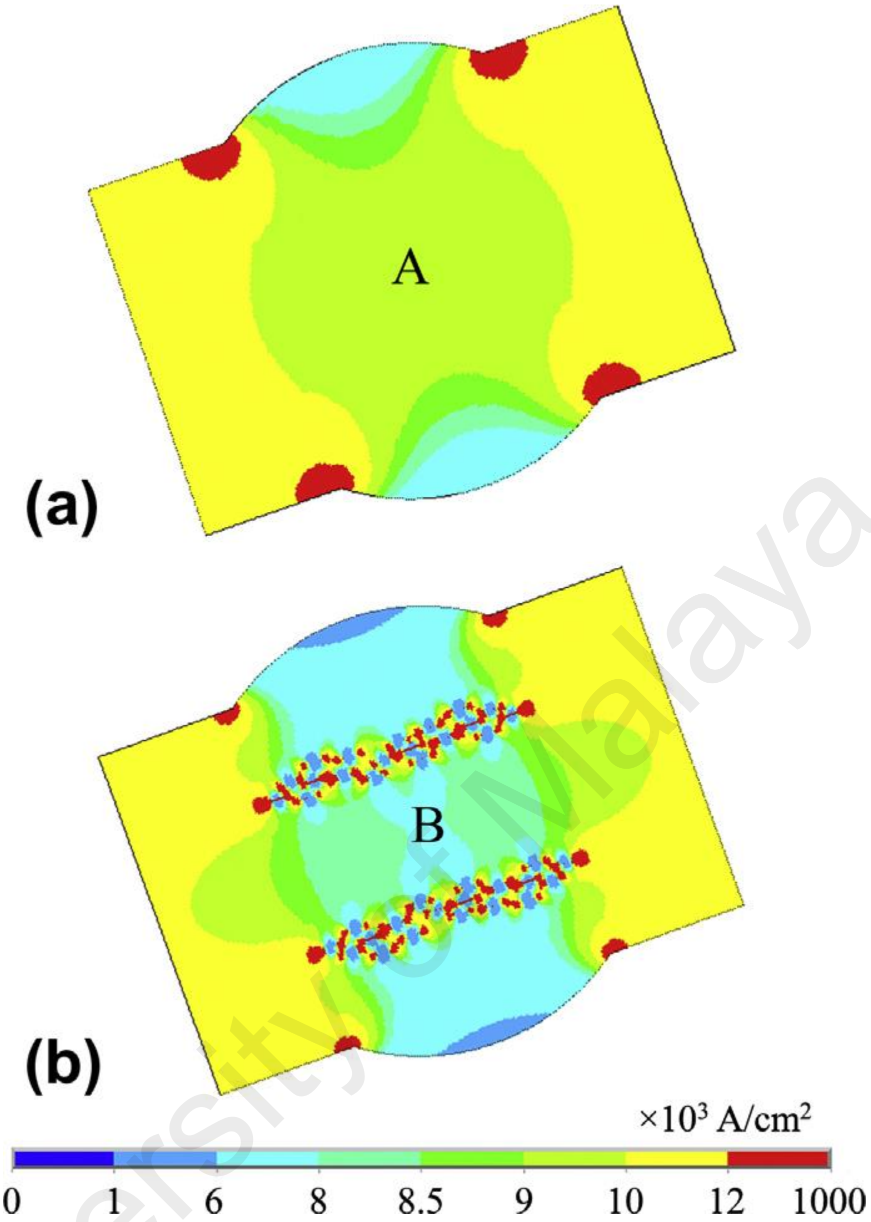

Figure 2.26: Current density distribution in the: (a) SAC solder joint and (b) SAC/1Ni–CNT solder joint (the resistivity of Cu, Sn, Cu_6Sn_5, and CNT is 1.7 Ωcm, 11 Ωcm, 18 Ωcm and 0.01 Ωcm, respectively) (Yang et al., 2013).

It was found that during electromigration, current mostly conducted through the carbon nanotube's network which reduced the current density inside the solder joint (Figure 2.26). By producing electric conduction path inside the solder and by reducing the current density inside the solder joint, the carbon nanotubes suppressed the effect of electromigration failures significantly (Yang et al., 2013).

2.8.4.2 Effect on mechanical properties of solder joint

Xu et al. investigated the effect of carbon nanotubes on microhardness and shear strength of the solder joints after the electromigration test (Xu et al., 2014). The carbon nanotubes controlled the IMC thickness at the anode side of the solder joint during the electromigration. It stabilized the IMC by affecting the reaction mechanism of Cu_5Sn_6 and Cu_3Sn IMC at the anode side during the electromigration. The stability of IMC at the interfaces and controlled thickness of the anodic IMC during the electromigration can enhance the mechanical properties of the solder joints positively. Xu et al. found that after addition of carbon nanotubes the microhardness and shear strength has improved in the solder joint (Xu et al., 2014).

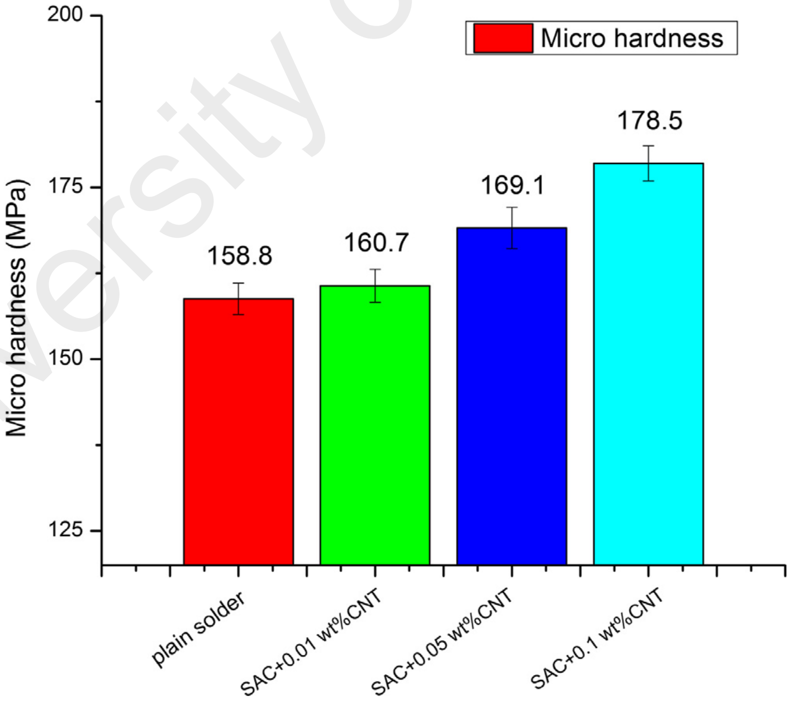

Figure 2.27: Measured microhardness for plain solder and composite solder (Xu et al., 2014).

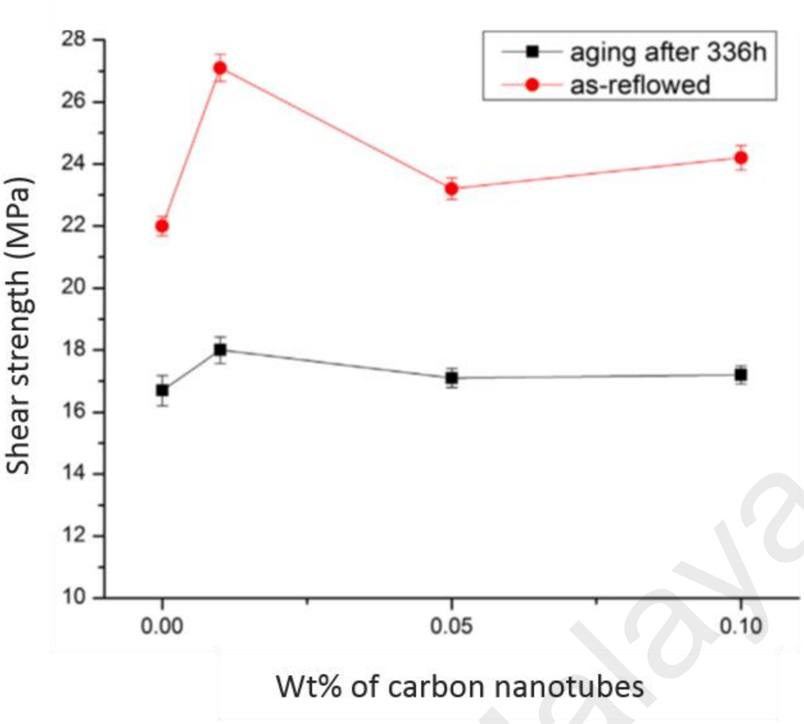

Figure 2.28: Measured shear strength for plain solder and composite solder (Xu et al., 2014).

Figure 2.27 describes the microhardness of the SAC solder and carbon nanotube containing solder. It was observed in the figure that the microhardness increased by increasing the wt% of carbon nanotubes in the solder joint (Xu et al., 2014) (Figure 2.27). The addition of Ni-coated carbon nanotube is found to be an efficient and very useful technique to minimize EM failures in the lead-free solder joint. But this technique was also found to be complicated to use in the industries compared to nanoparticle addition (Sujan, Haseeb, & Afifi, 2014).

2.9 Overall summary

Miniaturization of electronic device and increase in input current has increased the current density in the solder joints. High current density increases the occurrence of electromigration failures the solder joints. The electromigration failures include the formation of voids, cracks, and damage at the cathode side, reduction in thickness of cathodic interfacial IMC layer and rapid growth of anodic IMC layer. A number of efforts have been made in the past to minimize the electromigration failures and to improve the reliability of lead-free solder. Different types of methods were developed such as alloying method, the addition of microparticle, addition nanoparticle and the addition of carbon nanotubes in the solder joint. These methods were useful but less efficient and sample preparation was complicated. Recently, a flux mixing technique has been developed which allows the addition of nanoparticle at the solder/substrate interface and in the matrix. This technique is much easier to use for sample preparation and past studies found that this technique is more efficient than other technique. Reported studies on the particle addition mainly use paste mixing and ball milling methods. In both cases, the particles are mixed throughout the solder matrix. Alloying additions through metallurgical routes also mix the element throughout the bulk solder. Recently, a flux mixing technique has been developed which allows the addition of nanoparticle at the solder/substrate interface and in the matrix. In this technique, the nanoparticle undergo reactive dissolution and incorporate at interfaces and in the solder matrix during the reflow process. The characteristics of the intermetallic layers at the interface and the characteristics of β-Sn grain in the matrix play an important role in determining the reliability of the solder joints. The flux mixing technique of NP addition enables to study the effects of the modification of the interface and matrix caused by NP on the EM behavior of the solder joints. In this work, the effects of Ni and Co-NP addition in the Sn-3%Ag-0.5%Cu (SAC305) were investigated. The solder joints were prepared by the flux doping method. The process essentially involves the use of Ni and Co-NP doped commercial flux at the solder substrate interface prior to the reflow (Figure 3.2). To the best of our knowledge, this is the first time that the effects of the application of NP at the solder/substrate interface on the EM behavior have been reported. The key features of this study have been explained in chapter 1.

CHAPTER 3: METHODOLOGY

In this chapter, the experimental method of the study is explained in detail. This chapter contains five sections (1) Solder joint preparation (2) Electromigration test (3) Structural and chemical characterization (4) Mechanical properties and (5) Electrical resistance test. The research methodology used in this study is schematically shown in Fig 3.1. Four different sets of samples were prepared for electromigration tests. One set of samples was used to investigate the effect of NP on the microstructure of the SAC305 solder joint before EM. Before EM testing, the morphology of interfacial IMC, the grain sizes of interfacial IMC, structure, and size of the β-Sn grain in the matrix, structure, and thickness of IMC particles present in the eutectic region were investigated for as reflowed solder.

The second set of the samples was used to investigate the effect of NP on the microstructure of the SAC305 solder joint after EM test, EM damage at the cathode side, the anodic growth of interfacial IMC, rapid Cu diffusion from the cathode to anode side and reduction in cathodic IMC layer.

Microstructural properties before and after EM were characterized by using several analytical techniques, including field emission scanning electron microscopy (FESEM) energy dispersive X-ray (EDX) scanning electron microscopy (SEM) electron backscattered diffraction (EBSD) and optical microscopy (OM). For the characterization of as reflowed solder joint, the samples were etched. The etching was done in a solution of 2 %HCl, 3 %HNO_3 and 95 % (vol. %) ethyl alcohol for 5 seconds.

The third set was used for the mechanical test. To investigate the mechanical properties before and after electromigration, the micro tensile tests were conducted in a Shimadzu AGS-X Universal tensile testing machine before and after EM. The fourth set of samples was used for an electrical resistance test. To investigate the electrical properties of the doped and undoped solder joint, the electrical resistance and failure time of the solder joints were investigated (Figure 3.1).

During preparation of doped flux and preparation of solder joint, gloves and mask were used for the safety. During the electromigration test, a high-current density was applied. So for the safety, a thick insulation sheet was placed under the electromigration setup. The test was run on a wooden table.

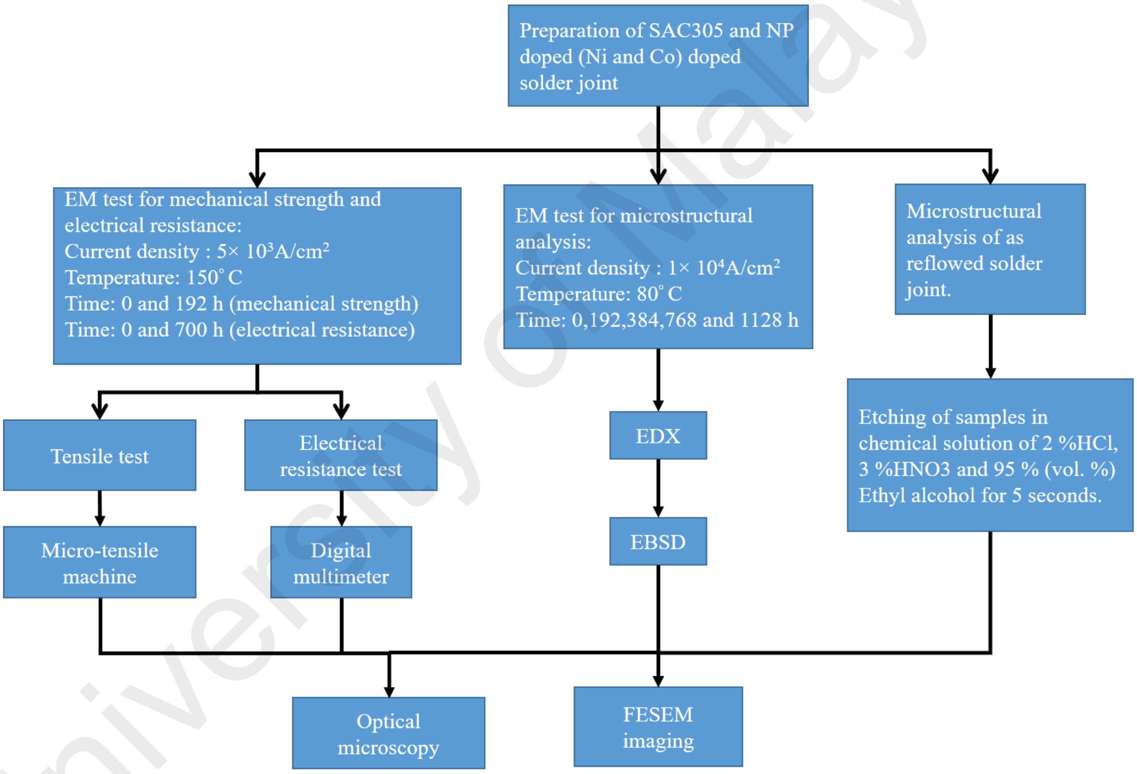

Figure 3.1: Flowchart of research methodology used.

3.1 Solder joint preparation

In this study, a commercially available water-soluble flux (Sparkle Flux WF-6317, Japan), lead-free Sn-3Ag-0.5Cu solder balls (Duk San Hi-metal, Ltd Korea) with a diameter of 0.45 mm, Ni and Co nanoparticle (Accumet materials, Co., USA) were used.

The size of Ni nanoparticle used in the present study was in the range of 24-93 nm (Sujan, Haseeb, & Afifi, 2014) and the average size of Co nanoparticle was in the range of 23-119 nm (Sujan et al., 2014).

In this study, three types of samples were prepared. The first type of samples was prepared by using lead-free Sn-3Ag-0.5Cu solder without the addition of nanoparticle and the samples were designated as a SAC305 solder joint. In the second type of samples, 2 wt% Ni nanoparticle were added into the lead-free Sn-3Ag-0.5Cu solder by using doped flux technique. This type of samples was designated as SAC305 + 2 wt% Ni NP-doped flux. The third type of samples was prepared by using Co nanoparticle. 2 wt% Co nanoparticle were added in lead-free Sn-3Ag-0.5Cu solder by using doped flux technique. The samples were then named as SAC305 + 2wt% Co NP-doped flux.

Water-soluble flux was used to remove the oxidation from the substrate and to protect the sample from further oxidation during the reflow process.

For the preparation of Ni and Co nanoparticle containing samples; first of all, two kinds of doped flux material were prepared.

1. Ni NP-doped flux
2. Co NP-doped flux

For the preparation of Ni NP-doped flux material, 2 wt% Ni NP was added to 98 wt% of water-soluble flux. After addition of 2 wt% Ni NP into water-soluble flux, the mixture was mixed mechanically for 30 minutes to make a good mixture. A similar technique was used to prepare Co NP-doped flux material. The reasons for using 2 wt% Ni and Co are because of their remarkable influence on improvement of the microstructure. In the past (Sujan et al., 2014), an effort was made to investigate the effects of Ni and Co on the SAC305 solder joint. The wt% of Ni and Co nanoparticle used in the experiment was 0-

2 wt%. It was found that 2wt% Co and Ni nanoparticle refined the morphology and improve the microstructure of the solder joint. In the present study, preliminary tests were conducted with different wt% of Ni and Co nanoparticle. It was found that 2 wt% Ni and Co converted the morphology of interfacial IMC from scallop type to planar type (Sujan et al., 2014). In the past studies, researchers found that the Cu migration is very fast in scallop type morphology due to valley areas (Chen et al., 2010; Lingyun Zhang et al., 2006). It was assumed that the planar type morphology of interfacial IMC would reduce the migration of Cu atoms during EM process. After preparation of NP-doped flux material, line type solder joints were prepared. The preparation of samples can be seen in Figure 3.2. Two copper wires with the length of 25 mm and diameter of 0.5 mm were used. One end of each copper wire was polished for about 10 minutes to achieve flat and smooth ends. After polishing, the polished ends of the Cu wires were cleaned with 10% H_2SO_4 and distilled water to remove any oxide and contamination.

For the preparation of Cu/SAC305/Cu solder joint, the polished ends of both wires were then dipped into the water-soluble flux. The copper wires were then placed in an aluminum die. A SAC305 solder ball with the diameter of 0.5 mm was mechanically pressed into a disk-shaped piece (as shown in Figure 3.2a). The thickness of solder disk was about 200 μm. The disk-shaped solder alloy was placed between dipped ends of copper wires. An optical microscope was used for the placement of copper wires, and a solder disk in the aluminum die to get a line type Cu/solder/Cu solder joint. For the preparation of Cu/SAC305 + 2wt%, Ni NP-doped/Cu solder joint, the polished ends of both wires were then dipped into the Ni NP-doped flux. After dipping, the copper wires were then placed in an aluminum die. A solder disk with similar shape and size as described earlier was placed between dipped ends of Cu wires, which were covered with Ni NP-doped flux. For the preparation of Cu/SAC305 + 2wt% Co NP-doped/Cu solder joint, the polished ends of Cu wires were dipped into Co NP-doped flux.

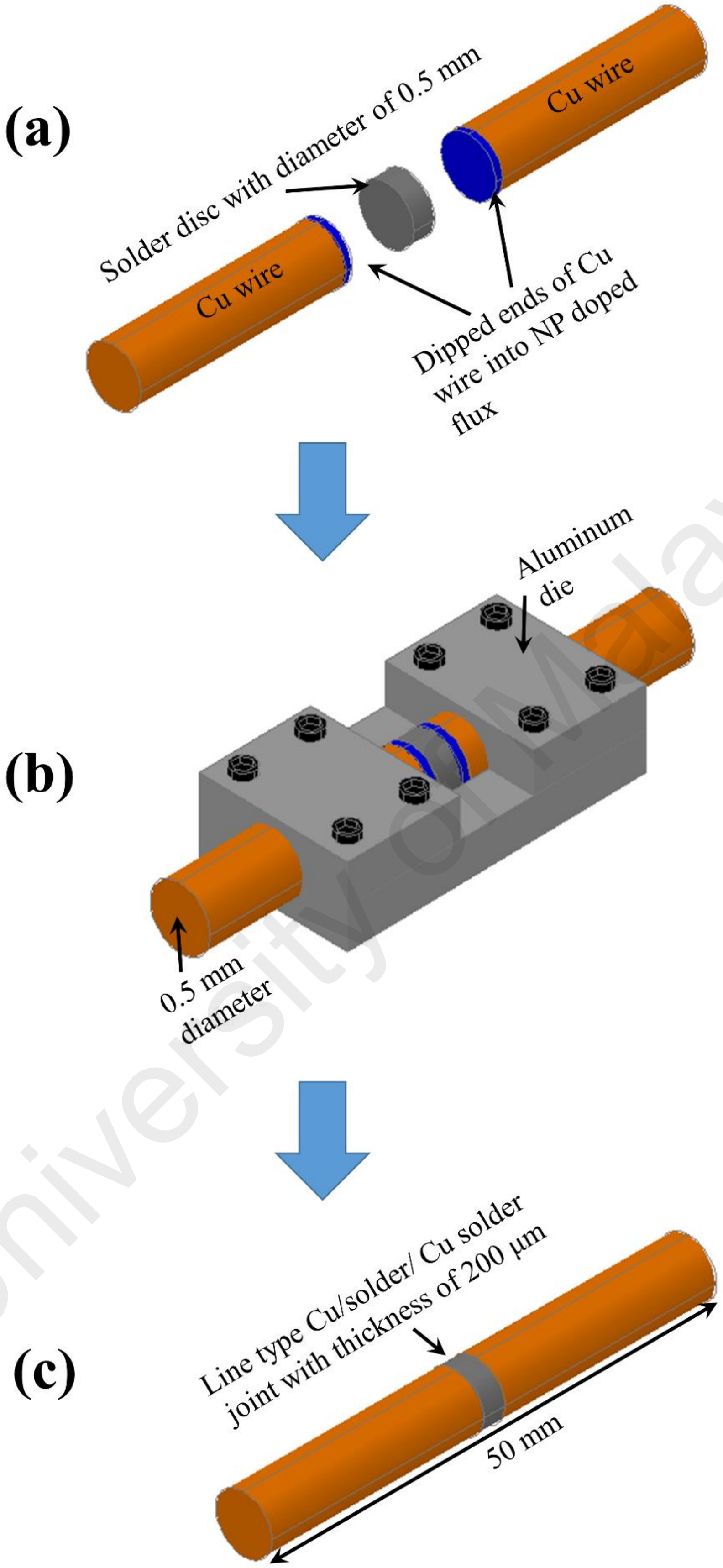

Figure 3.2: Schematic diagram for the preparation of line type Cu/solder/Cu sample: (a) Cu ends dipped into NP and solder disc, (b) Assembly of Cu wires and disc in an aluminum die, and (c) prepared line type Cu/solder/Cu solder joint.

The rest of the procedure was the same as that used for the preparation of Cu/SAC305/Cu solder joint and Cu/SAC305 + 2wt% Ni NP-doped/Cu solder joint. The assembled sample was then reflowed at 245° C for 45 seconds in a reflow oven (Forced Convection, FT02) to prepare the solder joint. The same reflow parameters were applied to all kinds of samples. After reflow, the samples were cleaned to remove the extra flux. For cleaning purposes, a solution of 10% H_2SO_4 and distilled water was prepared. All the samples were dipped into 10% H_2SO_4 and distilled water solution for one minute. After that, the samples were taken out and washed with pure distilled water and then were dried up by using an air blower.

3.2 Electromigration test

After preparation of line type Cu/solder/Cu samples, the electromigration tests were conducted on each type of sample. In this study, three kinds of investigations were performed under electromigration. (1) Structural and chemical characterization, (2) Mechanical properties and (3) Electrical test. During these investigations, different EM parameters were used. The detail of these parameters is also given in Table 3.1.

Table 3.1: Electromigration parameters used during different type of EM test.

Type of EM Test	Area of solder joint	Applied DC current	Current density	Temperature	EM time
EM test for microstructural analysis	0.05 mm^2	5 A	1×10^4 A/cm^2	80 °C	0 h, 192 h, 384 h, 768 h, 1128 h
EM test for Mechanical strength	0.19 mm^2	9.5 A	5×10^3 A/cm^2	150 °C	0 h, 192 h
Electrical test	0.19 mm^2	9.5 A	5×10^3 A/cm^2	150 °C	0 h, 700 h

In the flip chip package, the flip chip solder joint carries 0.2 A current (Tu, 2007). If the size of the solder joint is 50 μm, the 0.2 A current will generate a current density of 10^4 A/ cm^2 in the solder (Tu, 2007). Due to downscaling of flip chip devices, the size of the solder joint is expected to be reduced in the future, and the current density will also be increased.

In the present study, for structural and chemical characterization, 1×10^4 A/ cm^2 current density was used, which can be typically encountered in a flip chip solder joint (Tu, 2007). It is also known that high-current density generates joule heating effects inside the solder joint. The temperature produced by Joule heating could be distinctive in the different device due to their geometry and heat dissipation system. The cooling system in the flip chip devices maintains the temperature around 100°C during EM process (Tu, 2007). In the present study, the temperature was maintained at 80 ± 5°C during the EM tests by using pure silicon oil bath. As the sample was mounted in the epoxy resin and the melting temperature of the epoxy resin is around 130°C, so it was not possible to run the test close to 100°C. Preliminary tests were conducted to find the suitable temperature for the mounted sample. Formation of crakes was observed at 100°C temperature. But 80°C temperature was found to be suitable for the test. The tests were run in a silicon oil bath to maintain the temperature for a maximum duration of 1128 h. The purpose of the long-term test was to investigate the maximum effect of EM on the structure of the solder joints.

For investigation of mechanical properties, the EM test was run under a current density of 5×10^3 A/ cm^2. For the measurement of mechanical properties, the micro-tensile testing was done. A DC current 19A was required to generate the 1×10^4 A/ cm^2 current density. It was difficult to maintain the joule heating effect and constant temperature under high-current. Therefore, in the present study, a DC current 9.5 A was applied, which generated

5×10^3 A/ cm^2 current density in the solder joint. A constant temperature of 150 °C was maintained by using a silicon oil bath. The EM tests were run for a maximum time period of 192 h. As the long-time EM tests generate a lot of damage inside solder joints so the EM tests for tensile property evaluation were run for a shorter time because it is difficult to adjust the sample in the micro-tensile testing machine if the sample has already been heavily damaged by EM. The EM tests were run for five sets of samples under same parameters for all the samples, and the data were compared. In the past (Kumar et al., 2009; Ren et al., 2006; Wang et al., 2010) also investigated the mechanical strength of the Sn-based solder joint. The range of the parameters in their studies was close to the parameter used in the present study.

The electrical resistance tests were run to investigate the resistance changes and failure time of the solder joints. Due to the limitation of time, it was required to select the parameters which can generate maximum EM effects and can cause failure of the samples in a short period of time. It was found in the literature (Guo, Xu, Sun, et al., 2009; Lee et al., 2011b; Shen, Cao, Zhai, Zhao, & He, 2014; Yiwei Wang et al., 2012) that high-current density and high-temperature increase the effect of EM significantly in the solder joint due to which the solder joint fails early. In the current study, preliminary tests were performed to find the suitable parameters for an electrical resistance test. In preliminary tests, it was observed that the average failure time of the SAC305 solder was below than 700 h when the current density of 5×10^3 A/ cm^2 was applied under 150 °C. In the present study, the electrical tests were conducted under a current density of 5×10^3 A/ cm^2 at 150 °C temperature for 700 h. This test was repeated 3 times for each sample.

3.3 Structural and chemical characterization

In this section of the study, two types of the investigation were performed, (1) microstructural analysis and (2) crystallographic properties of the doped and undoped solder joint. First of all, the cross-sections of the samples were reduced to achieve a high-current density by applying a small amount of current. For this purpose, all types of solder joints were mounted and ground (Figure 3.4a and b). The cross-section area was reduced down to 0.05 mm^2 to get the current density of 1×10^4 A/cm^2 by applying 5 A DC current (Figure 3.4c and d). The mounting process is shown in Figure 3.3 while the cross-sectional area of the sample with all dimensions is illustrated in Figure 3.4.

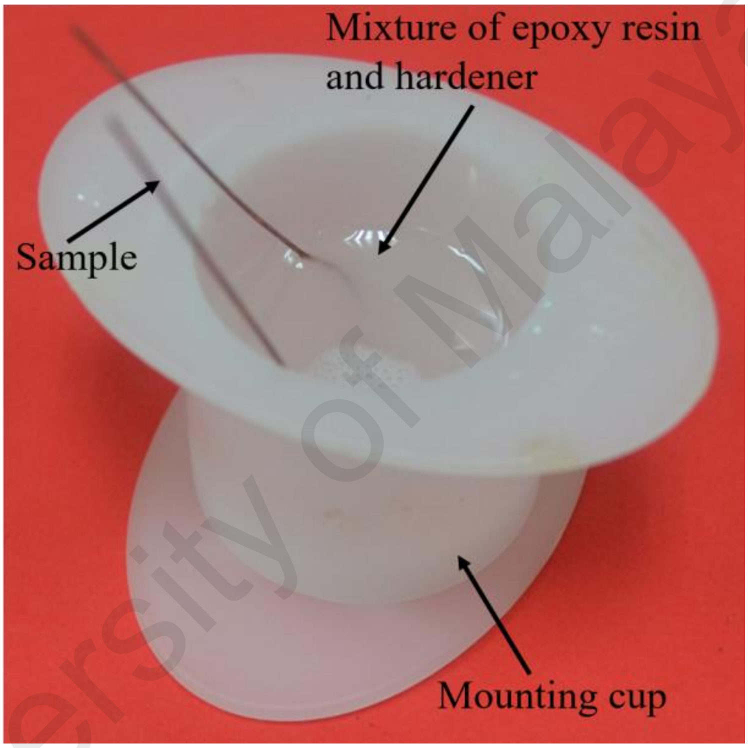

Figure 3.3: the Mounting process of samples by using epoxy resin and hardener.

The cross-sectional area of the solder joint was calculated by using following equation:

$$\text{Cross-sectional area} = \frac{R^2}{2} \quad \frac{\pi}{180} C \quad \sin C \qquad (3.1)$$

Where R is the radius of the whole sample, and C is the central angle as illustrated in Figure 3.4d. After preparation, the samples were placed into a silicon oil bath [Memmert

Kontakt] to maintain the required temperatures during EM test. A DC power supply [Leybold Didactic GMBH 521 55] were used to apply 5 A current for the periods of 0, 192, 384,768 and 1128 h at a constant temperature of 80° C.

3.3.1 Field emission scanning electron microscopy

After EM tests, the samples were polished for microstructural investigation under a field emission scanning electron microscopy (FESEM) and energy-dispersive x-ray spectroscopy (EDX) analysis. Field emission scanning electron microscopy (FESEM, FEI Quanta FEG450) was used for two main purposes. One is to take cross-sectional images of the samples, and the second is to do the elemental mapping. For the cross-sectional images, the samples were polished. After polishing the FESEM images were taken. The purpose of these images was to analyze the morphology of solder bulk and interfacial IMC layers before and after the electromigration and to monitor the thickness of IMC layers before and after the electromigration test. The elemental mapping was done for two purposes. One was to see the element distribution inside the solder bulk and at the interfacial IMC layer of as reflowed solder joints. The second was to analyze the movement of elements from the cathode to anode interface due to electromigration effects. For the analysis of elemental composition at interfacial IMC layers and in the solder bulk the energy dispersive x-ray spectroscopy (EDX, Horiba EMAX) analysis was performed. The scanning electron microscopy (SEM, Hitachi S3400N, Japan) images were taken to perform the EDX analysis.

3.3.2 Electron backscatter diffraction

The crystallographic properties of the samples were investigated by electron backscatter diffraction (EBSD). The analysis of the crystallographic structure of solder bulk and interfacial IMC layer were investigated at 0 h and 1128 h of EM.

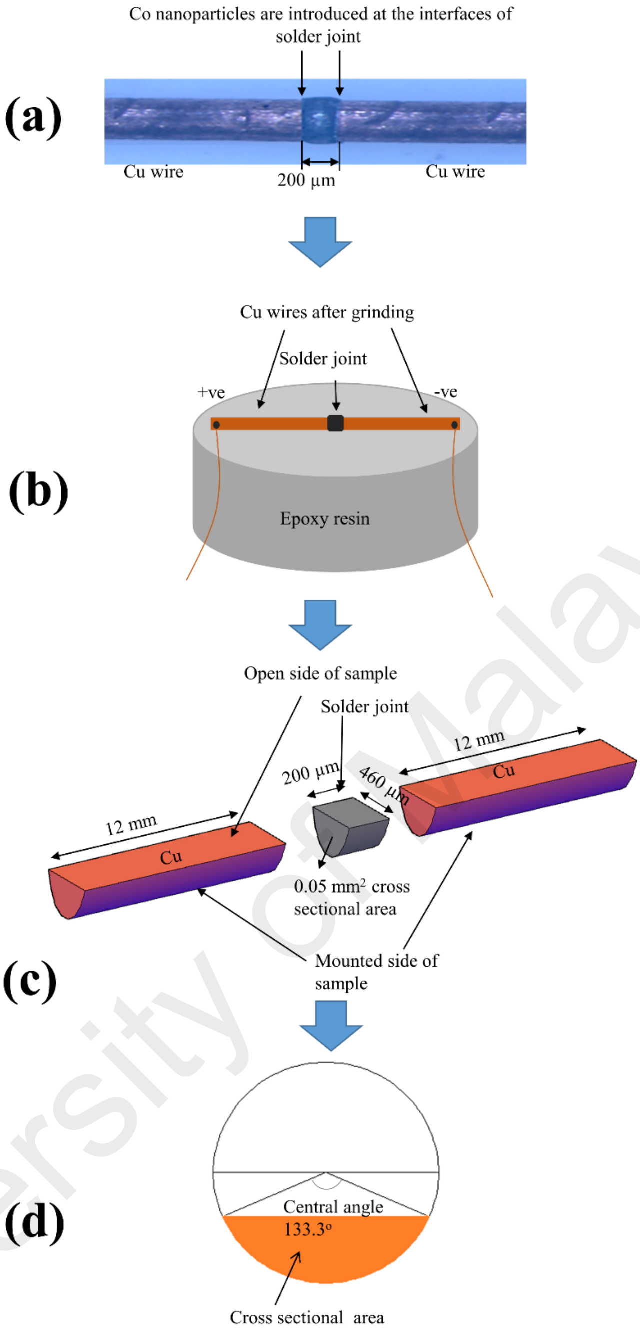

Figure 3.4: Illustration of sample preparation for electromigration test under high-current density (a) prepared line type Cu/solder/Cu solder joint, (b) mounted and ground sample in the epoxy resin, (c) dimensions of the ground sample and (d) cross-sectional area of the ground sample.

The purpose of EBSD (HIKARI XP2 9434.079.45400STBC) analysis was to investigate the grain size, grain structure, grain orientation and phase distribution in the solder bulk and at the interfacial IMC layers. The average thickness of IMC was measured by using following equation.

$$h = \frac{ar}{L} \tag{3.2}$$

Where the h is average thickness, ar is an area of interfacial IMC layers and L is a total length of the interfacial IMCs layer. A software (Olympus SZX10 image analyzer) was used to do the following measurements.

1. Total length of Interfacial IMC layer
2. The area of interfacial IMC layer
3. Grain size of interfacial IMC layer
4. size of β-Sn grain in solder matrix
5. Thickness of IMC particle in the eutectic region of the solder matrix.

3.4 Mechanical properties

To investigate the effect of electromigration on the mechanical strength in undoped and NP-doped solder joints, separate sets of samples with line type geometry were prepared. The total length of the samples was 50 mm. After reflow, the NP-doped and undoped samples were placed in a silicone oil bath to apply the maintained temperature of 150° C. After that, the EM tests were run by applying constant current density of 5×10^3 A/cm^2. The electromigration tests were conducted for the period of 0 and 192 h. After EM test, the tensile tests were conducted. As the size of the sample was very small and the sample was very sensitive, this is why a special micro-tensile testing machine (Shimadzu AGS-X Universal tensile testing machine with a load cell of 50 N) was used. This machine is only used for low load, and the maximum load of this machine is 50 N (Figure 3.5). The clamps of this machine are specially designed for micro size samples.

The clamps of the machine avoid the external forces during adjustment of the sample and during the tensile test. The tests were repeated five times for all kinds of solder joints with the strain rate of 6.59×10^{-5}/s. During the tensile tests, stress-strain curves and tensile strength were recorded. The tensile test process is illustrated in Figure 3.5.

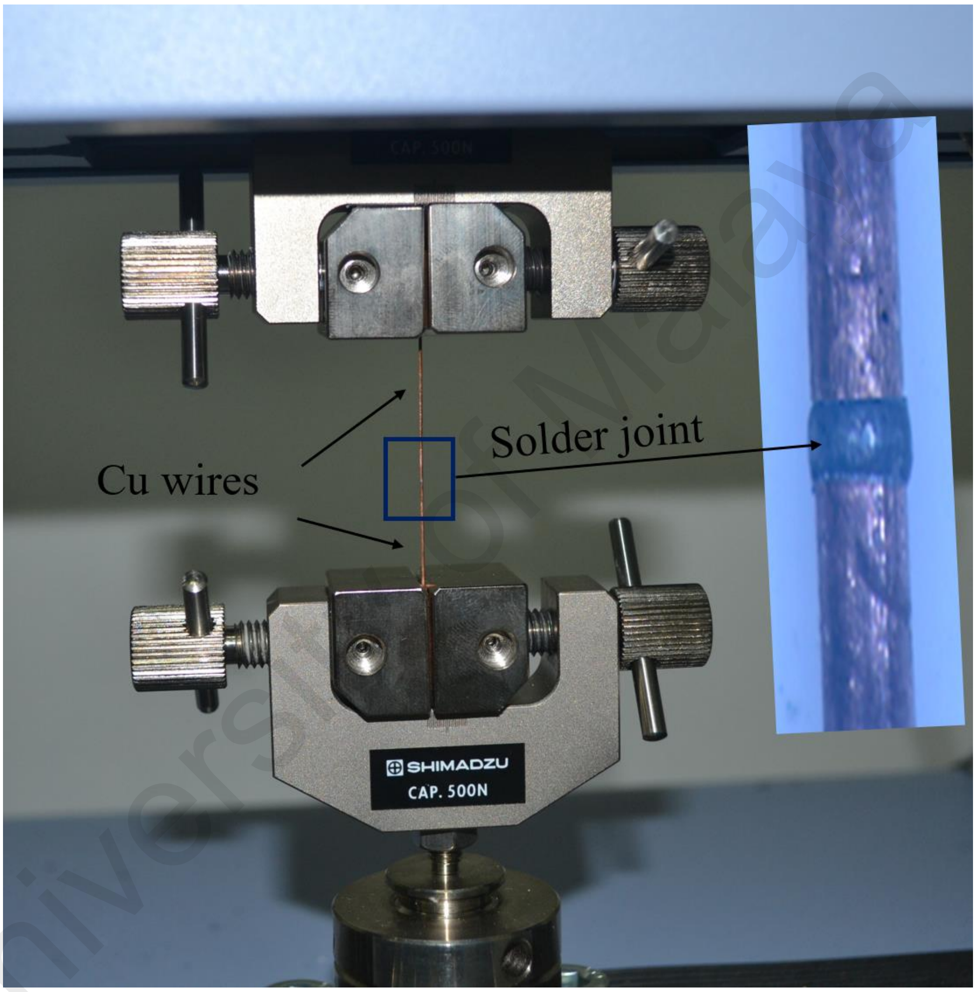

Figure 3.5: A Tensile test of line type solder in a tensile testing machine with 50 N load cell.

3.5 Electrical test

For the investigation of electrical resistance, the similar constant temperature of 150° C was applied in the silicon oil bath. The current density was also same as used for mechanical strength (5×10^3 A/cm^2). This test was done for 0 h and 700 h. The resistance was measured during the electromigration test. The tips of the probes were connected at the cathode and anode side of the samples (Figure 3.6). The resistance was measured for whole Cu/solder/Cu sample. The total length of the sample was 50 mm. To avoid the variation in the location of the samples, the tips were fixed at the cathode and anode side. The setup for the measurement of electrical resistance is given in Figure 3.6. A multimeter (FLUK 45 dual display multimeter) was connected with the samples to record the electrical resistance during the electromigration test. For the measurement of electrical resistance, the tips of multimeter were placed near the interfaces of solder joints. The values were recorded and plotted.

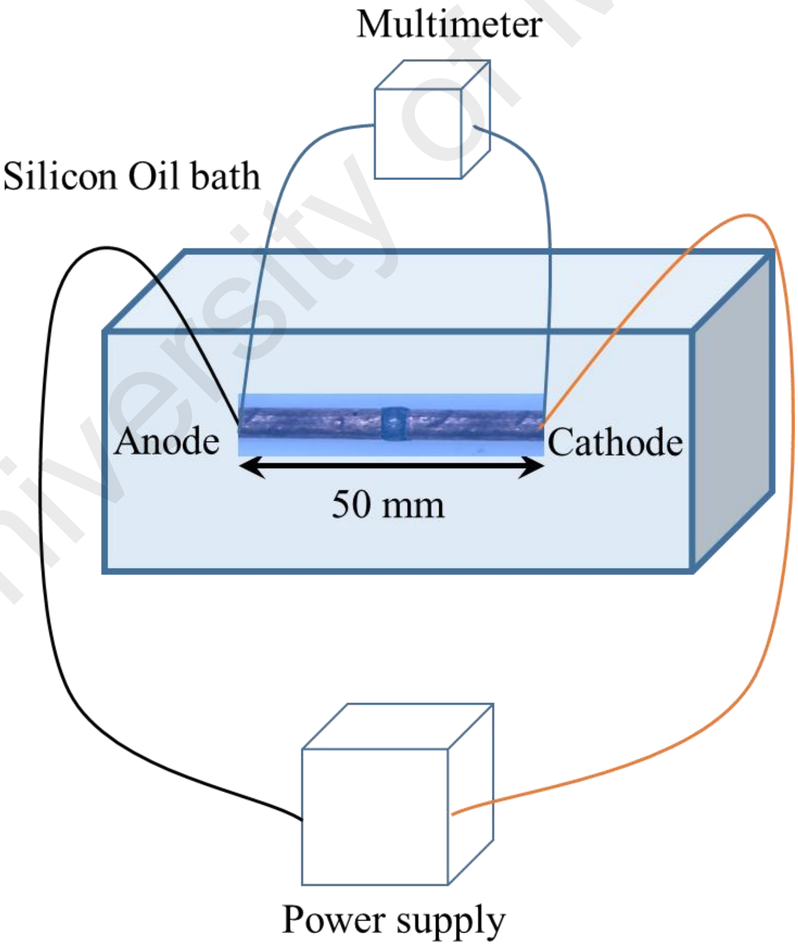

Figure 3.6 Schematic diagram for the measurement of electrical resistance during the electromigration test.

CHAPTER 4: RESULTS

4.1 Microstructure of doped and undoped solder after reflow

The effects of Ni and Co NP-doped flux addition were detected on the microstructure of the substrate/solder interface as well as in the microstructure of the matrix of the SAC305 solder joint. The detail of these effects is elaborated in the following two sections.

4.1.1 Interfacial microstructure

The microstructures of as reflowed SAC305 at interfaces are illustrated in Figure 4.1. After reflow, the microstructure of IMC was found to be scallop type. The average thickness of the IMC layer was 3.0 ± 0.3 µm. Cu_6Sn_5 and Cu_3Sn IMC were found by EDX analysis at interfaces at both ends. As the micrographs were taken at low magnification, the Cu_3Sn thin layer is not visible but it was observed at high magnification (Rao, Weng, Shen, Lee, & Zeng, 2010). Figure 4.1b shows the interfacial microstructure at one end of the SAC305+2 wt% Ni NPs solder joint. Upon adding Ni NPs to flux, a significant impact of Ni NPs on the interfacial microstructure of the solder joint was found. The morphology of the Cu_6Sn_5 IMC layer changed from scallop to planar type. A thin layer of Cu_3Sn IMC was also found between Cu substrate and the $(Cu, Ni)_6Sn_5$ IMC layer. The average thickness of the IMC layers becomes 3.9 ± 0.2 µm which is somewhat higher than that of the SAC305 sample.

Figure 4.1c represents microstructure of the SAC305 + 2 wt% Co-NP at the interface. The morphology of the interfacial IMC has also changed from scallop to planar type. The composition of IMC layer at interface changed from Cu_6Sn_5 to $(Cu, Co)_6Sn_5$ which was confirmed by EDX. The average thickness of IMC layer was 2.9 ± 0.1 µm. EDX spot analysis was performed to investigate the actual amount of Ni and Co-NP present in different positions. The spot analysis were made on three location of interfacial IMC

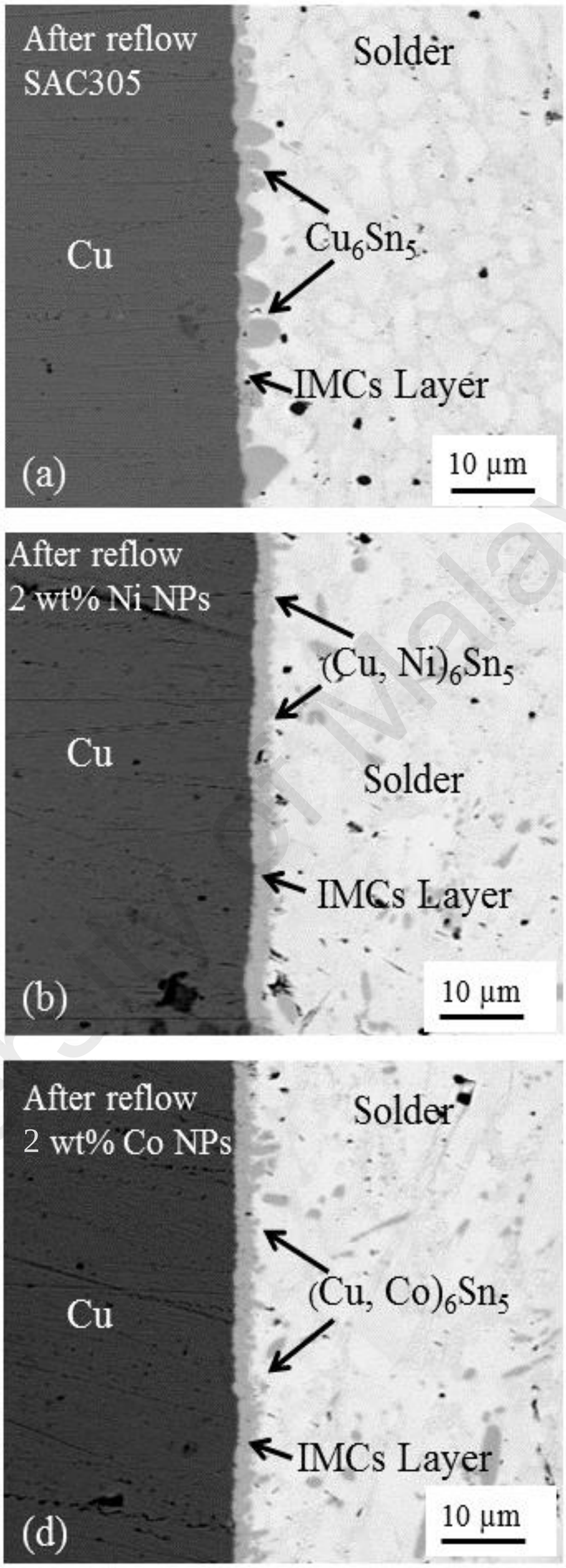

Figure 4.1: SEM back-scattered electron images of (a) SAC305, (b) SAC305+2 wt% Ni NP, and (c) SAC305+2 wt% Co-NP solder joints. Each micrograph corresponds to one end of the solder joint.

layer, (1) middle of the interfacial layer, (2) Interfacial IMC layer near to solder and (3) interfacial IMC layer near to Cu substrate. In each location, three spots were made. At each location, three different elemental compositions were detected. The average elemental composition of Ni and Co-NP was calculated and furnished in Table 4.1. It can be seen in the table that the interfacial IMC contains Ni and Co. The distribution of Ni in the interfacial IMC is not so uniform. At the solder side, the Ni content is 1.5 ± 0.1 wt% while it is lower at the substrate side (0.86 ± 0.51 wt%). A similar observation was made in an earlier work (Moon, Boettinger, Kattner, Biancaniello, & Handwerker, 2000; Tay et al., 2013). The average Co content of the interfacial IMC was 2.26 ± 0.23 wt% on the solder side, and 0.96 ± 0.6 wt% at the substrate side. The average Co content of the IMC particles situated in the solder matrix was 0.9 wt%. In the past, the calculation was made base on the amount of flux used in doped flux material, the amount of solder alloy and the rate of incorporation of NP with a solder joint. The amount of NP which can incorporate into solder joint was estimated to be 500 ppm (Sujan, Haseeb, Nishikawa, & Amalina, 2017).

4.1.2 Microstructure of solder matrix

To investigate the effect of Ni and Co-NP doped flux on the solder matrix, 3 sets of solder joints were prepared for each of type of samples, viz., SAC305, Ni-NP doped and Co-NP doped samples. The samples were polished and etched.)

Figure 4.2 describes the grain structure of β-Sn in the doped and undoped solder joint. Figure 4.2 a shows an overall microstructure of the SAC305 solder joint and Figure 4.2 b shows grain structure of β-Sn grain in the matrix of the SAC305 solder joint. It is found that in the SAC305 solder joint, β-Sn grains formed large size needle shape structure. In the case of Ni-NP doped solder joints, the structure of β-Sn grains was the globular shape and the area of β-Sn grain decreased significantly (Figure 4.2 c and d). Co-NP doped solder also showed the similar result as the Ni-NP doped solder joint. The morphology of β-Sn was found to be a globular shape in the Co-NP containing solder joint (Figure 4.2 e and f). Large size IMC particles were also detected in the solder matrix of Ni and Co containing solder joints. Detail on large size IMC particles in the solder matrix of Ni and Co contain solder joint is given in section 4.1.3.

Table 4.1: EDX elemental compositions of IMC phases in the SAC305 and NP-doped flux solder joints.

Solder joint	**Location**	**Element composition (wt%)**				
		Cu	**Ag**	**Sn**	**Ni**	**Co**
SAC305	Interfacial IMC layer	58.2 ± 1.0	0.9 ± 0.6	40.5 ± 0.1	---	---
Ni NP-doped	Interfacial IMC layer near to solder	54.24 ± 0.9	1.64 ± 0.7	42.62 ± 0.1	1.5 ± 0.1	---
	Interfacial IMC layer near to Cu substrate	55.01 ± 1.4	1.12 ± 0.3	43.01 ± 0.3	0.86 ± 0.5	---
Co NP-doped	Interfacial IMC layer near to solder	53.99 ± 1.1	0.39 ± 0.2	43.37 ± 0.9	---	2.26 ± 0.2
	Interfacial IMC layer near to Cu substrate	54.01 ± 2.1	0.23 ± 0.1	44.76 ± 0.8	---	0.96 ± 0.6

Figure 4.3 shows the average grain area of a β-Sn grain in the matrix of undoped and NP-doped solder joints. The area of β-Sn grains was measured by using (Olympus SZX10 image analyzer) software. Total 200 grains were found and the average area of a β-Sn grain in the matrix of the SAC305 solder joint was found to be 80.1 μm^2. In the case of the NP-doped solder, the average grain area significantly decreased. In Ni NP-doped solder joint the area of a β-Sn grain decreased from 80.1μm^2 to 35.2 μm^2 while in Co NP-doped solder joint decreased from 80.1 μm^2 to 29.2 μm^2.

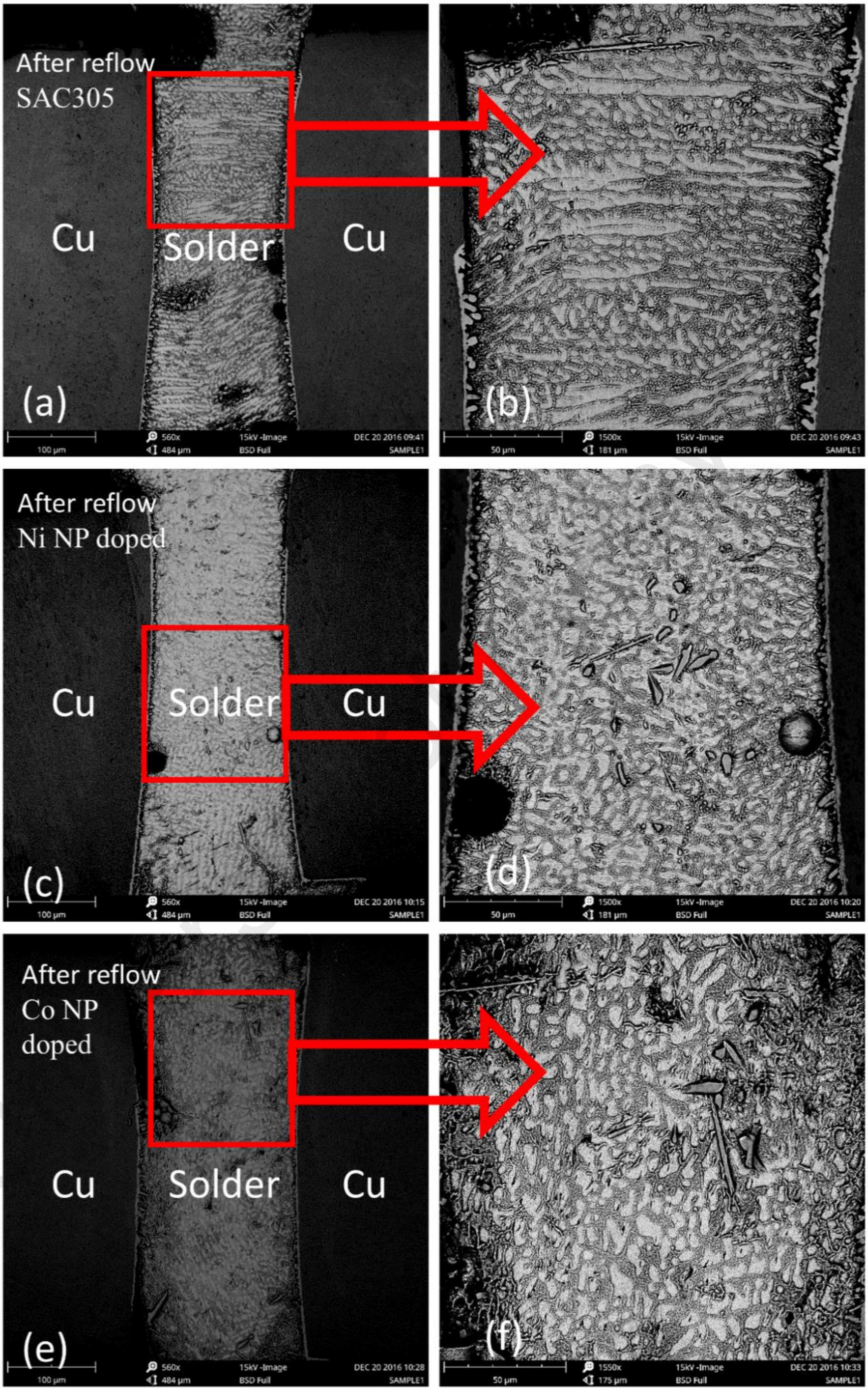

Figure 4.2: SEM images depicting grain structure in the matrix of (a and b) SAC305 (c and d) Ni-NP doped and (e and f) Co-NP doped solder joints.

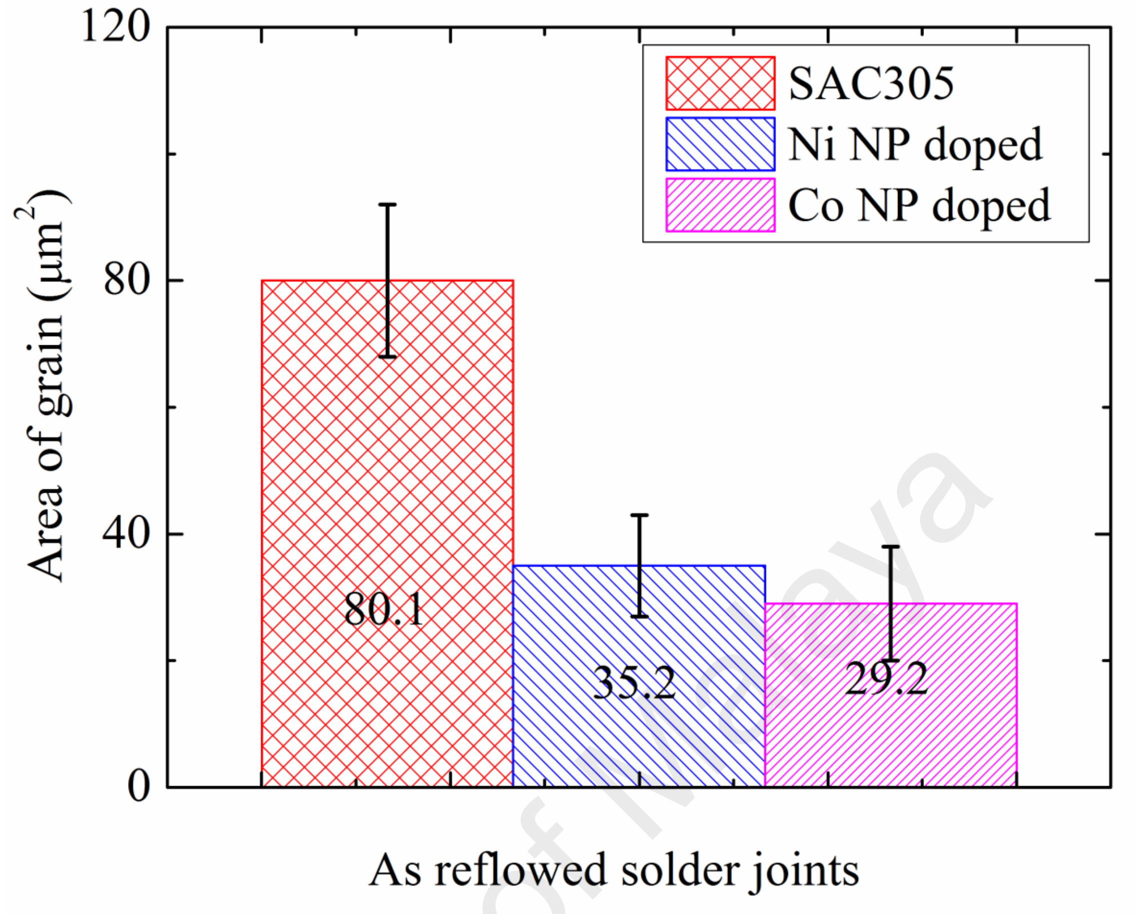

Figure 4.3: Averaged grain areas of β-Sn grain in as reflowed SAC305, Ni-NP doped and Co-NP doped solder joints.

Figure 4.4 describes the microstructure of IMC particles present in the eutectic region of solder matrix. It is seen that before addition of NP, the structure of IMC particles was found to be globular in the eutectic region (Figure 4.4 a). In the case of the NP-doped solder joint, the structure of IMC particles was found to be needle shape as shown in Figure 4.4 b and c.

The thickness of IMC particles present in the eutectic region of doped and undoped solder was measured by using software (Olympus SZX10 image analyzer). It was found that after addition of Ni and Co NP-doped flux, the thickness of IMC particles decreased as compared to IMC particles of the undoped solder joint. Figure 4.5 describes the thickness of IMC particles in the eutectic region of the doped and undoped solder joint. It is observed that the thickness of IMC particles in the eutectic region of undoped SAC305 was mostly greater than 0.9 µm. In the case of Ni and Co-doped solder joint, the thickness of the IMC particles was mostly below than 0.9 µm (Figure 4.5).

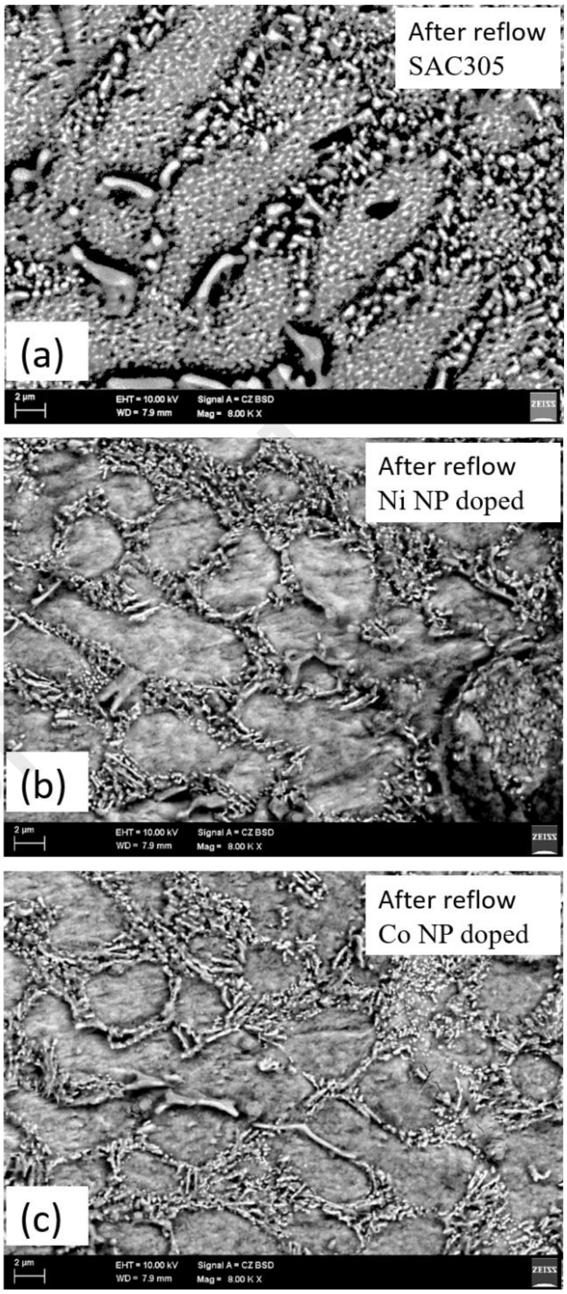

Figure 4.4: FESEM images depicting the structure of IMC particles present in the eutectic region of the matrix of (a) SAC305 (b) Ni-NP doped and (c) Co-NP doped solder joints.

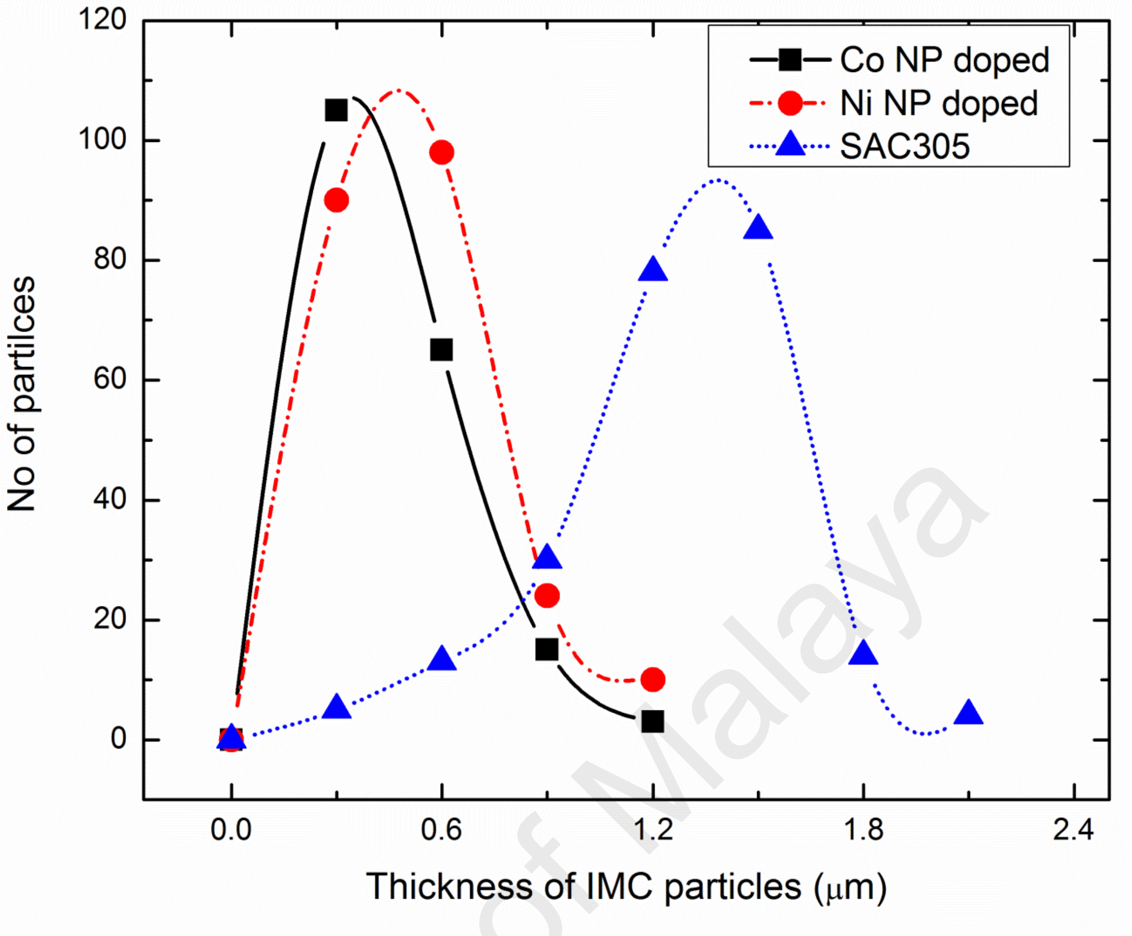

Figure 4.5: IMC particles thickness in eutectic region of matrix of doped and undoped solder.

4.1.3 Distribution of Ni and Co in solder joint

EDX elemental maps and EDX spot analysis were recorded to reveal Ni and Co-NP distribution in the SAC305 solder joint. The elemental mapping was done for the SAC305+2 wt% Ni-NP and the SAC305+2 wt% Co-NP solder joints. Figure 4.6 shows elemental maps for Cu and Ni in the SAC305 + 2 wt % Ni NP-doped flux solder joint. It is found that Ni is mainly concentrated at the interface. But a close observation of the Ni map reveals that Ni is also present in the solder matrix. Figure 4.7 shows elemental maps for Cu and Co in the SAC305 + 2 wt% Co-NP doped flux solder joint. In the figure, it can be seen that Co is mainly concentrated at interfacial IMC. A small concentration of

Co also found in the solder matrix (Figure 4.7b). It may be noted Co and Ni did not actually penetrate the Cu wire but that this is as artifact of the measurement.

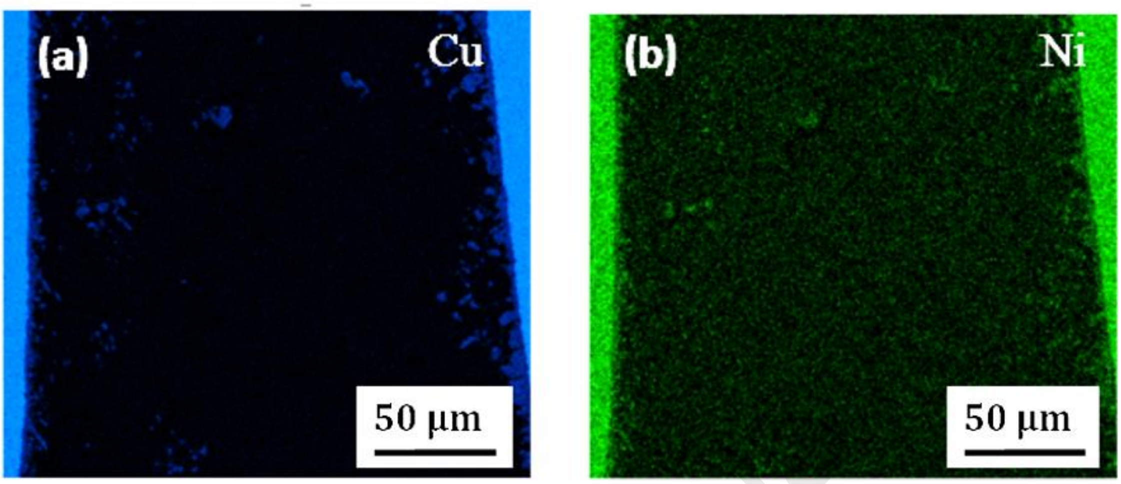

Figure 4.6: EDX elemental maps of the SAC305 + 2 wt% Ni NP solder joint. Elemental maps for (a) Cu and (b) Ni.

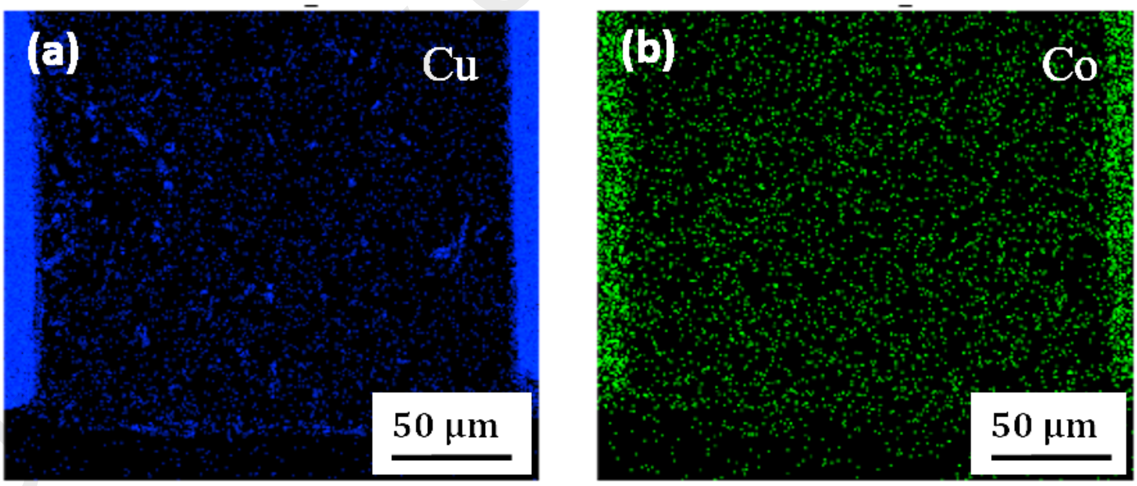

Figure 4.7: EDX elemental maps of the SAC305 + 2 wt% Co NP solder joint. Elemental maps for: (a) Cu and (b) Co.

After reflow, some large size IMC particles were found in the matrix of doped and undoped solder joints. EDX spot analysis was performed on these particles present in the solder matrix of Ni and Co NP-doped solder joint (Figure 4.8). EDX spot analysis confirmed that the composition of these IMC particles were (Cu, Ni)$_6$Sn$_5$ in the Ni-doped solder and (Cu, Co)$_6$Sn$_5$ in the Co-doped solder joint. The average elemental composition of Ni and Co-NP in the particles is given in EDX spot analysis of Ni and Co NP-doped solder joint. (a) overview of Ni NP-doped solder, (b) EDX spot on magnified image of (Cu, Ni)$_{6Sn5}$ large size particles in the matrix of Ni NP-doped solder (c) EDX analysis on figure b, (d) overview of Co NP-doped solder, (e) EDX spot on magnified image of (Cu, Co)$_{6Sn5}$ large size particles in the matrix of Co NP-doped solder and (f) EDX analysis on figure e.

It is seen in Table 4.2 that some of the IMC particles present in the solder matrix contains Ni and Co. The distribution of Ni in the IMC particles present in the matrix is not uniform. In the Ni NP-doped solder, IMC particles in the middle of solder matrix contain 1.60 wt% of Ni content while IMC particles in the solder matrix near to Cu substrate contain 0.9 wt% of Ni content. In the past, a similar study was performed by using paste mixing techniques (Tay et al., 2013). In their study, a similar finding was detected. In the Co NP-doped solder, 1.89 wt% Co was found in the IMC particle present in the middle of the solder matrix while 1.86 wt% Co was found in IMC particles present in the solder matrix near to Cu substrate. By EDX analysis it was observed that the chemical composition of large size IMC particles present in Ni NP-doped solder is (Cu, Ni)$_6$Sn$_5$ particles while (Cu, Co)$_6$Sn$_5$ in the Co NP-doped solder matrix. The EDX spot analysis was also done to measure the Ni and Co content in the β-Sn present in the solder matrix. It was found that Ni and Co did not dissolve in β-Sn. Ni and Co only dissolved into the IMC particles present in the solder matrix. After dissolution, they changed the composition of IMC particles from Cu$_6$Sn$_5$ to (Cu, Ni)$_6$Sn$_5$ and (Cu, Co)$_6$Sn$_5$. This result also follows the binary phase diagrams of Sn-Ni (Schmetterer et al., 2007) and Sn-Co (Jiang, Sato, Ohnuma, Kainuma, & Ishida, 2004).

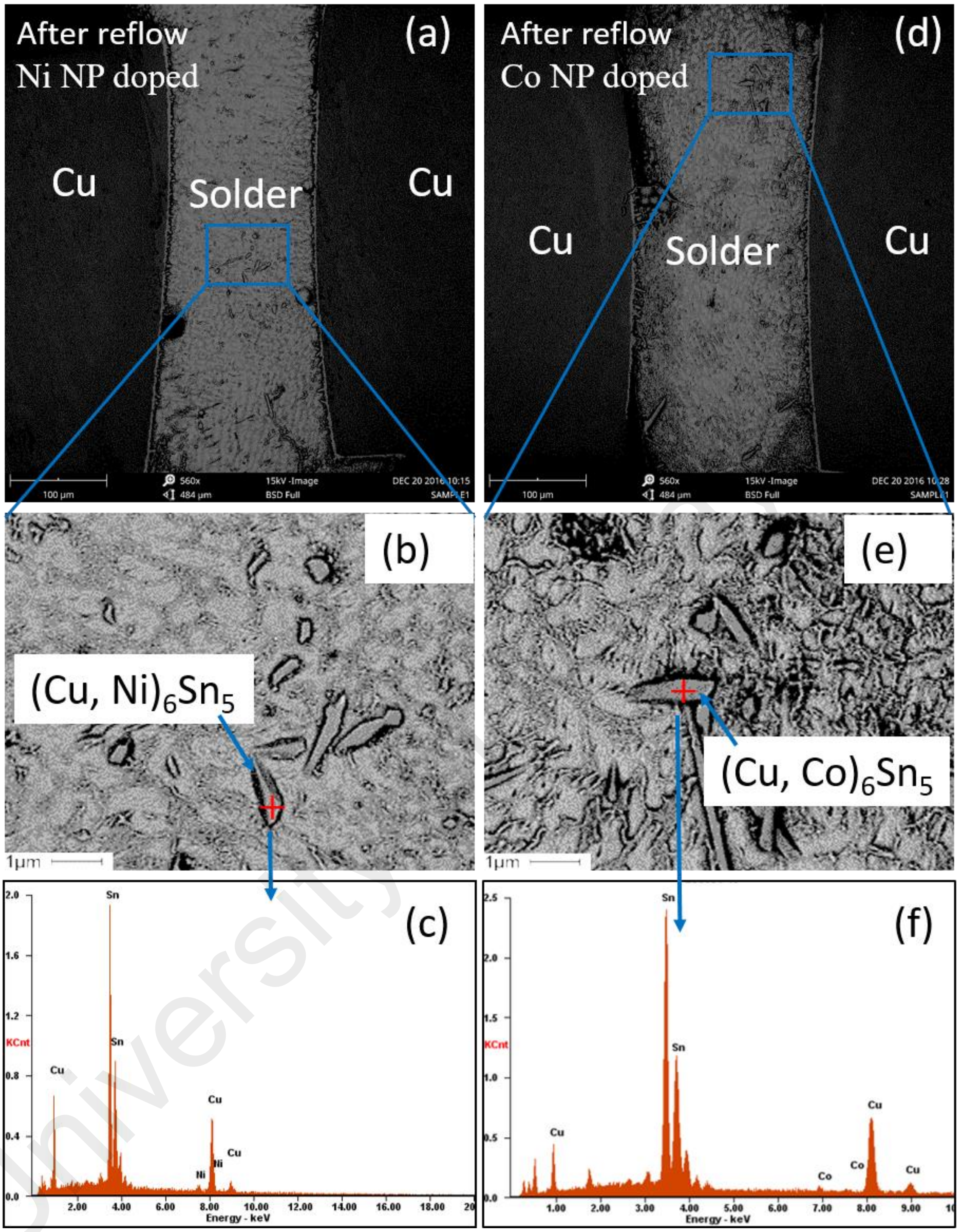

Figure 4.8: EDX spot analysis of Ni and Co NP-doped solder joint. (a) overview of Ni NP-doped solder, (b) EDX spot on magnified image of (Cu, Ni)$_6$Sn$_5$ large size particles in the matrix of Ni NP-doped solder (c) EDX analysis on figure b, (d) overview of Co NP-doped solder, (e) EDX spot on magnified image of (Cu, Co)$_6$Sn$_5$ large size particles in the matrix of Co NP-doped solder and (f) EDX analysis on figure e.

Table 4.2: EDX elemental compositions of IMC phases in the matrix of NP-doped flux solder joints.

Solder joint	Location	Element composition (wt%)			
		Cu	Sn	Ni	Co
Ni NP-doped	IMC particles in middle of solder matrix	35.20 ± 2.1	62.96 ± 1.5	1.60 ± 0.9	---
	IMC particles in solder matrix near to Cu substrate	50.35 ± 0.9	47.31 ± 0.8	0.9 ± 0.3	---
Co NP-doped	IMC particles in middle of solder matrix	33.04 ± 0.7	64.08 ± 2.4	---	1.89 ± 0.4
	IMC particles in solder matrix near to Cu substrate	51.21 ± 1	46.61 ± 0.6	---	1.86 ± 0.4

4.2 Interfacial microstructure after electromigration

The electromigration test was conducted in Ni and Co NP-doped flux solder joints and undoped (SAC305) solder joints. The test was run for 0, 192, 384 and 1128 h under a current density of 1×10^4 A/cm^2 in each type of samples. A temperature of 80 °C was maintained during the electromigration test. The test was run the in a silicon oil bath to maintain the temperature. The detail about the selection of parameters is given in chapter 3.2. The changes in the microstructure of doped and undoped solder joints are described below.

4.2.1 SAC305 solder joint

Figure 4.9 describes the effect of EM on the SAC305 solder joint after different time intervals. Figure 4.9 a, b, c and d show the cross-sectional microstructures of the cathode side after 192, 384, 768 and 1128 h respectively; while Figure 4.9 e, f, g, and h show the anode side after 192, 384, 768 and 1128 h respectively. At the cathode side, the thickness of the interfacial IMC layer decreased from 3.0 µm to 2.5, 1.7, 1.6 and 1.3 µm after the EM test at different time intervals. After 1128 h of EM, cracks appear at the cathode side. On the other hand, the thickness of IMC layer increased from 3.0 µm to 3.8, 4.8, 7.9 and 9.5 µm at anode side with the current stressing time. No crack or damage is found at the anode side.

4.2.2 Ni nanoparticle doped solder joint

Figure 4.10 a, b, c, and d show the cross-sectional microstructures of interfacial IMC at the cathode side of the SAC305+2 wt% Ni NPs samples subjected to EM tests for 192, 384, 768 and 1128 h respectively. The microstructures of the IMC at anode side are shown in Figure 4.10 e, f, g and h tested for EM time of 192, 384, 768 and 1128 h respectively. At the cathode side, no systematic change in the thickness or morphology of the interfacial IMC layer is observed. At 1128 h, cracks appear at the interface at the cathode side. However, the extent of cracking and damage at 1128 h is much lesser in the SAC305+2 wt% Ni NPs as compared with the SAC305 sample (Figure 4.9d and Figure 4.10d). The thickness of interfacial IMC at the anode side increase from 3.9 µm to 4.1, 4.4, 4.5 and 4.8 µm with the EM time. However, as compared with the SAC305, the increase in interfacial IMC at the anode side is much less in the SAC305+2 wt% Ni NPs sample (Figure 4.9 and Figure 4.10).

4.2.3 Co nanoparticle doped solder joint

Effect of EM on the SAC305 + 2 wt% Co-NP is shown in Figure 4.11. Interfacial microstructures at the cathode side are shown in Figure 4.11 a, b, c and d while the microstructures at the anode interface are shown in Figure 4.11 e, f, g, and h. After the EM tests conducted for 192, 384, 768 and 1128 hours, the average thickness of interfacial

IMC layers at the cathode decreased from 2.9 µm to 2.8, 2.6, 2.5 and 2.2 µm, respectively. On the other hand, the thickness at the anode side increased from 2.9 µm to 3.0, 3.2, 3.6 and 4.2 µm. No crack or damage was observed on the cathode side of solder joint when Co-NP doped flux was used.

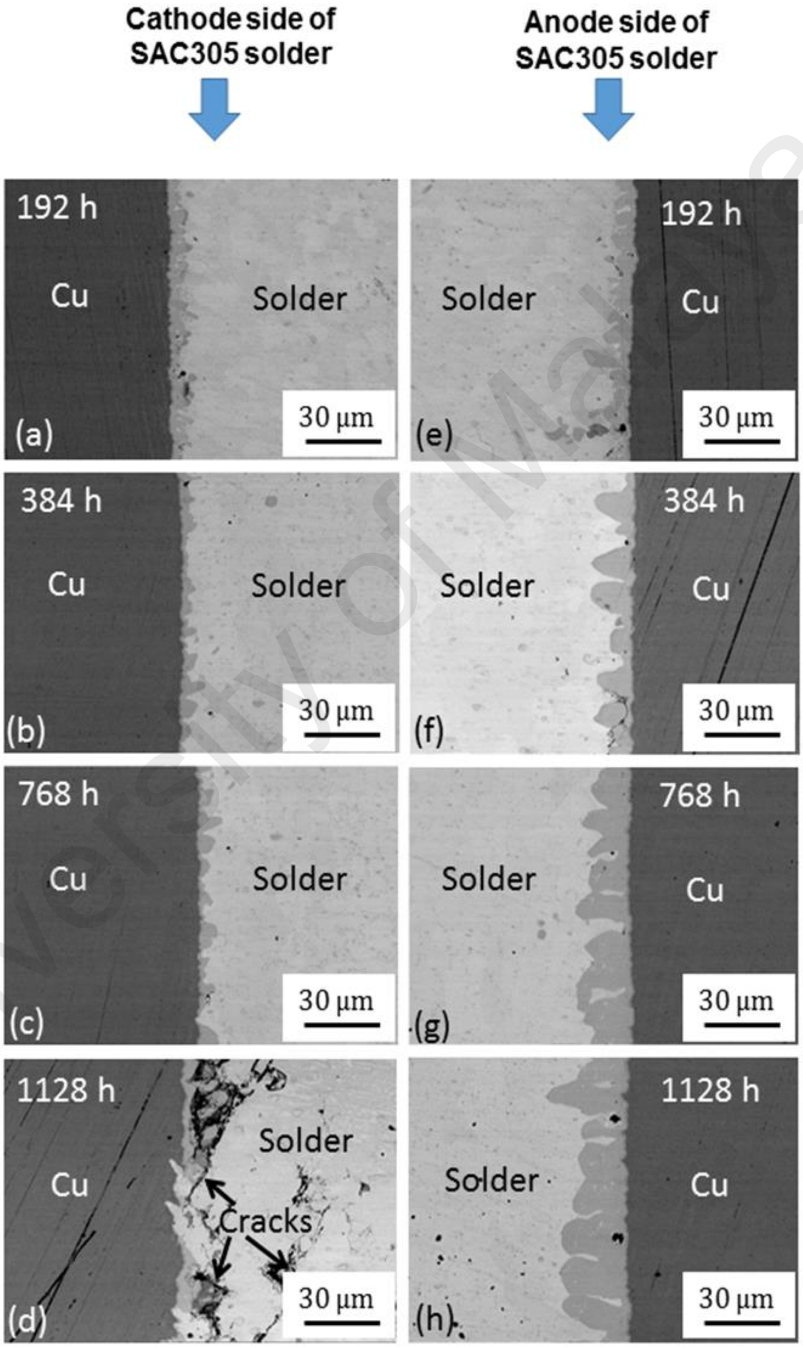

Figure 4.9: FESEM backscattered electron images of the SAC305 solder joint after EM test for 192, 384, 768 and 1128 h. (a), (b), (c) and (d) show cathode side, while (e), (f), (g) and (h) show anode side.

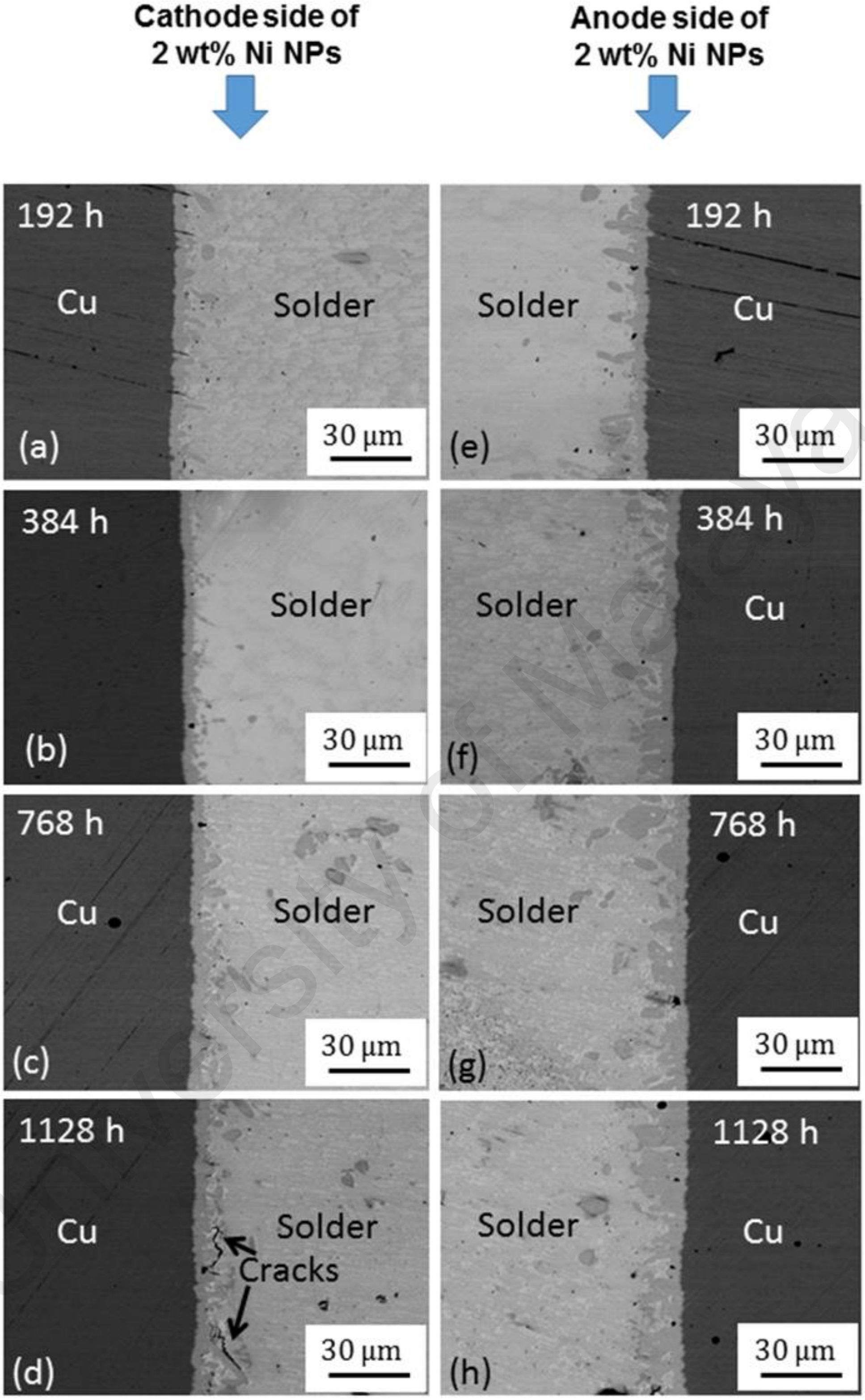

Figure 4.10: FESEM backscattered electron images of the SAC305 + 2wt% Ni NP solder joint after EM test for 192, 384, 768 and 1128 h. (a), (b), (c) and (d) show the cathode side, while (e), (f), (g) and (h) show the anode side.

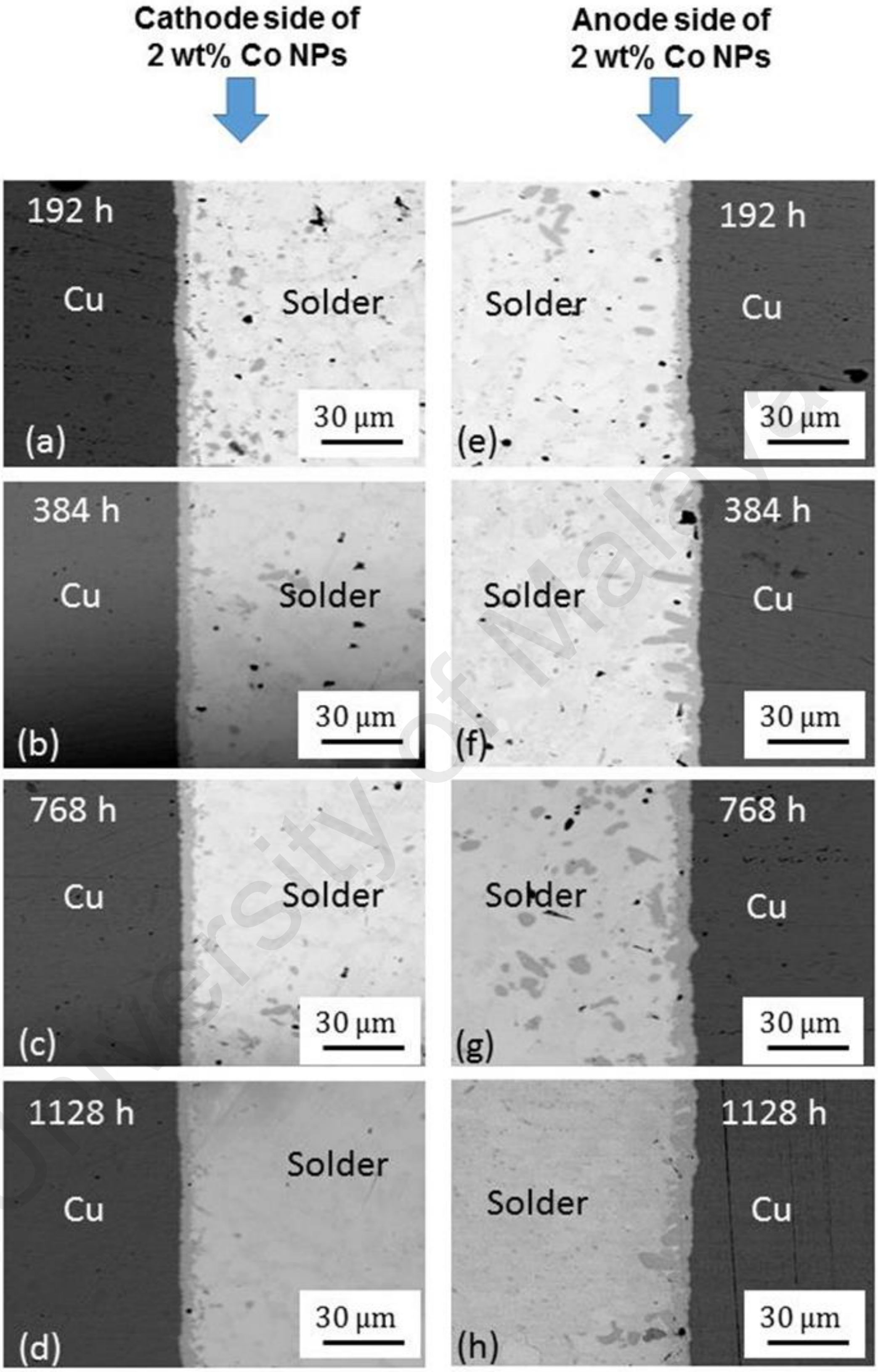

Figure 4.11: FESEM backscattered electron images of the SAC305 + 2wt% Co NP solder joint after EM test for 192, 384, 768 and 1128 h. (a), (b), (c) and (d) show the cathode side, while (e), (f), (g) and (h) show the anode side.

4.2.4 Comparison of thickness variation in interfacial IMC layers of doped and undoped solder

Figure 4.12a reveals that the thickness of interfacial IMC in the SAC305 sample markedly decreases at the cathode side while increases at the anode sides. In Figure 4.12 b and c, the change in the IMC thickness is much less at the cathode side as well as at the anode side due to the addition of Ni and Co. Ni NP and Co-NP doped flux significantly controlled the variation of IMC during the EM test.

Table 4.3 shows the growth rate of IMC at the anode side for the SAC305, SAC305, SAC305 + 2 wt% Ni and SAC305 + 2 wt% Co solder joints. In the SAC305 solder joint, the average anodic growth rate of the interfacial IMC layer is found to be 1.585×10^{-6}µm/s. In the case of Ni and Co-NP doped solder, the IMC growth rate at the anode side decreased significantly. The average anodic growth rate of Ni NP containing solder was 2.72×10^{-7} µm/s while for the interfacial IMC layer of Co-NP added solder joint was the growth rate is calculated to be 2.231×10^{-7}µm/s. The calculated values of anodic growth rate for all kind of samples and given in Table 4.3

4.3 Crystallographic structures of doped and undoped solder

The electron backscatter diffraction (EBSD) analysis was performed to investigate the effect of EM on the grain size of interfacial IMC of NP-doped solder joints and undoped SAC305 solder joints. The EBSD analysis was performed before and after EM tests conducted for 1128 h. The EBSD analysis was used for two kinds of investigation in the SAC305, Ni-NP doped and Co-NP doped solder joints. (1) Crystallographic structure and distribution of phases before electromigration, (2) crystallographic structure and distribution of phases after electromigration. The detail of these investigations is discussed below.

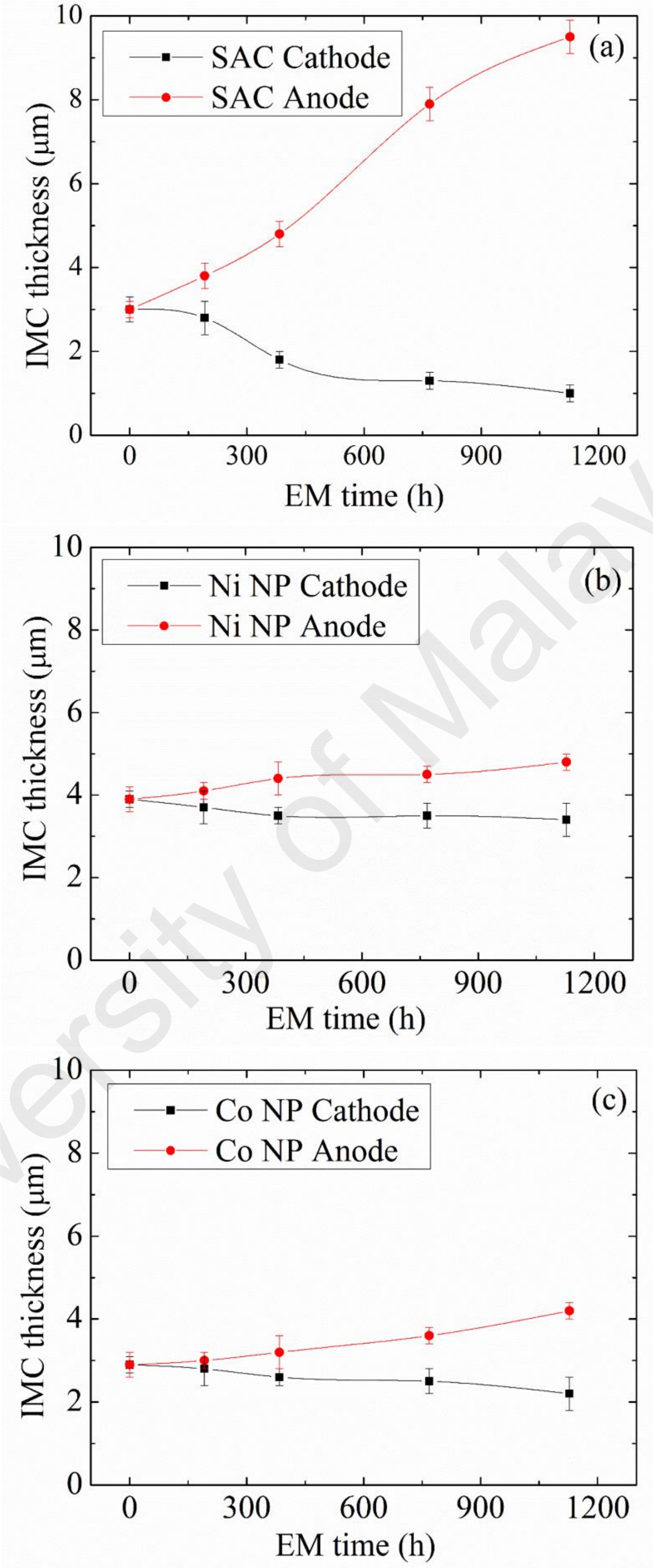

Figure 4.12: IMC thickness variation as a function of electromigration time at the cathode and anode sides of (a) SAC305, (b) Ni-NP doped and (c) Co-NP doped solder joint.

Table 4.3: Anodic growth rate of interfacial IMC in solder joints.

EM time (h)	SAC305	SAC305 + Ni NP doped flux	SAC305 + Co NP doped flux
192	1.591×10^{-6} µm/s	2.893×10^{-7} µm/s	1.44×10^{-7} µm/s
384	1.880×10^{-6} µm/s	3.616×10^{-7} µm/s	2.170×10^{-7} µm/s
768	1.591×10^{-6} µm/s	2.170×10^{-7} µm/s	2.531×10^{-7} µm/s
1128	1.280×10^{-6} µm/s	2.216×10^{-7} µm/s	2.201×10^{-7} µm/s
Average	$1.585 \pm 0.24 \times 10^{-6}$ µm/s	$2.72 \pm 0.68 \times 10^{-7}$ µm/s	$2.231 \pm 0.460 \times 10^{-7}$ µm/s

4.3.1 Crystallographic structure and distribution of phases before electromigration

Figure 4.13 represents the EBSD orientation maps at interfacial regions of as reflowed NP-doped and undoped solder joints. The mapping was performed to investigate the grain size of interfacial IMC at the interfaces of NP-doped and undoped solder joints. In Figure 4.13 (a) and (b), it is observed that Cu_6Sn_5 formed multi-grains inside the interfacial IMC layer. The average grain size of interfacial Cu_6Sn_5 IMC was found to be 2.7 ± 0.2 µm. After addition of Ni NP-doped flux into the SAC305 solder joint, It is found (Sujan et al., 2014) that the Ni substituted the Cu atoms in the interfacial Cu_6Sn_5 IMC and changed its composition from interfacial Cu_6Sn_5 IMC to $(Cu, Ni)_6Sn_5$. Ni NP-doped flux reduced the grain size of interfacial IMC significantly (Figure 4.13 c and d). The average grain size of interfacial $(Cu, Ni)_6Sn_5$ IMC was found to be 1.8 ± 0.1 µm. After the addition of Co NP-doped flux into the SAC305 solder, the composition of interfacial IMC changed from Cu_6Sn_5 to $(Cu, Co)_6Sn_5$. After the addition of Co NP-doped flux, the grain size of interfacial IMC also reduced (Figure 4.13 e and f). The average grain size of interfacial $(Cu, Ni)_6Sn_5$ IMC was found to be 2.1 ± 0.15 µm. The average grain size at interfaces of NP-doped and undoped solder are furnished in Table 4.4.

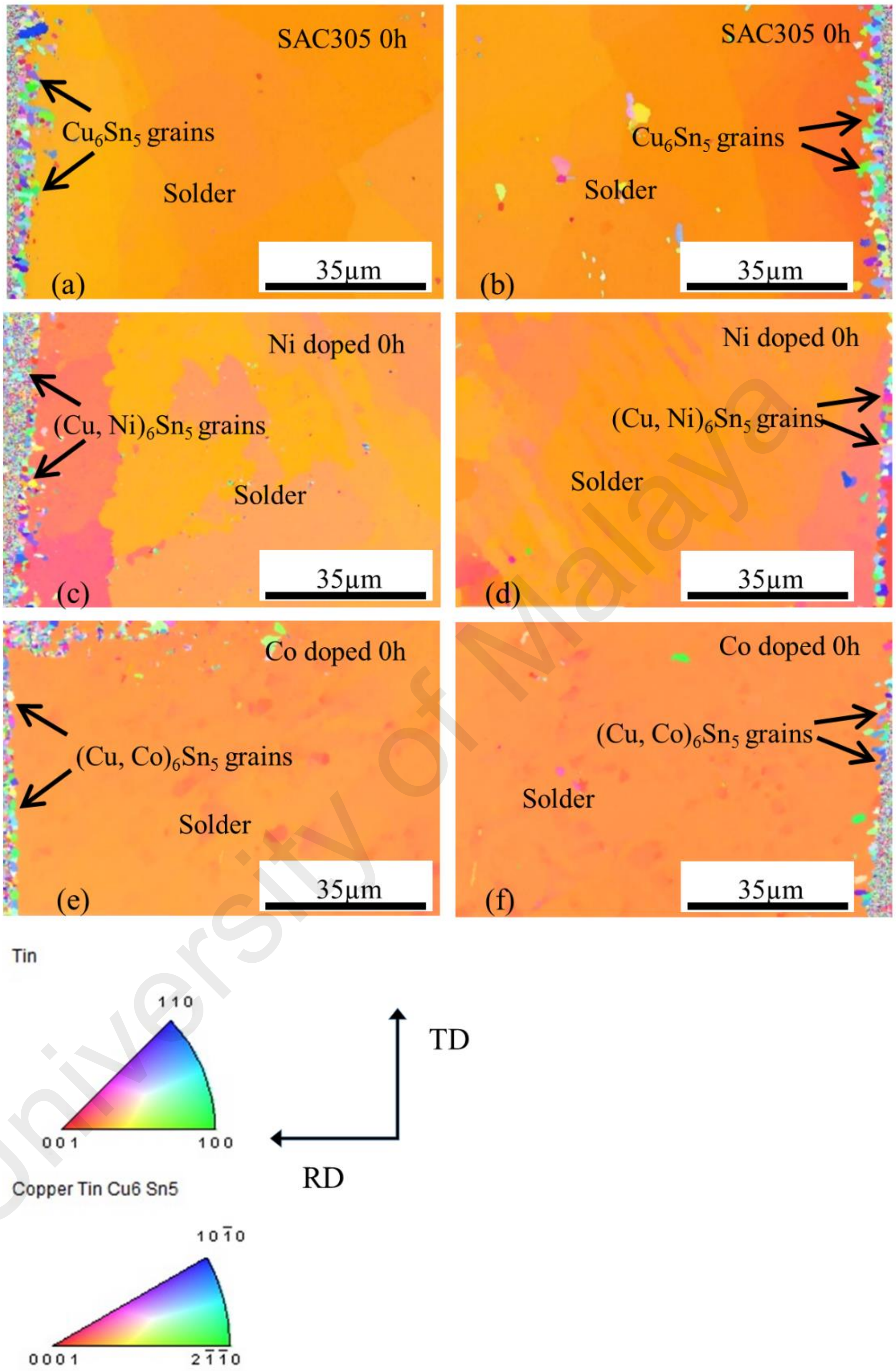

Figure 4.13: EBSD orientation mapping at interfaces of as reflowed (a and b) SAC305 solder joint, (c and d) Ni-NP doped solder and (e and f) Co-NP doped solder joints.

Table 4.4: Grain size of interfacial IMC of NP-doped and undoped solder joints.

Side	**Grain size of interfacial IMC (µm)**			
	EM Time (h)	**SAC305**	**Ni NP doped**	**Co NP doped**
Cathode	0	2.7 ± 0.2	1.8 ± 0.1	2.1 ± 0.15
	1128	1.3 ± 0.14	2.06 ± 0.15	2.4 ± 0.13
Anode	0	2.7 ± 0.12	1.8 ± 0.12	2.1 ± 0.1
	1128	6.7 ± 0.3	3 ± 0.14	3.6 ± 0.14

Figure 4.14 represents the phase mapping of NP-doped and undoped SAC305 solder joints. The phase mapping was done by using EBSD (HIKARI XP2 9434.079.45400STBC) machine. In the figure, the red color represents the Sn phase distribution while green color represents the Cu_6Sn_5 phase distribution. Figure 4.14 (a) and (b) show the phase distribution at both ends of the undoped SAC305 solder joint. It is found that the most of the area of solder bulk was covered by Sn phase (represented by red color). Cu_6Sn_5 phase is mainly found at the interfaces of the SAC305 solder joint (represented by green color).The Cu_6Sn_5 phase formed scallop type layer at interfaces of the SAC305 solder joint which can clearly be seen in Figure 4.14 (a) and (b). Particles of Cu_6Sn_5 can also be seen inside the solder bulk.

Figure 4.14 (c) and (d) show the phase distribution at interfaces and inside the solder bulk of Ni NP-doped flux solder joint. High concentration of Sn phase was found inside the solder (represented with red color). At the interfaces, a layer of $(Cu, Ni)_6Sn_5$ phase with a planar type morphology is found (represented by green color). Particles of $(Cu, Ni)_6Sn_5$ are also found inside the solder bulk.

Figure 4.14 (e) and (f) shows phase distribution in the Co NP-doped flux solder joint. It was found that Co-NP showed similar behavior as the Ni NP-doped solder joint. Co formed planar type (Cu, Co)$_6$Sn$_5$ IMC phase at the interfaces of the solder joint. Small particles of (Cu, Co)$_6$Sn$_5$ IMC were found inside the solder bulk.

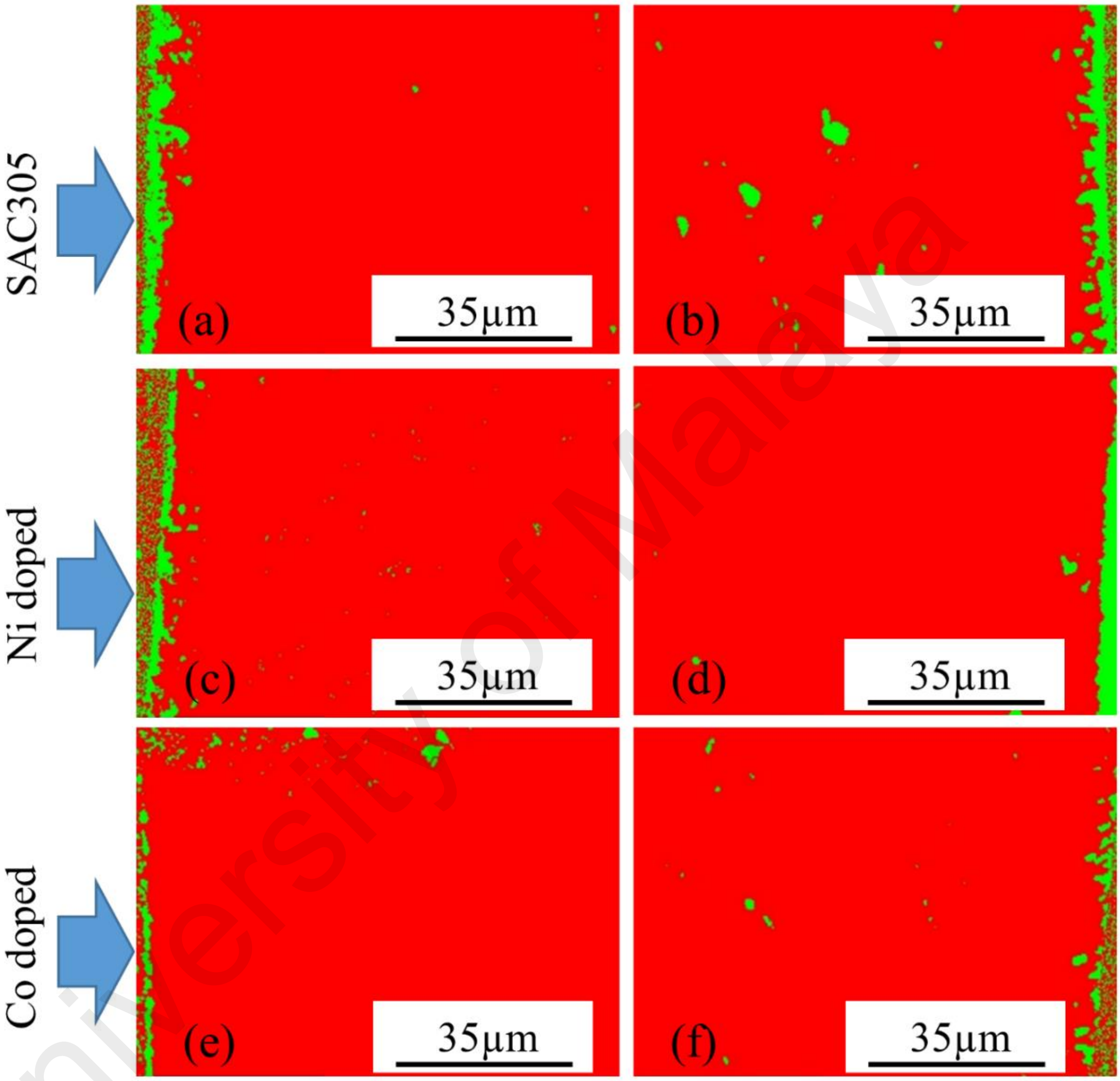

Figure 4.14: Phase mapping at the interface of as reflowed (a and b) SAC305, (c and d) Ni-NP doped and (e and f) Co-NP doped solder joints.

4.3.2 Crystallographic structure and distribution of phases after electromigration

Figure 4.15 shows EBSD orientation mapping of NP-doped solders and undoped SAC305 solder joint after the EM test. In Figure 4.15 (a) it can be seen that after EM test, the grain size of Cu_6Sn_5 interfacial IMC has been reduced from 2.7 ± 0.2 µm to 1.3 ± 0.14 µm at the cathode side while at anode side the grain size of Cu_6Sn_5 interfacial IMC has been significantly increased from 2.7 ± 0.2 µm to 6.7 ± 0.3 µm (Figure 4.15 (b). EM damage at the cathode interfaces of the solder joint and rapid growth of IMC at the anode side which was discussed in section 4.2.1 and can also be seen clearly in Figure 4.15 (a) and (b).

As Compared to the SAC305 solder joint, the Ni NP doping significantly reduced grain size at the cathode and anode side of solder joints after EM test (Figure 4.15 c and d). After EM test, the average grain size slightly increased from 1.8 ± 0.1 µm to 3 ± 0.14 µm at anode side while no significant change in grain size was found at the cathode interfaces. The addition of Co NP-doped flux also showed similar behavior as the Ni NP-doped flux. The Co NP-doped flux also controlled the grain size after the EM (Figure 4.15 e and f). It should be noted that some noise was detected during orientation mapping at the cathode interfaces of Co NP-doped solder joint Figure 4.15 e. The average grain size of Co NP-doped solder increased from 2.1 ± 0.15 µm to 3.6 ± 0.14 µm at the anode side. At the cathode side, no significant reduction in the grain size was observed. The average value of IMC grain size at the cathode and anode interfaces of NP-doped and undoped SAC305 solder joint is tabulated in Table 4.4.

4.3.3 Variation of grain size of interfacial IMC layers

Effect of electromigration on the grain size of interfacial IMC was investigated by using EBSD analysis. The grain size was measured by using software (Olympus SZX10 image analyzer). Figure 4.17 shows the variation of grain size of interfacial IMC of the undoped SAC305 solder joint and NP-doped solder joints before and after EM test. In Figure 4.17a it can be seen that at 0 h of EM, the SAC305 solder contains bigger grains in interfacial IMC compared with Ni and Co-doped solder joints (Figure 4.17 b and c).

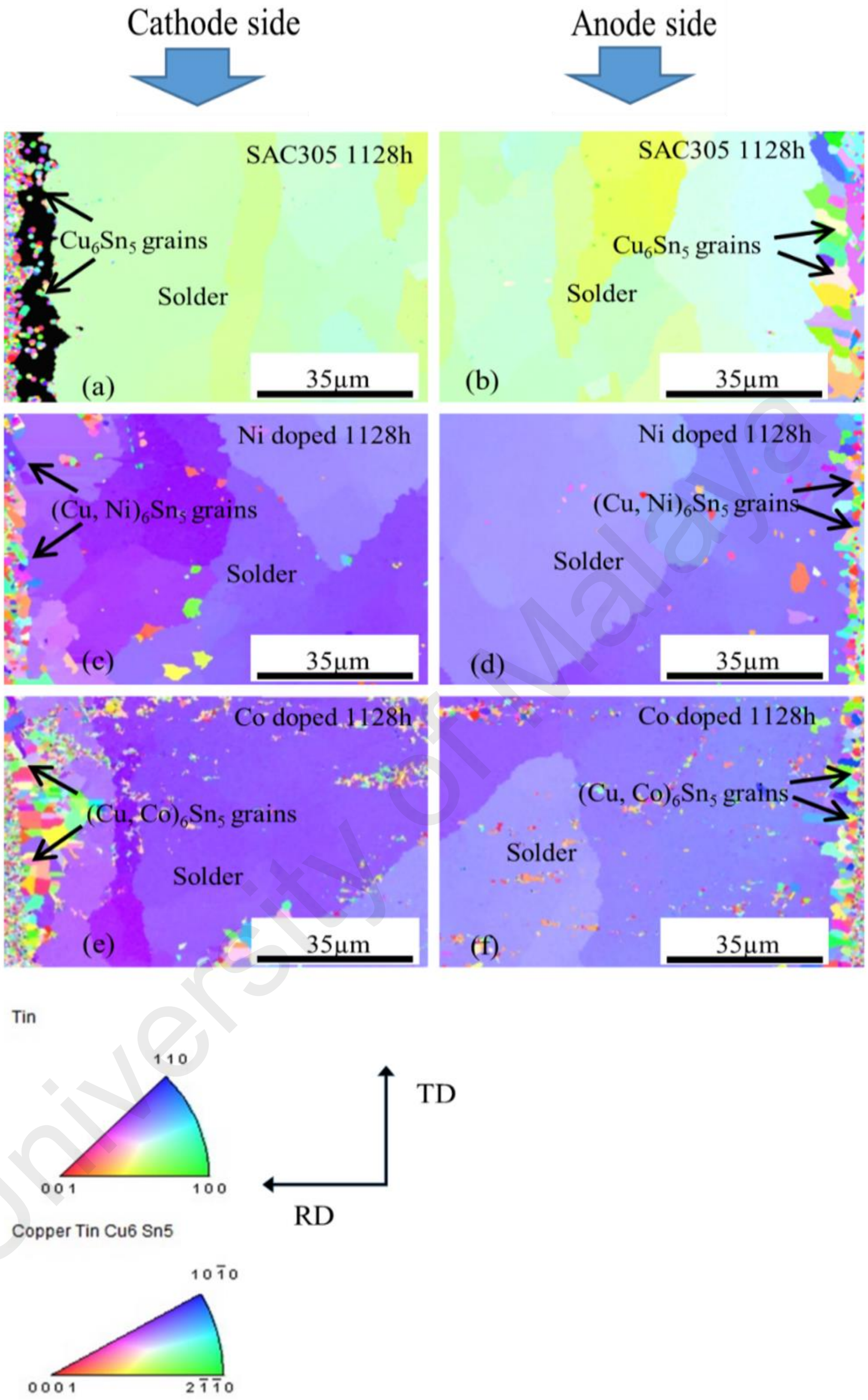

Figure 4.15: EBSD orientation mapping at interfaces of (a and b) SAC305, (c and d) Ni-NP doped and (e and f) Co-NP doped solder joint after the electromigration.

After EM test the grain size of the SAC305 solder joint significantly increased on the anode side while Ni and Co-NP doping controlled the growth of grain size at anode side after the EM test (Figure 4.17 a, b and c).

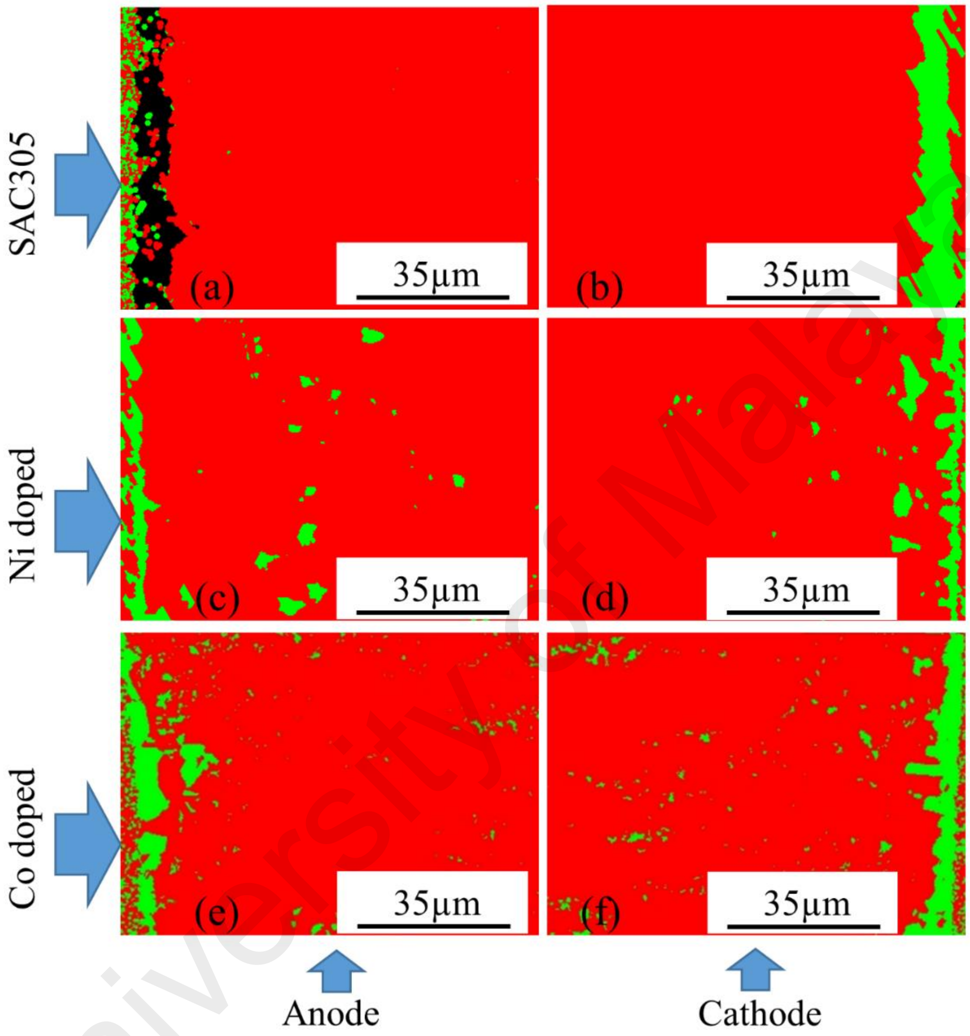

Figure 4.16: Phase mapping at the interface of (a and b) SAC305, (c and d) Ni-NP doped and (e and f) Co-NP doped solder joints after EM test of 1128 h.

4.4 Measurement of electrical resistance in doped and undoped solder

Electrical resistance tests were conducted on the SAC305, Ni-NP doped and Co-NP doped solder joints to investigate the effect of EM on the electrical resistance of the solder joints and failure time of the solder joints. Due to the difference in dimension of the samples, the parameters for this test were different than the parameters used in microstructure analysis. The information about parameters used in this study is given in Table 3.1 and section 3.2.

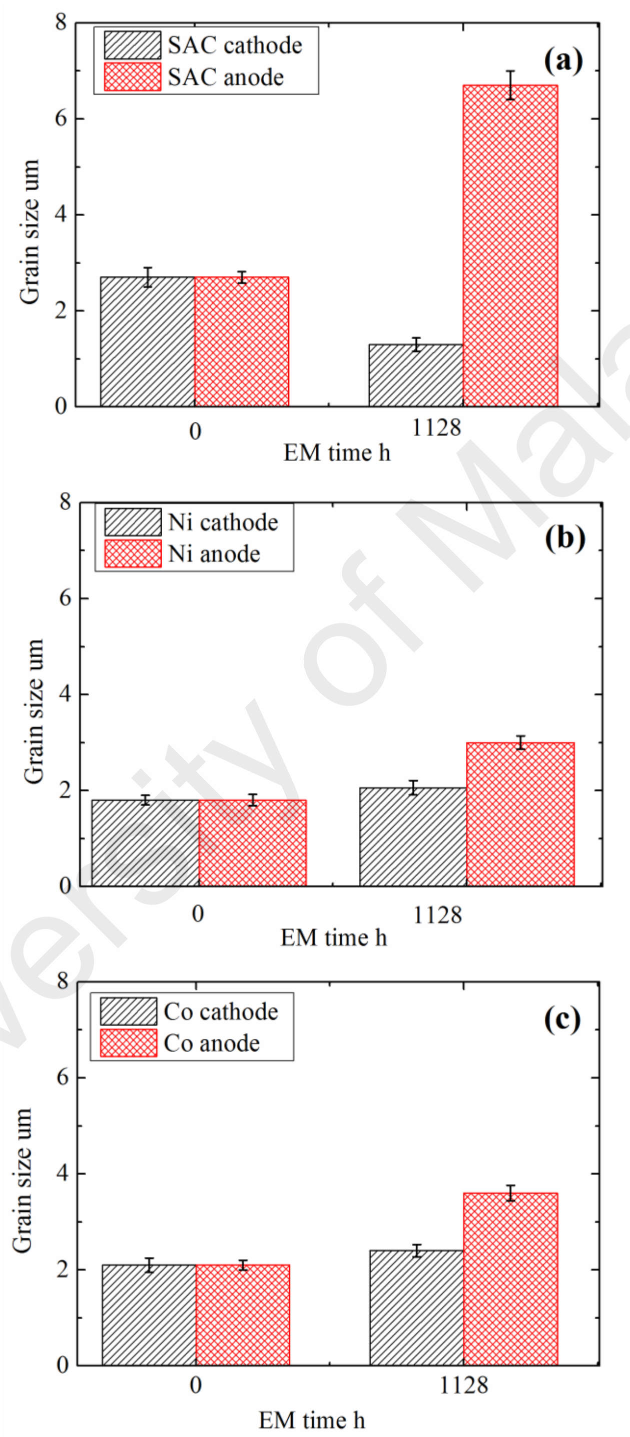

Figure 4.17: Variation of grain size of interfacial IMC of NP-doped and undoped SAC305 solder joint before and after the EM test.

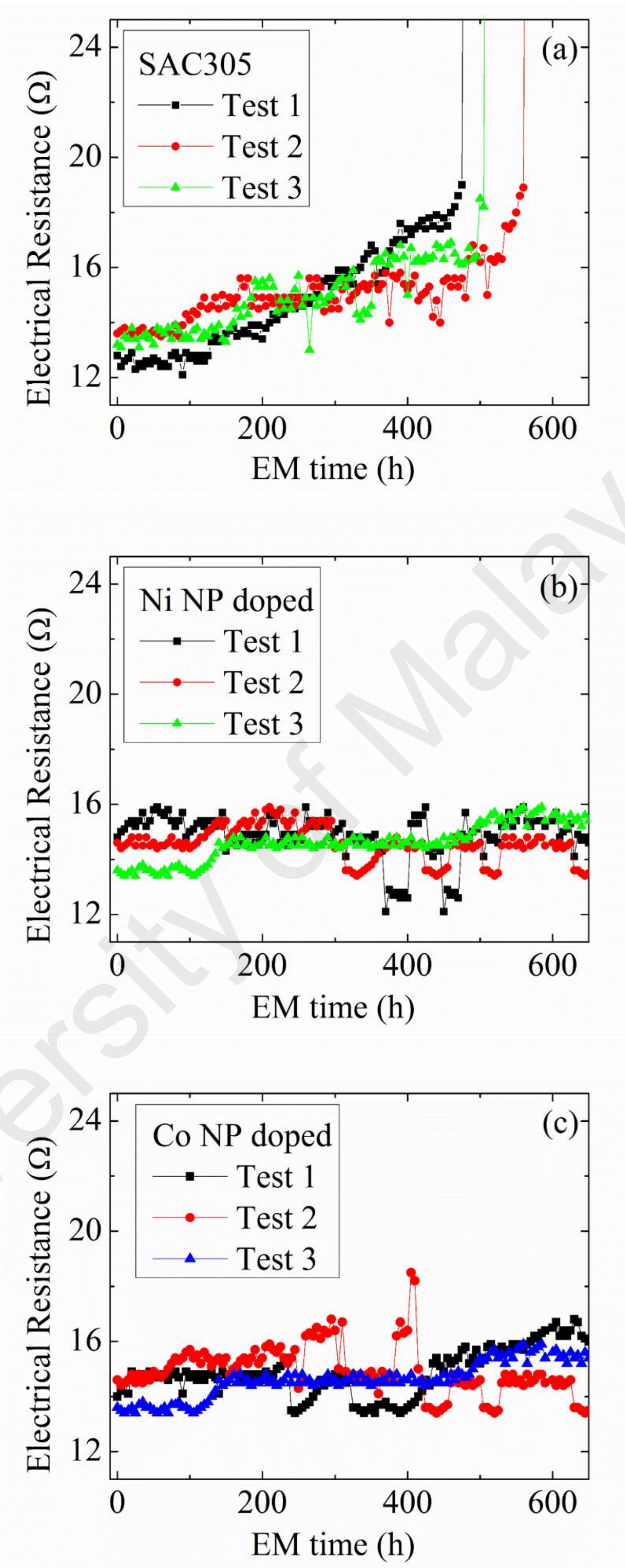

Figure 4.18: Changes in electrical resistance of (a) SAC305, (b) Ni-NP doped and (c) Co-NP doped solder joints as a function of EM time.

The EM test was run for 0 h and 192 h under a current density of 5 × 10^3 A/cm^2. A constant temperature of 150 °C was maintained by using a silicon oil bath. The test was repeated three times for each type of samples. Figure 4.18 describes the electrical resistance of the SAC305, Ni-NP doped and Co-NP doped solder joints as a function of EM time. In the SAC305 solder joints, the electrical resistance tends to increase during EM. The failure time of the samples was between 500 h to 600 h as indicated by the abrupt raise in the resistance values (Figure 4.18a). In the case of Ni and Co-doped solder, the electrical resistance slightly increased but the sample did not fail until 700 h of EM test.

4.5 Influence of nano doped flux on mechanical strength of SAC305 solder

The effect of Ni and Co-NP on mechanical strength was investigated. The micro tensile tests were done for the SAC305, Ni-NP doped and Co-NP doped solder joints. The micro tensile tests were repeated 5 times for each type of samples at 0 and 192 h of EM. Stress-strain values, maximum tensile strength, and fracture behavior were studied and recorded during the micro tensile test. Detailed explanation on a micro-tensile test of the SAC305, Ni-NP doped and Co-NP doped solder joints is given below in section 4.5.1, 4.5.2 and 4.5.3.

4.5.1 Stress-strain values

Figure 4.19a-f illustrate the stress-strain curves for the samples, SAC305, SAC305 + 2 wt% Ni-NP and SAC305 + 2 wt% Co-NP solder joints subjected to 0 h and 192 h of EM test. Figure 4.19 a exhibits the stress-strain curves for the SAC305 solder joint without EM test. The stress values for all as-reflowed SAC305 samples solder joints lie between 55 to 65 MPa. The as reflowed SAC305 exhibit plastic deformation and most of the strain values are above 0.6%. Figure 4.19 b shows the stress-strain curves for the SAC305 solder joints after 192 h of EM. In this figure, it is observed that the samples broke at low loads. The values of maximum stress are less than 40 MPa for all these samples.

After addition of Ni NP-doped flux into the SAC305 solder joint, considerable changes in tensile behavior were found. At 0 h of EM, the maximum stress is between 95 to 110 MPa and strain% is below 0.5% in most of the curves. After EM test of 192 h, the maximum stress is between 70 to 85 MPa and strain% is less than 0.5 in most of the curves. The stress-strain curves for the SAC305 + Ni NP-doped solder can be seen in Figure 4.19 c and d respectively for 0 and 192 h of EM test. In the case of Co-NP containing solder joints the maximum stress values are between 85 to 95 MPa and the strain values are less than 0.6% strain at 0 h of EM tests. All the samples of Co-NP containing solder broke at the higher value of strength. It can be seen in Figure 4.19 e that most of the Co-NP containing solder joints did not exhibit the lower plastic strain values. The stress-strain curves after 192 h of EM test are shown in Figure 4.19 f for Co-doped solder joints. After electromigration of 192 h, the strength of the SAC305+2wt% Co-NP samples slightly decreased. The values of maximum stress are above than 70 MPa which is higher than the strength values of the SAC305 solder joints after EM test of 192 h.

4.5.2 Mechanical strength

Figure 4.20 summarizes the average values of the tensile strength of the SAC305, SAC305 + 2 wt% Ni-NP and the SAC305 + 2 wt% Co-NP solder joints at 0 and 192 h. In the case of the SAC305 solder joint, the average strength value is 60.34 MPa at 0 h EM test. But after 192 h of EM experiment, the tensile average strength diminishes significantly to 22.36 MPa. In the case of Ni NP-doped samples, the average tensile strength is found to be 100.99 MPa at 0 h of EM test which is higher than the corresponding values for the SAC305 solder joints. After EM for 192 h, the average tensile strength decreased to 77.23 MPa for Ni NP-doped samples.

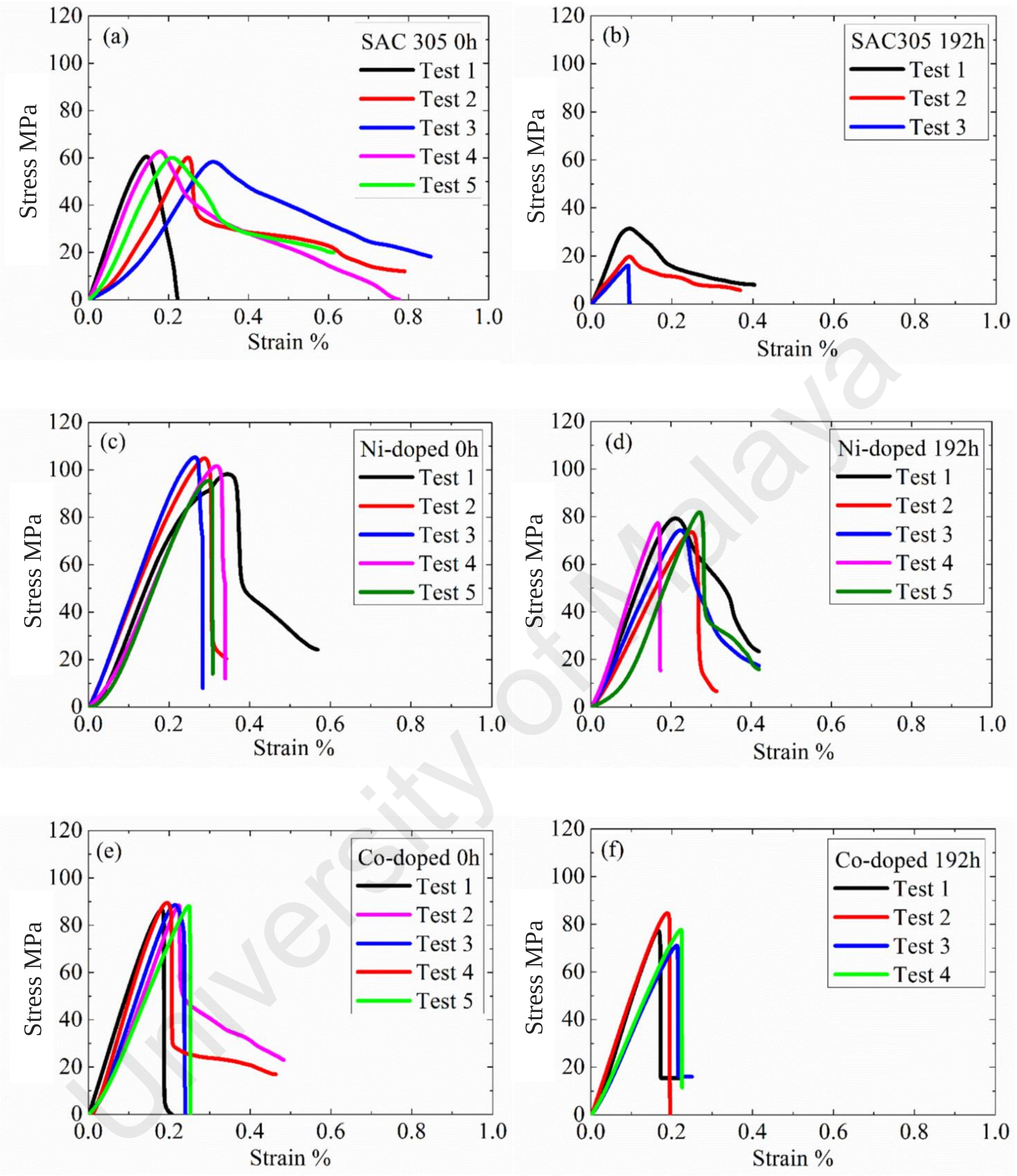

Figure 4.19: Stress-strain curves of the SAC305solder (a) 0 h and (b) 192 h of EM, SAC305 + 2 wt% Ni NP solder (c) 0 h and (d) 192 h of EM and SAC305 + 2 wt% Co-NP (e) 0 h and (f) 192 h of EM.

On the other hand, the average value of tensile strength for the SAC305+2 wt% Co-NP solder joint is found to be 88.19 MPa at 0 h and 78.17 MPa at 192 h EM test. Overall the tensile strength of the SAC solder was decreased by 63% after EM. For Ni NP containing solder joint tensile strength decreased by 23.5% after 192 h of current stressing. Whereas tensile strength of Co-doped SAC305 solder joints down trend by 11%. The tensile strength was degraded in all type of solder joints after the electromigration test. In the case of the SAC305 solder joint, the strength degraded significantly because of electromigration damage. But in the Ni and Co NP-doped solder joints, the electromigration damage were minimized due to which the degradation of mechanical strength was significantly reduced compared to the SAC305 solder joint.

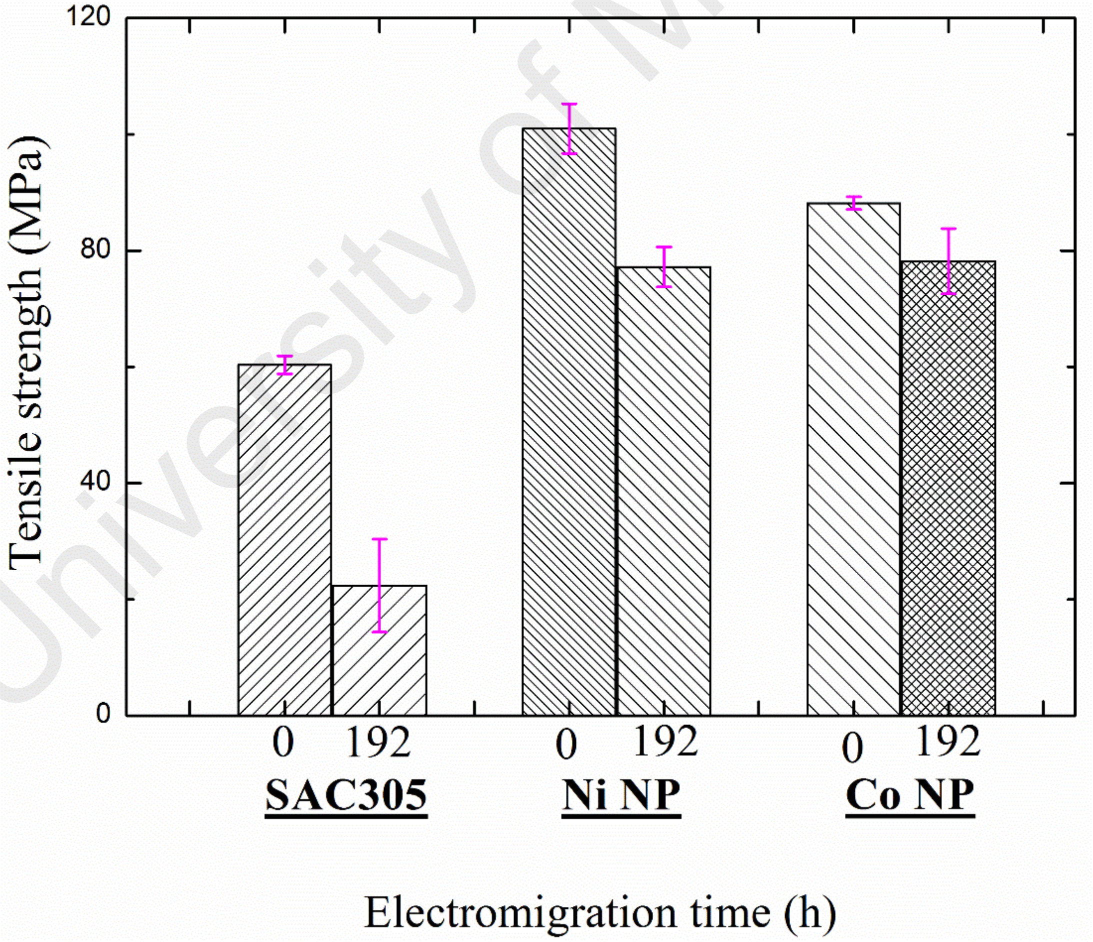

Figure 4.20: Tensile strength of the SAC305, SAC305 + 2wt% Ni-NP and SAC305 + 2wt% Co-NP solder joints after reflow and after electromigration for 192 h.

4.5.3 Fracture behaviour

Figure 4.21 and Figure 4.22 show typical fracture path in the SAC305, SAC305 + 2 wt% Ni NP and SAC305 + 2 wt% Co-NP solder joints before and after electromigration test. The SAC305 solder joints exhibit ductile fracture (Figure 4.21a) and the fracture occurred inside the bulk at 0 h of EM. A cup-and-cone type fracture is visible in Figure 4.21a. The fracture path after 192 h of EM for the SAC305 solder joint can be seen in Figure 4.22a. After EM test for 192 h, the fracture path of the SAC305 solder joint shifted to the cathode side. The fracture occurred in brittle manners.

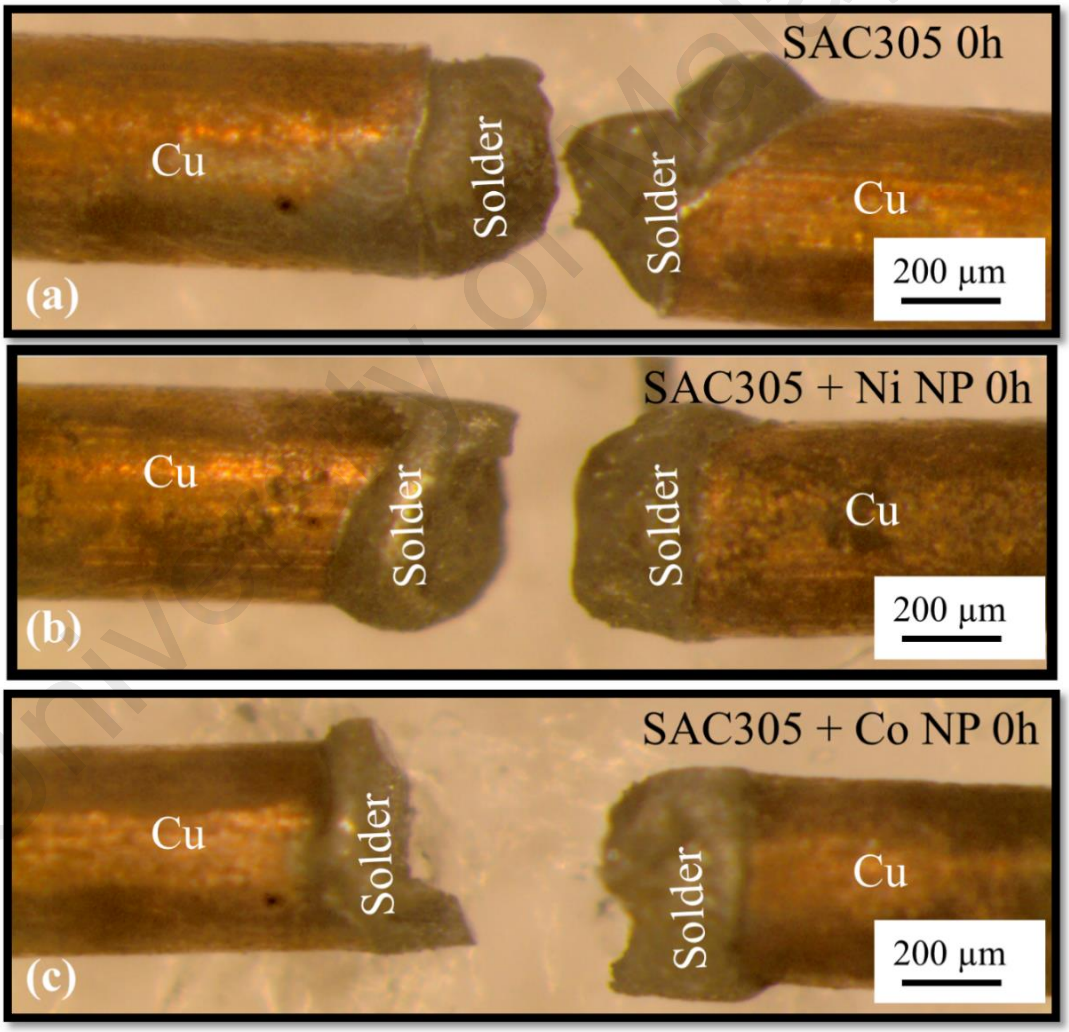

Figure 4.21: Description of fracture path in (a) SAC305, (b) SAC305 + 2 wt% Ni-NP doped and (c) SAC305 + 2 wt% Co-NP doped solder joints at 0 h and 192 h EM test.

In Ni NP-doped solder joints, the fracture path is still inside the bulk solder at 0 h of EM, but the solder appears to show lower ductility (Figure 4.21b). The fracture path after 192 h of EM for the SAC305 + Ni solder joint can be seen in Figure 4.22b. After EM test, the fracture path remained inside the solder bulk. The fracture path of the SAC305+2wt Co-NP solder joint is shown in

Figure 4.19c at 0 h and Figure 4.22c at 192 h of EM. At 0 h the fracture appeared in the solder bulk and fracture showed lower ductility. After EM of 192 h, the fracture progressed partly at the cathode interface and partly at the solder bulk.

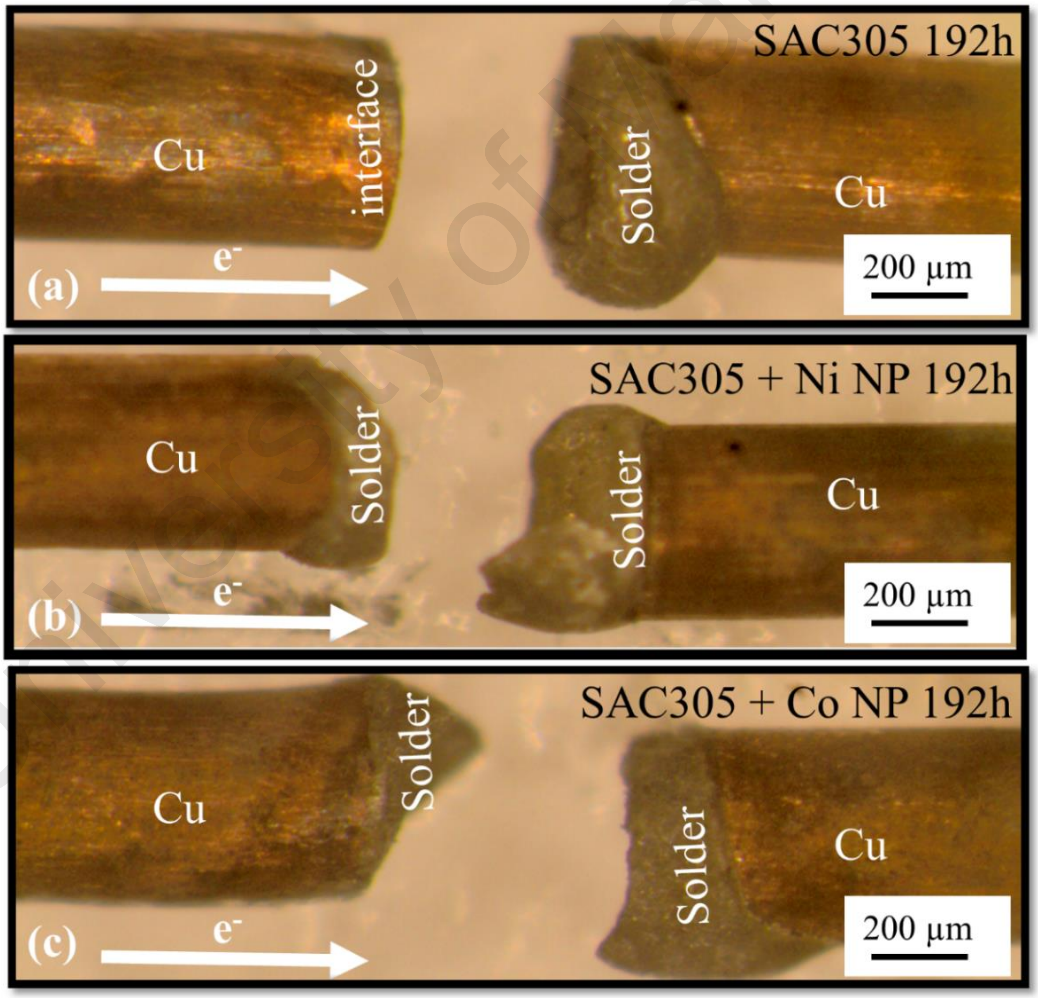

Figure 4.22: Description of fracture path in (a) SAC305, (b) SAC305 + 2 wt% Ni-NP doped and (c) SAC305 + 2 wt% Co-NP doped solder joints at 0 h and 192 h EM test.

CHAPTER 5: DISCUSSION

5.1 Reactive dissolution of nanoparticle in SAC305 solder

This study has focused on the effects of the addition of Ni and Co metallic nanoparticle (NP) to the SAC305 solder joints by flux mixing. Commercial water-soluble flux mixed with 2 wt% Ni and Co-NPs were used for solder preparation. The resulting effects on the microstructure of interfacial IMC and solder matrix and the electromigration performance of the solder joints have been investigated. During the reflow process, nanoparticle incorporated into the interfaces and in the solder matrix (Figure 5.1). It is seen that the addition of Ni and Co-NP to the flux has a decisive influence on the as-reflowed microstructure of the solder joint at the interfaces as well as in the matrix. Ni and Co-NP addition changed the usual scallop type morphology of Cu_6Sn_5 into a planer type. Ni and Co-NPs particles also decreased the area of the β-Sn grain in the matrix and IMC particles in the eutectic region.

In earlier studies, researchers added the Ni and Co into the solder joint by using different technique such as, paste mixing technique (Haseeb & Leng, 2011; Tay et al., 2013), alloying method (Bobet, Akiba, & Darriet, 2001; Bobet, Akiba, Nakamura, & Darriet, 2000; Yano, Kataoka, Yamashita, Uchida, & Watanabe, 2007) and doped flux technique (Sujan et al., 2014; Sujan et al., 2017). They also observed that Ni and Co-NP underwent reactive dissolution during reflow and entered into the solder joint. It is therefore suggested that when Ni and Co-NPs doped fluxes are applied to the solder ball/substrate interface, Ni and Co NPs undergo reactive dissolution and are incorporated into the solder joint through in-situ alloying. It was reported earlier that when Ni and Co NPs were added to solder paste, less than one-third of Ni and Co entered into the solder joint after reflow. The rest was discarded to the flux residue. In the present case, Ni and Co-NP are added to the flux at 2 wt%. It is highly likely that only a fraction of it entered the solder. It is difficult to find out exactly how much of Ni and Co NPs are retained in the solder matrix and how much at the interfaces.

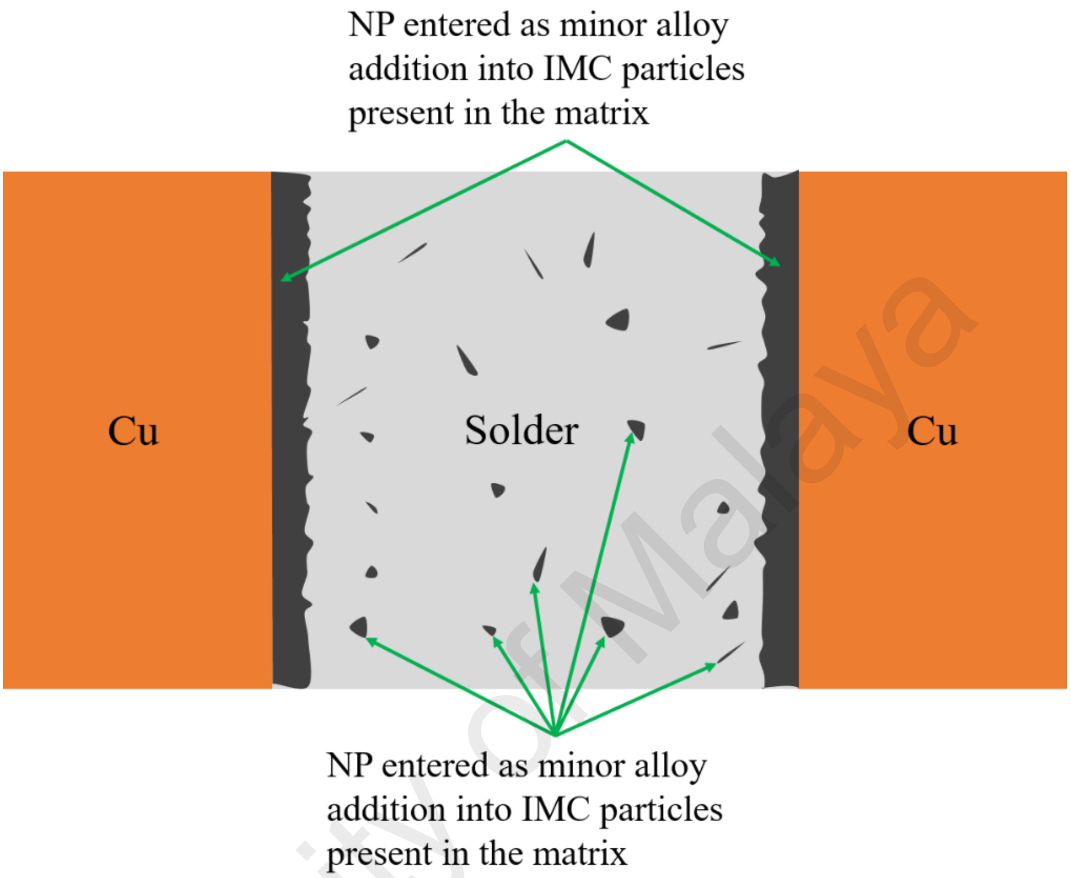

Figure 5.1: Schematic diagram of SAC305 + NP-doped solder joint which represents the incorporation of NP into the SAC305 solder joint during the reflow process.

However, it is clear that doping of the flux with 2 wt% Ni and Co NPs resulted in the incorporation of enough Ni and Co in the solder so as to have a distinct influence. Ni and Co-NP addition are also seen to influence the characteristics of the solder joint which is suggested to be related to the alloying effect. Sujan et al. added 0.1 wt% Co into the SAC305 solder joint. They estimated the amount of NP entered into the solder joint during reflow in doped flux method (Sujan et al., 2017). The calculation was made based on the amount of flux used in doped flux material, the amount of solder alloy and the rate of incorporation of NP into a solder joint. The amount of NP which was incorporated into a solder joint by doped flux technique was estimated to be 500 ppm (Sujan et al., 2017).

During the reflow process, Ni and Co-NP can undergo rapid diffusion in the liquid solder which is mainly liquid Sn in the present study. In previous studies, the diffusion coefficient of Ni, Sn, Zn, Ag, Cu and Al in liquid Sn was calculated in the temperature range of 240°C-280°C (Careri & Paoletti, 1955; Ma & Swalin, 1960). The calculated values of diffusion coefficient for Ni, Sn, Zn, Ag, Cu and Al in liquid Sn obtained by the researchers are given in Table 5.1. Based on the value of diffusion coefficient of Ni in liquid Sn, the distance traveled by Ni in liquid Sn can be calculated for the current study by using the following equation.

$$x^2 = Dt \tag{5.1}$$

Where,

x = distance traveled by Ni during the reflow

D = diffusion coefficient of Ni

t = reflow time.

In the present study, the solder was reflowed for 45 seconds under 245°C for which the distance traveled by Ni atoms into liquid Sn was calculated to be 1017.3 μm. It should be noted that during the reflow process, the effect of Marangoni flows and effect of convection will further increase the travelling distance of the Ni atoms into liquid Sn. As the total thickness of solder joint in the present case is 200 μm then the Ni atoms are expected to travel and cover the whole solder joint. Indeed, EDX spot analysis confirmed the presence of Ni in different places in the solder joint. EDX analysis also detected the presence of Co in the solder matrix. As Ni and Co have similar reaction behavior with Sn, it is expected that the diffusion rate of Co will be close to the diffusion rate of Ni.

Table 5.1: Diffusion coefficient of different elements in liquid Sn.

Elements	Diffusion coefficient	References
Al	1.9×10^{-3} cm^2/s	(Ma & Swalin, 1960)
Zn	6.2×10^{-4} cm^2/s	
Ag	2.6×10^{-4} cm^2/s	
Cu	1.8×10^{-4} cm^2/s	
Ni	2.3×10^{-4} cm^2/s	
Sn	2.2×10^{-4} cm^2/s	(Careri & Paoletti, 1955; Ma & Swalin, 1960)

Based on binary Sn-Ni phase diagram (Schmetterer et al., 2007), the Ni and Sn form 4 types of intermetallic compounds; $NiSn_4$ Ni_3Sn, Ni_3Sn_2, and Ni_3Sn_4 and 13 kinds of variant reactions (Schmetterer et al., 2007; Belyakov & Gourlay) (Figure 5.2). But for soldering process, in presence of 99.67at % Sn and 231°C temperature, the Ni and Sn form only one eutectic reaction (L = (Sn) + Ni_3Sn_4) (Massalski & International, 1996; Nash & Nash, 1985). Earlier studies observed that during the reflow process, Ni atoms substitute the Cu atoms in the sublattice of Cu_6Sn_5 IMC in the bulk of the solder joint (Gao, Qu, & Takemoto, 2010; Mattila, Laurila, & Kivilahti, 2005; Tay et al., 2013). In the present study, a very small amount of Ni was added into the solder joint most of which will enter into Cu_6Sn_5 phase and formation of Ni_3Sn_4 will not take place due to a shortage of Ni atoms. Ni also does not react with Ag_3Sn IMC particles during the reflow process (Lis, Park, Arroyave, & Leinenbach, 2014; Wang, Chin, Yeh, & Gan, 2015). The distribution of Ni at interfaces and in the matrix was investigated by EDX in the present study. It was found that Ni was mainly concentrated in the interfacial Cu_6Sn_5 layer. Ni was also detected in the Cu_6Sn_5 IMC particle in the matrix. Ni and Cu have similar face-centered cubic crystallographic structure. It has been found that Ni atoms substitute the Cu atoms in the sublattice of Cu_6Sn_5 IMC interfaces and in the bulk of the solder joint

(Gao et al., 2010; Mattila et al., 2005; Tay et al., 2013). The substitution of Cu with Ni reduces the formation energy of Cu_6Sn_5 and changes the IMC composition from Cu_6Sn_5 to $(Cu, Ni)_6Sn_5$. The change in the composition of IMC can be expressed by the following equation.

$$Cu_6Sn_5 + Ni \longrightarrow (Cu,Ni)_6Sn_5 \tag{5.2}$$

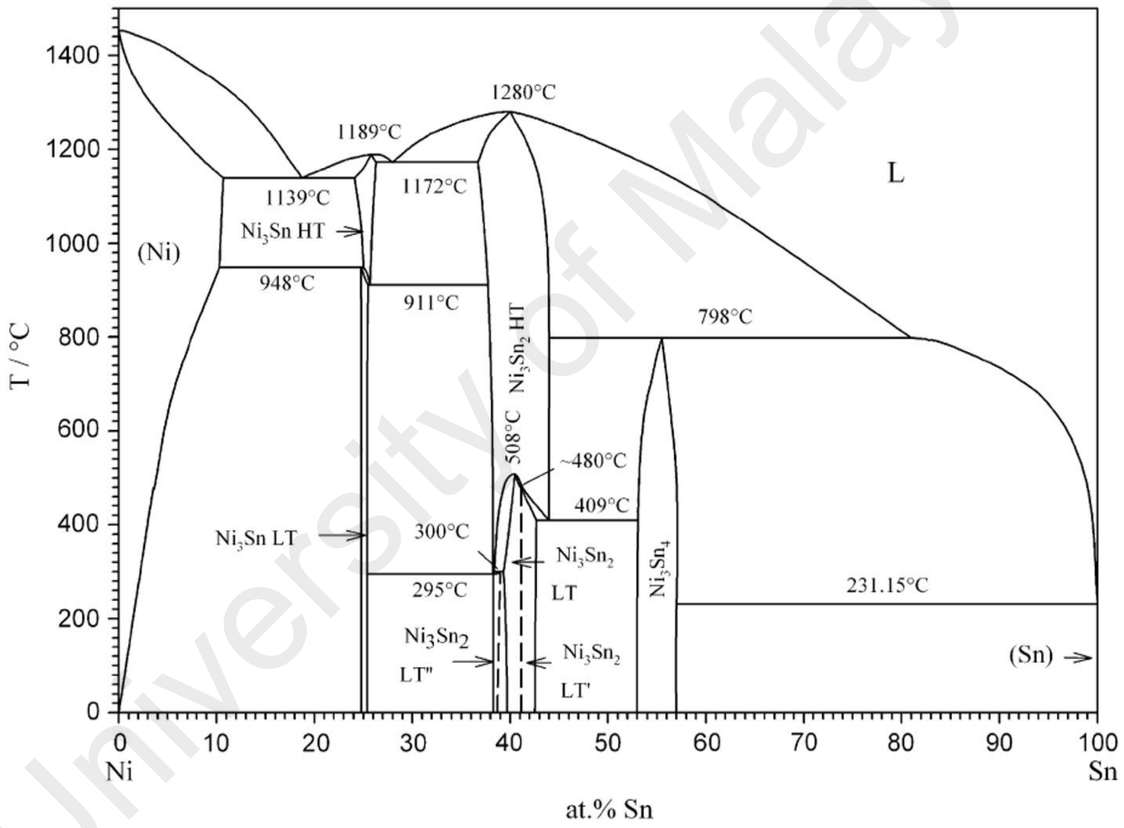

Figure 5.2: Binary Sn-Ni phase diagram from Ref. (schmetterer et al., 2007).

Based on Sn-Co phase diagram (Jiang, Sato, Ohnuma, Kainuma, & Ishida, 2004) (Figure 5.3), Sn-Co system forms 4 terminal solid solution (αCo) and (εCo) in the Co-rich region, (βSn) and (αSn) in the Sn-rich region. This system also forms 6 kinds of intermetallic compound (βCo_3Sn_2, αCo_3Sn_2, CoSn, $CoSn_2$, $\beta CoSn_3$ and $\alpha CoSn_3$). The formation of IMCs and the formation of the invariant require a high percentage of Co and Sn. But in the present study, a very low percentage of Co was used. Thus Sn will not form any IMC when there is a very small percentage of Co during the reflow process. Earlier studies also suggested that Co does not form IMC with Ag_3Sn during the reflow process (Chen, Chen, Chang, Hsu, & Chen, 2014; Yakymovych, Mudry, Shtablavyi, & Ipser, 2016).

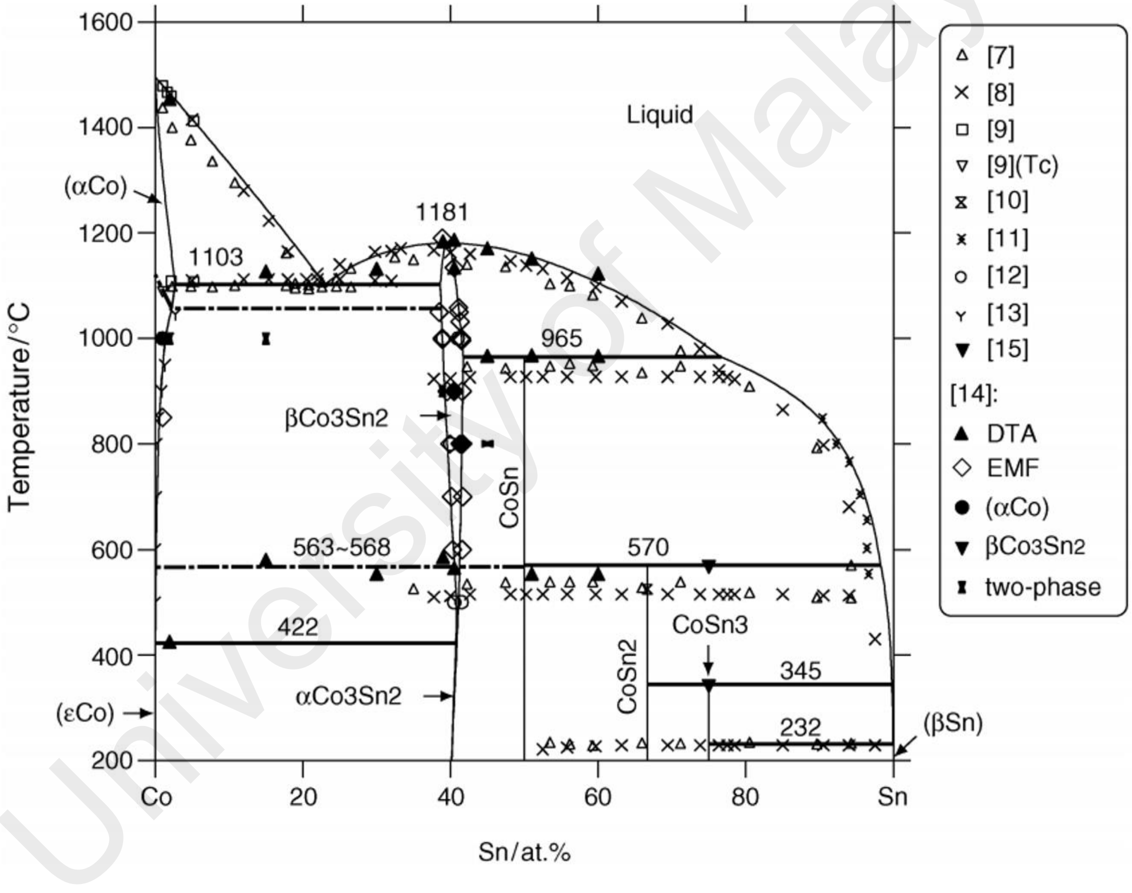

Figure 5.3: Binary phase diagram of Sn-Co from Ref. (M. Jiang et al., 2004).

In the past, it has been found that Ni (Tay et al., 2013), Co (Haseeb & Leng, 2011)and Zn (Haseeb et al., 2014) nanoparticle mainly dissolve in Cu_6Sn_5. This has indeed been confirmed for Co nanoparticle in the present work by EDX analysis. The composition of interfacial IMC has also been changed from Cu_6Sn_5 to $(Cu, Co)_6Sn_5$ in Co-NP doped joints.

$$Cu_6Sn_5 + Co \longrightarrow (Cu, Co)_6 Sn_5 \tag{5.3}$$

Gao et al. (Gao, Takemoto, & Nishikawa, 2006) who also obtained similar results suggested that during IMC formation, Co atoms enter the Cu sublattice of Cu_6Sn_5 and substitutes some of the Cu atoms leading to the formation of $(Cu, Co)_6Sn_5$.

5.2 Effect of nanoparticle on microstructure after reflow

Significant influences of metallic nanoparticle were detected on the microstructure of interfacial IMC and solder matrix of the SAC305 solder joint. These influences are explained in detail in the following subsections.

5.2.1 Effect on interfacial IMC

The formation enthalpies of Cu_6Sn_5 to $(Cu, Ni)_6Sn_5$ and $(Cu, Co)_6Sn_5$ were calculated by Zhang et al. (Zhang et al., 2016) in the past. It was found that Ni reduces the formation enthalpies of Cu_6Sn_5 phase. The reduction in the formation enthalpies was found to be in the range of -40meV/atom to -100meV/atom in Ni-containing Cu_6Sn_5 IMC phases (Zhang et al., 2016). Gao et al. have also shown using a thermodynamic calculation that $(Cu, Ni)_6Sn_5$ and $(Cu, Co)_6Sn_5$ IMCs are comparatively more stable than Cu_6Sn_5 (Gao, T Takemoto, & H Nishikawa, 2006). They concluded that Ni-Sn and Co-Sn have a higher affinity as compared with Cu-Sn. The higher affinity of Ni-Sn and Ni-Co increase the nucleation rate of IMC in interfacial layer (Gao et al., 2006). This also promotes a planar interfacial IMC morphology (Sujan et al., 2014; Sujan et al., 2017). In a previous study (Sujan et al., 2014; Sujan et al., 2017; Tay et al., 2013), after the addition of Ni and Co-NPs, the interfacial IMC morphology was refined and was more planar which indicates that the nucleation rate of IMC was increased after the addition of Ni and Co-NPs. The addition of Ni and Co-NP also reduces and refines the grain area of IMC which improves the mechanical properties of the solder (Gao et al., 2006; Laurila, Vuorinen, & Paulasto-Kröckel, 2010). Moreover, Ni and Co-NP addition also suppresses the growth of Cu_3Sn and reduces void formation (Maeshima, Ikehata, Terui, & Sakamoto, 2016) which also improve the mechanical properties of the solder joint.

5.2.2 Effect on solder matrix

In the present study, it is observed that the addition of Ni and Co-NP doped flux reduced the area of the βSn grain in the solder matrix. It also reduced the thickness of IMC particles present in the eutectic region. Similar results were detected when the Co was added into the SAC305 solder as a minor alloying element (Ma, Belyakov, & Gourlay, 2016). It was found that Co significantly suppressed the nucleation undercooling of β-Sn (Cheng, Nishikawa, & Takemoto, 2008; Cho, Kim, Seo, & Lee, 2009; Kim, Cho, Seo, & Lee, 2009; Song, Huang, & Chuang, 2006). The addition of Co refined and reduced the area of β-Sn grain and improved the mechanical strength of the solder joint (Ma et al., 2016). It was observed that β-Sn nucleation undercooling suppressed from 14.6 K to 0.2 K after addition of 0.05 wt% Co and area of β-Sn significantly reduced from 378 μm to 175 during the reflow process (Ma et al., 2016). Daly et al. investigated the effect of minor alloying Ni and Sb on SAC105 solder joint (El-Daly, Hammad, Fawzy, & Nasrallh, 2013). They found that Ni and Sb significantly reduced the undercooling, refined the Sn grains and increased the eutectic area in the matrix. Similar results were found when Ni and Co were added together into the SAC305 solder as a minor alloying element (Cheng et al., 2008). Hence it can be said that after addition of Ni and Co-NP doped flux into the SAC305 solder, Ni and Co entered into the solder matrix during the reflow process and influenced the nucleation undercooling of β-Sn. Ni and Co suppressed the area of β-Sn grain and increased the eutectic area significantly. In the present study, IMC particles were found in the solder matrix of the doped and undoped solder joint. In the case of the undoped solder joint, the thickness of IMC particles was smaller while it was larger in NP-doped solder joints (Figure 4.1 and Figure 4.8). EDX analysis confirmed the particles as Cu_6Sn_5 IMC in the undoped solder joint while $(Cu, Ni)_6Sn_5$ and $(Cu, Co)_6Sn_5$ IMC in the Ni and Co-doped solder joint. The occurrence of Cu-Sn based IMC particles in the solder matrix may result from spalling of interfacial IMC. During the interfacial reaction process, some of the IMC particles move from interface to the solder matrix. This process is called spalling of IMC particles. Spalling of Co-Sn and Ni-Sn IMC was commonly observed by researchers during the interfacial reaction process (Ho, Lin, Yang, Kao, & Jiang, 2006; Hong, Lee, & Wu, 2013; Kim et al., 2009; Sharif & Chan, 2007; Sohn, Yu, Kang, Shih, & Lee, 2004). The researchers suggested that the possible reason of spalling is a limited supply of Cu atom from the SAC305 joint at the interfaces during reflow (Ho et al., 2006). As $(Cu, Ni)_6Sn_5$ and $(Cu, Co),_6Sn_5$ are Cu-bearing IMC and due to the limited supply of Cu from the solder side to the interface affect the interfacial reaction. Reduction in Cu supply changes the equilibrium phase of interfaces and destabilizes the interfacial IMC layers which result in the spalling of the IMC into solder matrix (Ho et al., 2006). IMC spalling was suggested as a reliability concern because too much spalling may cause dewetting in molten solder (Kim, Jang, Lee, & Tu, 1999; Liu, Chen, Mal, & Tu, 1999). Excessive spalling may decrease the shear strength and tensile strength of the solder joint (Liu et al., 1999). In the present study, the extent of spalling was limited. In spite of IMC spalling, Ni and Co improved the tensile strength. Improvement of microstructure viz., refinement of both interface and matrix structure is believed to have contributed to the improved properties of NP added solder.

5.3 Influence of nanoparticle on solder after electromigration

With a high-current density (order of 1×10^4 A/cm^2), EM usually influences migration of Cu atoms from the substrate to the solder joint. This leads to reliability concern for the solder joint. The rapid growth of IMCs at the interface could be well controlled by managing the diffusion of Cu atoms from the substrate. Other than current density, diffusion of Cu atoms also depends on temperature and duration of EM. Therefore, the duration of EM test was increased to see the further effect on Cu diffusion. In the SAC305 solder joint, a substantial increase of IMC thickness at the anode side was observed during the study with a decrease at the cathode side as the duration of EM test increased. High-current density causes heavy electron wind flow through the sample. Cu atoms start to migrate in the direction of electron flow from the cathode towards the anode side because of drifting caused by a collision with the electrons. Gradually, Cu atoms begin to form a thicker layer of IMCs such as Cu_6Sn_5 at the anode side by reacting with Sn atoms present at anode side (Gan & Tu, 2005). If IMCs become thicker, it could reduce the mechanical reliability of the solder joints because of brittleness in the IMC's structure (Ren et al., 2006). On the other hand, directional migration of Cu atoms towards the anode side creates vacancies, cracks, and voids in the cathode side (Zhao et al., 2013). Serrated cathode dissolution phenomenon was found in the SAC305 solder joint after a long period of EM. The addition of a small quantity of Ni and Co NPs slowed down the dissolution process at the cathode. Figure 5.4 shows the schematic diagram representing microstructure changes at the interfaces of the SAC305, SAC305 + 2 wt% Ni NPs and the SAC305 + 2 wt% Co NPs solder joints before and after EM. During EM, Cu atoms are accumulated at anode but depleted at the cathode which results in more vacancies at the cathode than at the anode side as proposed in the Nabarro-Herring model. The results of the current study show that in the SAC305 + 2 wt% Ni NPs and the SAC305 + 2 wt% Co NPs solder joints, Cu diffusion was suppressed significantly. It also reduced Cu diffusion into the solder joint and resisted the rapid growth of interfacial IMCs at the cathode and anode side. Similarly, Ran et. al found the suppression of Cu diffusion by the addition of Ni and Co in the SAC solder joint (Tu et al., 2001; Zhao et al., 2013). After migration of Cu atoms the created vacancies at the cathode side produce voids at interfaces.

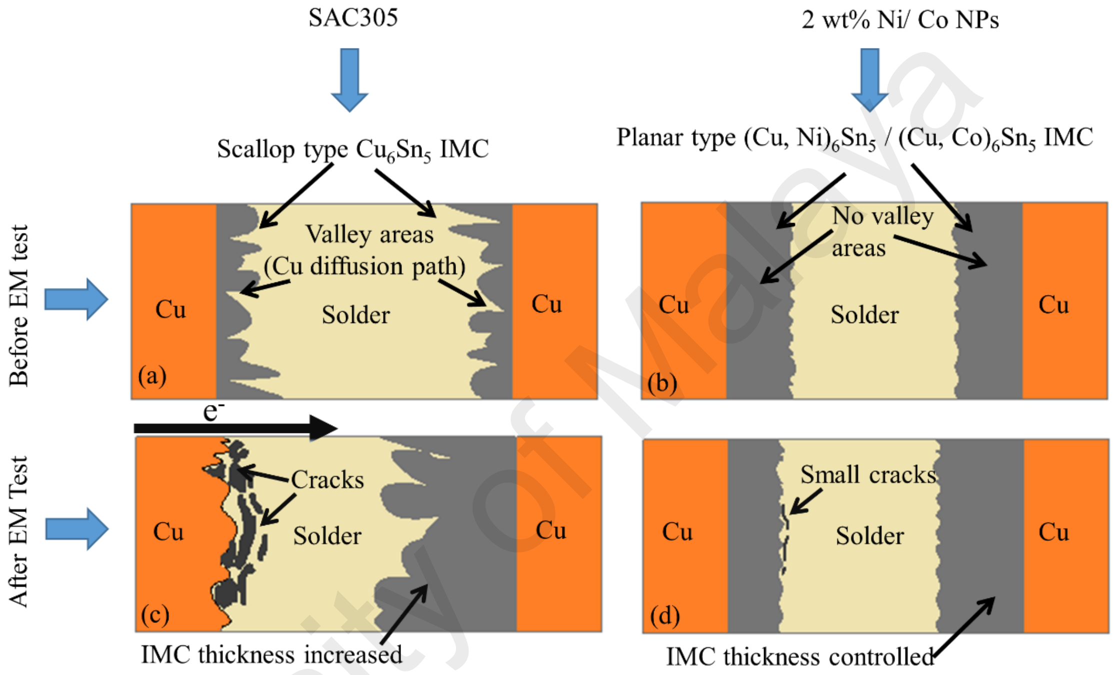

Figure 5.4: Schematic diagrams presenting microstructure changes in the SAC305 and Ni/Co-NP- doped flux solder joints (a, b) before while (c, d) after EM test.

These voids reduce the conductivity of current and increase the resistance in the solder joint (Chang, Liang, & Chen, 2006). In this case, heavy electron wind changes its conducting path and tries to flow from the connected area of the joint. Most of the electron wind leaves the disconnected area of joint and attacks at the connected area which causes the non-uniform distribution of current at that area. Non-uniformity of current distribution and joule heating effect are the root causes of Cu diffusion. Due to joule heating effect, Cu atoms get more energy to leave their position and increase the Cu diffusion rate, produce more void and cracks at the cathode side(Hsu & Chen, 2013; Sun et al., 2011; Xie et al., 2014), increase the rapid growth of IMC at anode side (He, Xu, & Guo, 2010) and finally lead to the failure and separate the solder joint from substrate at the cathode interfaces. It is observed that Ni and Co nanoparticle can reduce the formation of cracks which leads to better resistance stability as compared to the SAC305 samples. From all the experiments, the positive effects of Ni and Co addition on solder joints are found.

The reasons for the improved EM failure resistance of Ni and Co-NP doped solder can be related to a number of factors including i) favorable interfacial IMC morphology (Chen et al., 2010; Lingyun Zhang et al., 2006), ii) improved stability of interfacial IMC layer when Co and Ni dissolves in it (Gao et al., 2010, iii) change in microstructure and grain orientation (Huang, Yang, Ke, Li, & Kao, 2013; Yang et al., 2015), iv) segregation of Co atoms to grain boundaries (Hu, Nozawa, Koizumi, Fujiwara, & Uda, 2015; Westbrook, 1964). These factors are briefly discussed below.

It has been found (Chen et al., 2010; Lingyun Zhang et al., 2006) that scallop type morphology of the interfacial Cu_6Sn_5 IMC layer facilitates the rapid diffusion of Cu atoms from the substrate to the solder. This is because Cu atoms can diffuse faster through the valleys between the scallops as the valleys provide shorter diffusion paths. In the present study, the addition of Ni and Co-NP has changed the scallop shaped interfacial IMC into a planar one. The planar IMC morphology eliminates the valleys between scallops and eliminates the shorter diffusion channels for Cu atoms (Figure 5.4). This is believed to have contributed to the improved EM resistance in Ni and Co-NP doped solders. Gao et al. Investigated the thermodynamic stability of $(Cu, Co)_6Sn_5$ and $(Cu, Ni)_6Sn_5$ IMCs compared with Cu_6Sn_5. During electromigration, Cu atoms from the substrate have to pass through the interfacial IMC layer. Higher stability of $(Cu, Ni)_6Sn_5$ and $(Cu, Co)_6Sn_5$ in Ni and Co-doped solder means that the release of Cu atoms through this layer will be slower compared with that through the Cu_6Sn_5 interfacial IMC layer in the undoped SAC305 sample. This is also believed to have contributed to the increased EM resistance of Ni and Co-doped solder. It has been suggested (Huang, Yang, Ke, Li, & Kao, 2013; Yang et al., 2015) that Cu diffusion can also be slowed down by controlling the orientation of βSn grains in solder. Cu atoms require an activation energy of 16.8 kJ/mole to diffuse along the c-axis. While an activation energy of 33.18 kJ/mole is needed for Cu atoms to diffuse along a- axis (Yang et al., 2015). Thus, electromigration resistance can also be improved by controlling the crystallographic orientation of grains in solder joints (Huang et al., 2014; Wang et al., 2012). It is beyond the scope of this study to find out the effect of Ni and Co-NP addition on the orientation of solder grains. Further studies are suggested to be conducted along this direction. It is known that solute atoms can segregate to grain boundaries in an effort to minimize the free energy of the system (Hu, Nozawa, Koizumi, Fujiwara, & Uda, 2015; Westbrook, 1964). Thus, Ni and Co atoms by segregating to solder grain boundaries can retard the grain boundary diffusion of Cu atoms during electromigration. Further study is necessary to confirm this in Ni and Co-doped solders.

5.4 Effect of NP-doped flux on kinetics of anodic IMC formation

Thermodynamic investigation reveals that two kinds of driving forces are responsible for mass transportation during electromigration process (Lu, He, En, Wang, & Zhuang, 2009). These forces accelerate atom diffusion towards anode which results in rapid growth of IMC at the anode side. One force is called chemical force J_{chem} while another one is an electrical force J_{em}. The electromigration flux equation can be expressed as (He et al., 2010).

$$j = J_{chwm} + J_{em} = C\frac{Df}{kTm}\left(-\frac{\partial\mu}{\partial\mu}\right) + C\frac{Df}{kTm}Z^{*}ej\rho \qquad (5.4)$$

Where,

C = concentration,

Df = the diffusivity,

K = Boltzmann’s constant,

Tm = the absolute temperature,

$\partial\mu \ / \ \partial\mu$ = chemical potential gradient,

Z^* = the effective charge number,

e = the electron charge,

J_{em} = electrical force, J_{em}

J_{chem} = chemical force,

p = is resistivity.

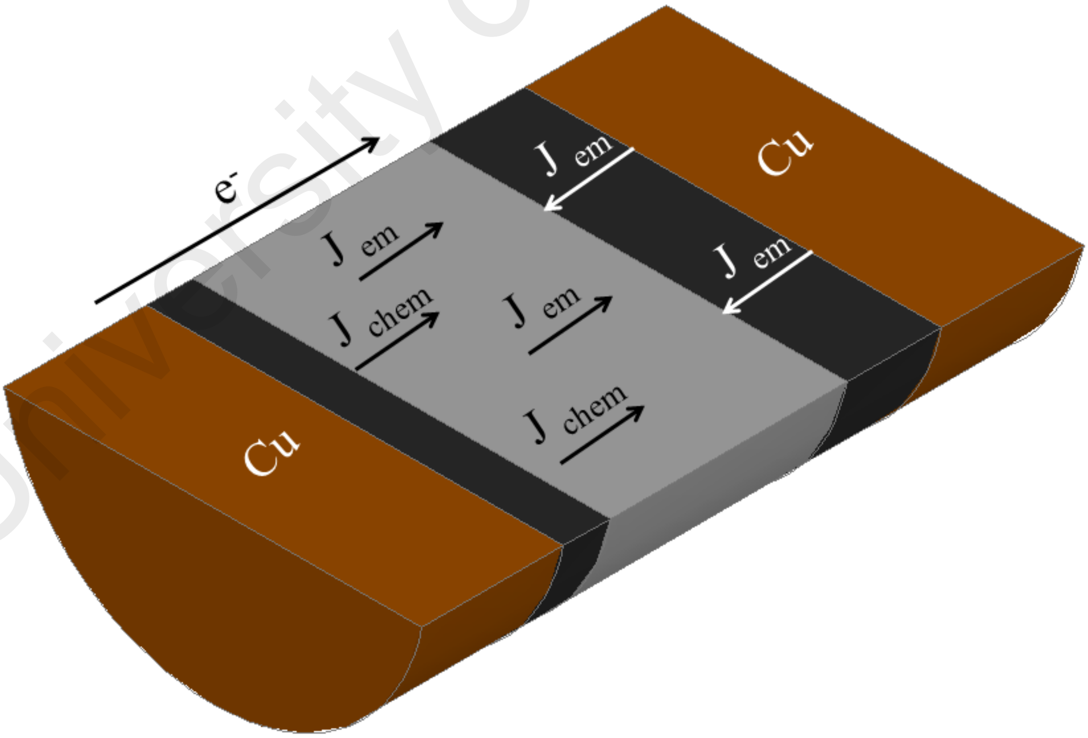

Figure 5.5: Schematic diagram illustrating the contribution of chemical and electrical forces during EM test.

In the absence of J_{em}, the J_{chem} usually enhances the both interfaces of the solder joint but in the presence of electric force, both forces work competitively. If J_{em} is higher than the anode side, IMC growth will be accelerated while at the cathode side it will be retarded. But if J_{em} is weaker, then J_{chem} will accelerate IMC growth at the cathode side as well. In the present study, a high-current density was applied during electromigration test. Due to which the influence of J_{em} was higher than the chemical force. Higher influence of J_{em} creates electromigration damage at the cathode interface and the thickness of anodic IMC layer rapidly increased (Figure 5.5). But after addition of 2 wt% Ni and Co-NPs doped flux, the effect of J_{chem} and J_{em} forces will be reduced due to which the electromigration damage decreased and the average anodic growth rate of $(Cu, Ni)_6Sn_5$ IMC decreased by five and seven times compared to Cu_6Sn_5.

Further analysis was performed to investigate the kinetics of IMC growth at anodic interfacial by using the following equation (Chiu & Lin, 2012):

$$d = A\exp\left(-\frac{Q}{RT}\right)t^n = kt^n \tag{5.5}$$

Where,

d = is the thickness of anodic interfacial IMC,

Q = is activation energy of IMC formation,

T = is the absolute temperature,

t = is Electromigration time,

k = is the growth rate constant,

A = constant,

n = constant.

The estimation of n and k values can be done by fitting following equation which is derived from taking the natural log of equation 5.5 (Chiu & Lin, 2009, 2012).

$$\ln d = \text{const} + n \ln t \tag{5.6}$$

Where ln t is independently variable and ln d is the dependent variable. The researchers found that there are two type of IMC growth mechanism (1) diffusion-controlled mechanism and (2) reaction-controlled mechanism (Chiu & Lin, 2009, 2012). The diffusion-controlled mechanism occurs during the aging process and reaction-controlled mechanism occurred during the electromigration process. The n value for the diffusion-controlled mechanism is estimated to be 0.5 (Chao et al., 2006; Chao et al., 2007). In the case of electromigration, the value of n was found to be 0.88 in the past (Chiu & Lin, 2009). In the present study, the curve fitting can be seen in Figure 5.6. The calculated values of these parameters are tabulated in Table 5.2. In the present study, a similar value of n was found which is 0.88. For comparison, a couple of literature data are also shown. In the present study, the value of n for the SAC305 solder was estimated to be 0.88. While the value of n was found to be 1.2 and 1.4 for the Ni and Co NP-doped solders. Usually, n value is expected to be 0.5 for a diffusion controlled process (Chen et al., 2010; Hu, Chan, Zhang, & Yung, 2013). However, in our study, the obtained values of n is greater than 0.5. This indicates the effect of the additional driving force applied by a strong electric wind. The significant influences of NPs doped flux can be seen by comparing the values of growth rate constant, k for all kinds of samples. The k value of

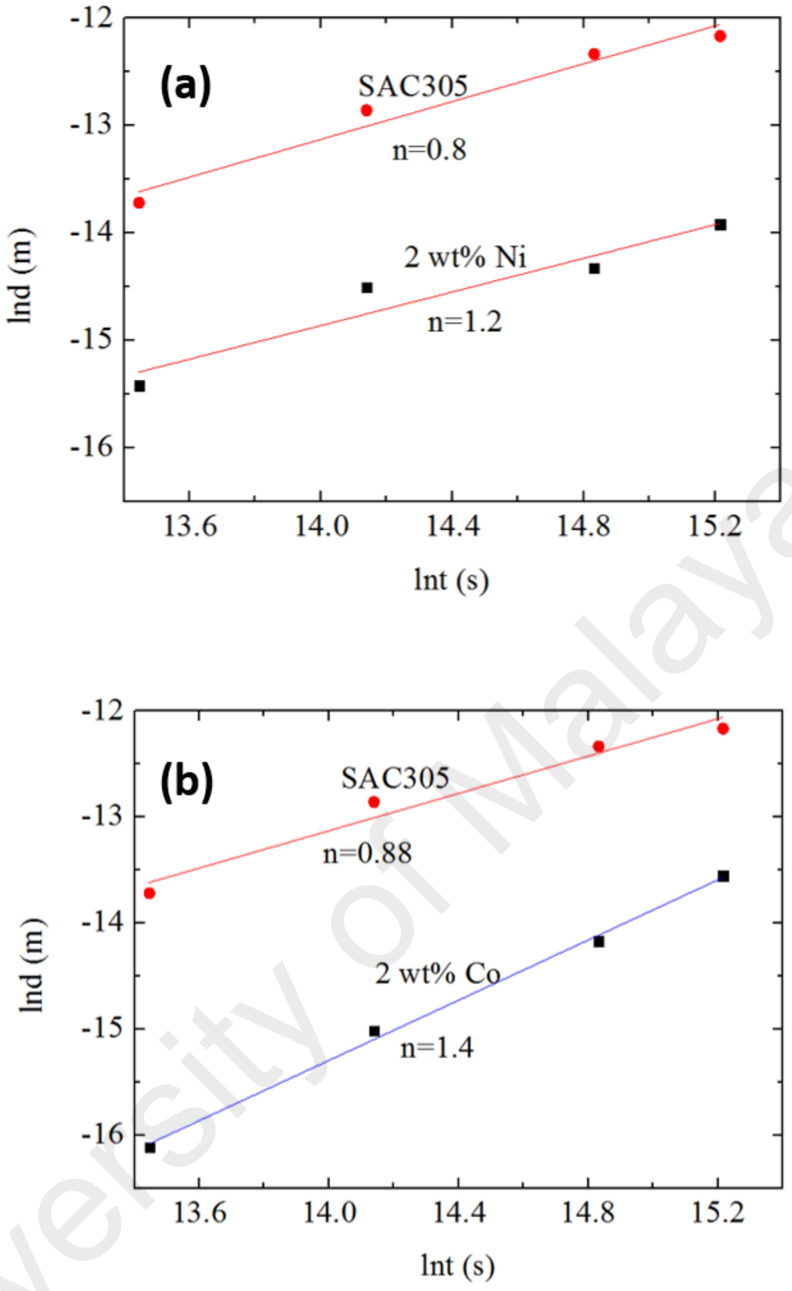

Figure 5.6: Estimated value of constant n of equation (5.3) by using curve fitting technique (a) Ni-doped solder joint (b) Co-doped solder joint.

the SAC305 solder was calculated to be 8.85 × 10^{-12} m^2/s (Table 5.2). The values of k obtained under the same experimental conditions as used in this study are not available in the literature for a direct comparison. A couple of k values obtained by Chiu and Lin (Chiu & Lin, 2009), although under different experimental conditions, seem to be reasonably close to the value obtained here for SAC. The values of k for Ni, Co-doped solder were calculated to be 1.01×10^{-16} and 6.31×10^{-16} and which is much smaller than the corresponding value for the SAC305 solder.

Table 5.2: Comparison of the estimated value of n and k with literature.

Composition	n	k **(m^2/s)**	**Current density A/cm²**	**Temp T(k)**	**Maximum EM time t (h)**	**References**
Cu/SAC+Ni/Cu	1.21	1.01×10^{-16}	1.0×10^{4}	353	1128	Present study
Cu/SAC+Co/Cu	1.40	6.31×10^{-16}	1.0×10^{4}	353	1128	
Cu/SAC/Cu	0.88	8.85×10^{-12}	1.0×10^{4}	353	1128	
Cu/Sn3.5Ag/Au	0.88	-----	2.6×10^{3}	393.15	480	(Chiu & Lin, 2012)
Cu/SAC/Cu	0.65	5.72×10^{-13}	1.0×10^{3}	343	360	(Chiu & Lin, 2009)
Cu/SAC/Cu	0.63	1.41×10^{-12}	2.0×10^{3}	343	360	

5.5 Effect of nanoparticle doping on Cu diffusion

During EM, the high-current density applies force on the atoms present at the cathode interfaces of the solder joint. It was found that Cu atoms require low activation energy compared to Sn atoms which result in rapid migration of Cu atoms from the cathode to anode side during EM (Yang et al., 2015). During EM, Cu migration from the cathode to anode side is expected to occur in two ways: one is Cu migration from Cu substrate and another one is Cu migration from interfacial IMC layer at the cathode side. In the first case, the Cu atoms from the Cu substrate migrate through the interfacial IMC layer during the EM. In scalloped shape interfacial IMC layers, the Cu atoms mostly migrate through the valley areas (Zhao et al., 2013) (Figure 5.7a). As the Ni and Co atoms change the morphology of interfacial IMC from scallop to planar shape so it eliminates this easy Cu diffusion path (Zhao et al., 2013) (Figure 5.7b). When Cu atoms try to migrate from the Cu substrate to anode side through the planar shape $(Cu, Ni)_6Sn_5$ and $(Cu, Co)_6Sn_5$ interfacial IMC layer then Ni and Co atoms react with diffused Cu atoms and reduce further diffusion. In the second case of Cu migration, Cu atoms rapidly migrate from

Cu_6Sn_5 interfacial IMC layer in undoped solder and reduce the thickness of IMC layer significantly. But when doped with Ni and Co atoms they reduce the Cu diffusion significantly from the $(Cu, Ni)_6Sn_5$ and $(Cu, Co)_6Sn_5$ interfacial IMC layers due to their higher thermodynamic stability (Gao et al., 2006). This retards the rapid reduction of IMC thickness at the cathode side. Ni and Co control the rapid growth of IMC at the anode interfaces and reduces the void and crack formation at the cathode side.

Thus it can be suggested that thermodynamic stability and refined geometry of interfacial IMC layer in Ni and Co-NP doped solder joints significantly retard the EM damage in the solder joint.

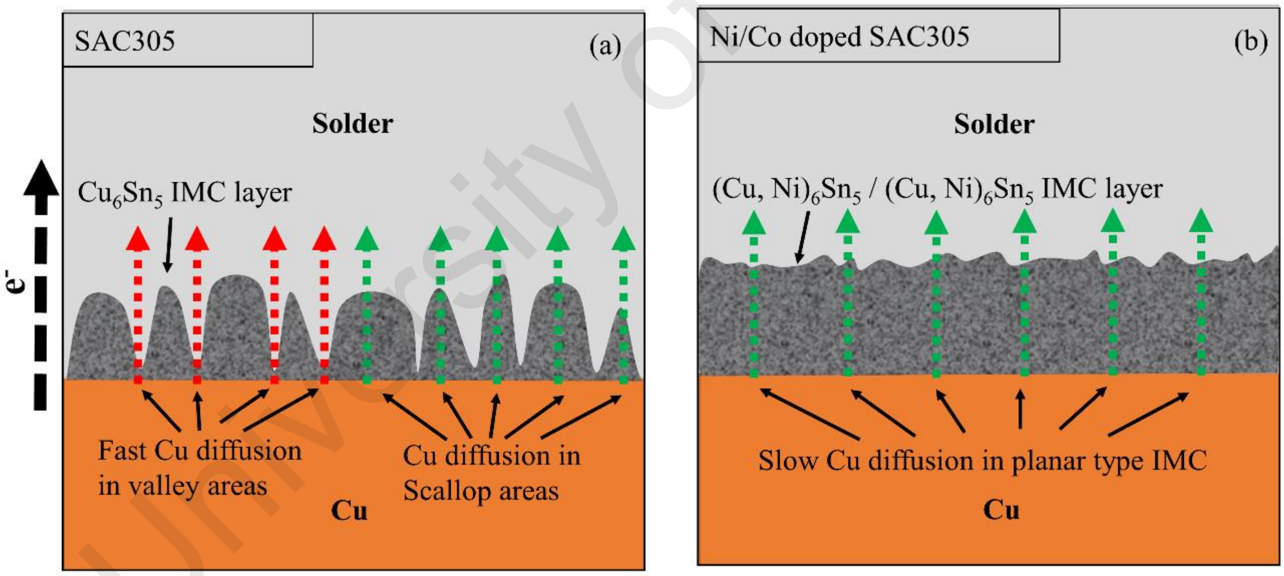

Figure 5.7: Schematic diagrams describing Cu migration in undoped SAC305 and Ni/Co NP-doped solder joint during EM.

5.6 Influence of Ni NP on tensile strength

In the present study, the Ni and Co-NP doped flux containing solder joints possess significantly higher values of maximum stress before EM tests. EM causes a lowering of the maximum tensile stress values. No significant changes are found in the values of maximum strain% before and after EM tests.

Table 5.3 illustrates the average tensile strength of Ni NP-doped solder joints calculated from the results of the present study. Corresponding values collected from the literature are also shown for comparison purposes. The strength of Co-doped solder was also investigated before and after the EM test in the present study. It is found that Co-doped solder showed similar behavior to Ni-doped solder, that is Co-NP doping helped to maintain high tensile strength after EM (Table 5.3). A comparison of strength values for doped and undoped solder joints with available literature values (Ren et al., 2006; Wei, Yao, & Shi, 2011; L Zhang et al., 2007) can also be seen in Table 5.3. Although values of different parameters used in the investigation described in the literature are not exactly the same as ours, our tensile strength values for undoped joints are reasonably close to literature values before and after EM.

Table 5.4 shows the average strain % of Ni NP containing solder calculated from the result of the present study. Literature values are also shown for comparison. The average strain % of Ni-doped solder was 0.37 % before the EM test and 0.35 % after the EM test. Although the average strain value of Ni NP-doped joints after EM seem higher, the average value of maximum strain % of undoped solder joints is found to be 0.65 % and 0.29 % respectively before and after EM. Literature values of a strain of undoped SAC solder joints (Ren et al., 2006; L Zhang et al., 2007) vary from each other (Table 5.4). But these are generally higher than the corresponding values found in our results for undoped solder. Strain values of Co-NP doped solder are close to that of Ni NP-doped solder (Table 5.4).

Table 5.3: Average tensile strength of Ni NP-doped solder joints and its correlation with literature.

Solder composition	EM parameters	Avg tensile Strength MPa		References
		Before EM	After EM	
Sn-3Ag-0.5Cu	J = 5 × 10^3 A/cm^2 T = 150 °C t = 0-192 h	60.34 ± 1.5	22.36 ± 8	Present study
Sn-3Ag-0.5Cu + Ni NP	J = 5 × 10^3 A/cm^2 T = 150 °C t = 0-192 h	100.99 ± 4.2	77.23 ± 3.4	
Sn-3Ag-0.5Cu + Co NP	J = 5 × 10^3 A/cm^2 T = 150 °C t = 0-192 h	88.18 ± 1	78.16 ± 5.6	
Sn-3Ag-0.5Cu	J = 1.78 × 10^4 A/cm^2 T = 100 °C t = 0-200 h	52	28	Estimated values from (Wei et al., 2011)
Sn-3.8Ag-0.7Cu	J = 5.03 × 10^3 A/cm^2 T = 145 °C t = 0-48 h	47	17	Estimated values from (Ren et al., 2006)
Sn-3.8Ag-0.7Cu	J = 3 × 10^4 A/cm^2 T = 145 °C t = 0-98.5 h	55	35	Estimated values from (Zhang et al., 2007)

The structural degradation of the interfaces can impose serious effects on mechanical performance of the solder joint. In the present study, it is observed that the fracture shifted to the cathode interfaces. The fracture was cup and cone shaped with ductile behavior before EM but after 192 h, it converted from ductile to brittle. Ren et al. (Ren et al., 2006) found that EM converts the ductile to brittle fracture and fracture path migrated to the cathode interfaces of the SAC solder joint. The value of maximum strain and stress also reduced (Ren et al., 2006). Kumar et al. also concluded that EM caused the brittle fracture in Sn-Ag solder due to high current density and as a result, the also degraded (Kumar et al., 2009). Wang et al. reported that by increasing the current stressing time the shear strength of the SAC solder decreased and the fracture migrated to the cathode interfaces with brittle behavior (Wang et al., 2010). Similar results were also reported elsewhere (Zhang et al., 2007). After the addition of Ni and Co-NP, the EM effects on the microstructures were reduced and the strength of IMC joints was improved significantly both before and after the EM test. No significant effect of EM was found on the fracture behavior of Ni and Co-NP containing solder joints. The maximum stress slightly decreased but no significant effect was found for maximum strain values after the EM test.

Table 5.4: Average maximum tensile strain of Ni NP-doped solder joint and its correlation with literature.

Solder composition	**EM parameters**	**Strain rate used for tensile tests**	**Avg maximum tensile Strain %**		**References**
			Before EM	**After EM**	
Sn-3Ag-0.5Cu	J = 5 × 10^3 A/cm^2 Temp = 150 °C time = 0-192 h	6.59 × 10^{-5}/s	0.65 ± 0.25	0.29 ± 0.16	Present study
Sn-3Ag-0.5Cu + Ni NP	J = 5 × 10^3 A/cm^2 Temp = 150 °C time = 0-192 h	6.59 × 10^{-5}/s	0.37 ± 0.12	0.35 ± 0.10	
Sn-3Ag-0.5Cu + Co NP	J = 5 × 10^3 A/cm^2 Temp = 150 °C time = 0-192 h	6.59 × 10^{-5}/s	0.33 ± 0.13	0.2 ± 0.02	
Sn-3.8Ag-0.7Cu	J = 5.03 × 10^3 A/cm^2 Temp = 145 °C time = 0-48 h	6 × 10^{-3}/s	0.52	0.35	Estimated values from (Ren et al., 2006)
Sn-3.8Ag-0.7Cu	J = 3 × 10^4 A/cm^2 Temp = 145 °C time = 0-98.5 h		0.97	0.89	Estimated values from (Zhang et al., 2007)

In the past studies, it was found that Ni and Co-NP doped flux reduced the area of the βSn grain in the solder matrix. It also reduced the thickness of IMC particles present in the eutectic region (Ma, Belyakov, & Gourlay, 2016). It was found that Co and Ni significantly suppressed the nucleation undercooling of β-Sn (Cheng, Nishikawa, & Takemoto, 2008; Cho, Kim, Seo, & Lee, 2009; Kim, Cho, Seo, & Lee, 2009; Song, Huang, & Chuang, 2006). Due to which the area of grain reduced and thickness of the eutectic region increased. Reduction in grain area improves the mechanical properties of the solder joint (Ma et al., 2016). IMC particles present in the eutectic region are brittle and reduce overall ductility of the solder joint. In the present study, it was observed that after addition of Ni and Co, the area of β-Sn grain was decreased and the area of the eutectic region was increased. Due to which Ni and Co containing solder joint showed less ductility compared to the SAC305 solder joint. Overall the addition of Ni and Co-NP-doped flux improved the structural properties of the SAC305 solder joint due to which the mechanical strength also improved. During the reflow process, Ni and Co-NP reduced the area of β-Sn in the matrix. Reduction in area of β-Sn improved the mechanical strength of the solder joint. Similar results were found when the Co and Ni were added into the SAC solder as a minor alloying element (Cheng et al., 2008; Ma et al., 2016). It was observed that the addition of Co and Ni refined and reduced the area of β-Sn which improved the mechanical strength of the solder joint (Cheng et al., 2008). Daly et al. investigated the effect of minor alloying Ni and Sb on SAC105 solder joint (El-Daly et al., 2013). They also observed that Ni and Sb refined and reduce the theickness β-Sn grain and improved the creep properties of the solder joint. Therefore, by correlating of our findings with literature, it can be concluded that reduction in area of β-Sn grain, thermodynamic stability of IMC, less variation in IMC size during EM, reduction in EM damage, favourable morphology of interfacial IMC and reduction in Cu diffusion could be some of the possible reasons for improvement in electrical and mechanical properties of Ni and Co-NP-doped flux containing solder joint after the EM.

CHAPTER 6: CONCLUSION

6.1 Conclusion

Two types of nanoparticle Ni and Co were introduced at the interfaces of Cu/SAC305/Cu solder joints by using the nanoparticle-doped flux technique. Based on the results obtained, the following conclusions can be made:

1. Ni and Co-NP doped flux have a decisive influence on the as-reflowed microstructure of the solder joints, both at the interfaces and in the matrix. During the reflow process, nanoparticle dissolved and got incorporated in the solder. Ni and Co-NP addition changed the usual scallop type morphology of interfacial Cu_6Sn_5 layer into a planer type and thermodynamically stabilized the IMC. Ni and Co-NP also decreased the area of the β-Sn grain in the matrix and the thickness of IMC particles in the eutectic region.

2. Ni and Co-NP significantly reduced the effects of EM at the cathode and anode sides. Ni and Co retarded the migration of Cu atoms at the cathode side. As a result the extent of EM damage, voids and cracks was reduced at the cathode side, while the rapid growth of anodic interfacial IMC layer was significantly halted. Ni and Co-NP doped flux reduced the effect of electron wind imposed by high-current density as well as chemical force of diffusion of copper atoms.

3. The average anodic growth rate in the SAC305 solder joint was found to be 1.585×10^{-6} µm/s while in Ni and Co-doped solder joints, the average anodic growth rate was found to be 2.72×10^{-7} µm/s and 2.231×10^{-7}µm/s which are 5 and 7 times lower than that in the undoped solder joint.

4. After the reflow process, undoped SAC305 solder joints showed bigger grain size in the interfacial Cu_6Sn_5 layer but Ni and Co-NP doped flux reduced the grain size. After electromigration process, the grain size of anodic interfacial IMC of undoped SAC305 solder joint significantly increased but Ni and Co NP-doped flux controlled the grain growth in the anodic interfacial IMC layer.

5. During electrical resistance test, the resistance of SAC305 solder joint significantly increased and samples failed before 600 h of the test. Ni and Co NP-doped flux showed better performance in the electrical resistance test and the sample did not fail until the end of the test conducted for 700 h.

6. Ni and Co-NP containing solder joints improved the mechanical strength of reflowed samples and reduced the degradation of mechanical strength after EM test. The fracture path did not shift towards the cathode side and stayed inside the solder bulk after EM test. The mechanical strength of SAC305 solder joint significantly decreased after EM test and the fracture path shifted to the cathode interface due to EM effects.

7. Therefore it can be concluded that the use of Ni and Co nanoparticle doped flux is beneficial in retarding the electromigration damage and in improving the properties and life of the SAC305 solder joints. This technique can easily be applied in the industry for better reliability of solder joints without the need for the change of the production process steps.

6.2 Recommendations

In this study, the effect of Ni and Co metallic nanoparticle on microstructure, mechanical and electrical properties of the SAC305 solder joint under electromigration was investigated. For the future work, this study recommends the following suggestions.

1. NP-doped flux has significantly retarded the EM issue in the solder joint, so it is suggested to use this method to study the effect of NP-doped flux on thermomigration in the solder joint as well.

2. Due to Miniaturization and increment in current density, it is expected that the effects of electromigration on micro-sized solder joint will be increased significantly. The significant increase in electromigration can convert the solder joint into IMC joint. It is suggested to study the electromigration effects on properties of nanoparticle-doped and undoped IMC joint.

3. The electromigration process is much faster in thin solder film which degrades the properties of the thin film. It is suggested to study the effect of nanoparticle on electromigration issue of thin solder film.

4. Metallic nanoparticle other than Ni and Co-NP, those have a chemical affinity with liquid Sn can be used to investigate their effect on EM failures in the SAC305 solder joint.

5. The orientation of the c-axis of β-Sn grain plays an important in the migration of Cu atoms during the EM process. A study is recommended to be conducted on the effect of Ni and Co-NP doped flux on grain orientation of β-Sn grain during the EM process.

6. In the present study, it was detected that Ni and Co-NP reduced the IMC particles in the eutectic region of solder matrix. It is suggested to investigate the hardness of the eutectic region after the addition of Ni and Co-NP.

7. During the EM process, the formation of voids at the cathode side was found to be reduced in the current study by the addition of Ni and Co-NP. It is suggested to investigate the nano-hardness of the interfacial IMC layers after EM test.

REFERENCES

Abtew, M., & Selvaduray, G. (2000). Lead-free solders in microelectronics. Materials Science and Engineering: R: Reports, 27(5), 95-141.

Arafat, M., Haseeb A.S.M.A, & Johan, M. R. (2011). Interfacial reaction and dissolution behavior of Cu substrate in molten Sn-3.8 Ag-0.7 Cu in the presence of Mo nanoparticles. Soldering & Surface Mount Technology, 23(3), 140-149.

Association, S. I. (2009). International technology roadmap for semiconductors, 2009 edition. International SEMATECH, Austin, Texas.

Basaran, C., Lin, M. H., & Ye, H. (2003). A thermodynamic model for electrical current induced damage. International Journal of Solids and Structures, 40(26), 7315-7327. doi:DOI 10.1016/j.ijsolstr.2003.08.018.

Bauer, R., Fischer, A. H., Birzer, C., & Alexa, L. (2011). Electromigration Behavior of Interconnects between Chip and Board for Embedded Wafer Level Ball Grid Array (eWLB). 2011 Ieee 61st Electronic Components and Technology Conference (Ectc), 317-325.

Belyakov S.A. & Gourlay C.M. (2012). NiSn4 Formation in As-Soldered Ni-Sn and ENIG-Sn Couples. , Journal of electronic materials, 41(12), 3331-3341. DOI: 10.1007/s11664-012-2277-1.

Bobet, J.-L., Akiba, E., & Darriet, B. (2001). Study of Mg-M (M= Co, Ni and Fe) mixture elaborated by reactive mechanical alloying: hydrogen sorption properties. International journal of hydrogen energy, 26(5), 493-501.

Bobet, J., Akiba, E., Nakamura, Y., & Darriet, B. (2000). Study of Mg-M (M= Co, Ni and Fe) mixture elaborated by reactive mechanical alloying—Hydrogen sorption properties. International journal of hydrogen energy, 25(10), 987-996.

Careri, G., & Paoletti, A. (1955). Self-diffusion in liquid indium and tin. Il Nuovo Cimento (1955-1965), 2(3), 574-591.

Chae, S. H., Zhang, X. F., Chao, H. L., Lu, K. H., Ho, P. S., Ding, M., . . . Ramanathan, L. N. (2006). Electromigration lifetime statistics for Pb-free solder joints with Cu and NiUBM in plastic flip-chip packages. 56th Electronic Components & Technology Conference 2006, Vol 1 and 2, Proceedings, 650-656.

Chae, S. H., Zhang, X. F., Lu, K. H., Chao, H. L., Ho, P. S., Ding, M., . . . Ramanathan, L. N. (2007). Electromigration statistics and damage evolution for Pb-free solder joints with Cu and NiUBM in plastic flip-chip packages. Journal of Materials Science-Materials in Electronics, 18(1-3), 247-258. doi:DOI 10.1007/s10854-006-9026-2

Chan, Y., Arafat, M., & Haseeb A.S.M.A. (2013). Effects of reflow on the interfacial characteristics between Zn nanoparticles containing Sn-3.8 Ag-0.7 Cu solder and copper substrate. Soldering & Surface Mount Technology, 25(2), 91-98.

Chang, Y., Liang, S., & Chen, C. (2006). Study of void formation due to electromigration in flip-chip solder joints using Kelvin bump probes. Applied physics letters, 89(3), 032103.

Chao, B., Chae, S.-H., Zhang, X., Lu, K.-H., Ding, M., Im, J., & Ho, P. S. (2006). Electromigration enhanced intermetallic growth and void formation in Pb-free solder joints. Journal of applied physics, 100(8), 084909.

Chao, B., Chae, S.-H., Zhang, X., Lu, K.-H., Im, J., & Ho, P. S. (2007). Investigation of diffusion and electromigration parameters for Cu–Sn intermetallic compounds in Pb-free solders using simulated annealing. Acta Materialia, 55(8), 2805-2814.

Chen, C., & Liang, S. (2007). Electromigration issues in lead-free solder joints Lead-Free Electronic Solders (pp. 259-268): Springer.

Chen, C., Tong, H., & Tu, K. (2010). Electromigration and thermomigration in Pb-free flip-chip solder joints. Annual Review of Materials Research, 40, 531-555.

Chen, J., Shen, J., Min, D., & Peng, C. (2009). Influence of minor Bi additions on the interfacial morphology between Sn–Zn–xBi solders and a Cu layer. Journal of Materials Science: Materials in Electronics, 20(11), 1112-1117.

Chen, L., Huang, M., & Zhou, S. (2010). Effect of electromigration on intermetallic compound formation in line-type Cu/Sn/Cu interconnect. Journal of Alloys and Compounds, 504(2), 535-541.

Chen, S.-w., Chen, T.-K., Chang, J.-s., Hsu, C.-m., & Chen, W.-A. (2014). Interfacial Reactions in Sn-Ag/Co Couples. Journal of electronic materials, 43(2), 636-639.

Cheng, F., Nishikawa, H., & Takemoto, T. (2008). Microstructural and mechanical properties of Sn–Ag–Cu lead-free solders with minor addition of Ni and/or Co. Journal of materials science, 43(10), 3643-3648.

Chiu, T.-C., & Lin, K.-L. (2009). The difference in the types of intermetallic compound formed between the cathode and anode of an Sn–Ag–Cu solder joint under current stressing. Intermetallics, 17(12), 1105-1114.

Chiu, T.-C., & Lin, K.-L. (2012). The growth of intermetallic compound in Cu/Sn3. 5Ag/Au solder joints under current stressing. Intermetallics, 23, 208-216.

Cho, M. G., Kim, H. Y., Seo, S.-K., & Lee, H. M. (2009). Enhancement of heterogeneous nucleation of β-Sn phases in Sn-rich solders by adding minor alloying elements with hexagonal closed packed structures. Applied physics letters, 95(2), 021905.

Chung, D. (1995). Materials for Electronic Packaging, Butterworth: Heinemann.

Diehl, D. S. (1968). Semiconductor or write tri-layered metal contact: Google Patents.

Ding, M., Wang, G., Chao, B., Ho, P. S., Su, P., & Uehling, T. (2006). Effect of contact metallization on electromigration reliability of Pb-free solder joints. Journal of applied physics, 99(9), 094906.

Dudek, M., & Chawla, N. (2009). Oxidation behavior of rare-earth-containing Pb-free solders. Journal of electronic materials, 38(2), 210-220.

Dudek, M., & Chawla, N. (2010). Effect of rare-earth (La, Ce, and Y) additions on the microstructure and mechanical behavior of Sn-3.9 Ag-0.7 Cu solder alloy. Metallurgical and Materials Transactions A, 41(3), 610-620.

Dusek, M., Okoro, C., & Hunt, C. (2006). Establishing the stress/strain behaviour of solder alloys under multiple constant strain cycles with isothermal conditions. ESTC 2006: 1st Electronics Systemintegration Technology Conference, Vols 1 and 2, Proceedings, 942-946.

Dyson, B., Anthony, T., & Turnbull, D. (1967). Interstitial diffusion of copper in tin. Journal of applied physics, 38(8), 3408-3408.

Ebersberger, B., Bauer, R., & Alexa, L. (2005). Reliability of lead-free SnAg solder bumps: influence of electromigration and temperature. Paper presented at the Electronic Components and Technology Conference, 2005. Proceedings. 55th.

El-Daly, A., Hammad, A., Fawzy, A., & Nasrallh, D. (2013). Microstructure, mechanical properties, and deformation behavior of Sn–1.0 Ag–0.5 Cu solder after Ni and Sb additions. Materials & Design, 43, 40-49.

Gan, H., & Tu, K. (2005). Polarity effect of electromigration on kinetics of intermetallic compound formation in Pb-free solder V-groove samples. Journal of applied physics, 97(6), 063514.

Gao, F., Qu, J., & Takemoto, T. (2010). Additive occupancy in the Cu 6 Sn 5-based intermetallic compound between Sn-3.5 Ag solder and Cu studied using a first-principles approach. Journal of electronic materials, 39(4), 426-432.

Gao, F., Takemoto, T., & Nishikawa, H. (2006). Effects of Co and Ni addition on reactive diffusion between Sn–3.5 Ag solder and Cu during soldering and annealing. Materials Science and Engineering: A, 420(1), 39-46.

Gao, F., Takemoto, T., & Nishikawa, H. (2006). Morphology and growth pattern transition of intermetallic compounds between Cu and Sn-3.5 Ag containing a small amount of additives. Journal of electronic materials, 35(12), 2081-2087.

Glazer, J. (1994). Microstructure and mechanical properties of Pb-free solder alloys for low-cost electronic assembly: a review. Journal of electronic materials, 23(8), 693-700.

Guo, F., Xu, G., & He, H. (2009). Electromigration behaviors in Sb particle-reinforced composite eutectic SnAgCu solder joints. Journal of materials science, 44(20), 5595-5601.

Guo, F., Xu, G., Sun, J., Xia, Z., Lei, Y., Shi, Y., & Li, X. (2009). Resistance changes in eutectic sn-bi solder joints during electromigration. Journal of electronic materials, 38(12), 2756-2761.

Guo, R., Gao, L., Li, M., Mao, D., Qian, K., & Chiu, H. (2015). Microstructure evolution of Ag–8Au–3Pd alloy wire during electromigration. Materials Characterization, 110, 44-51.

Harper, C. (2004). Electronic packaging and interconnection handbook: McGraw-Hill, Inc.

Haseeb A.S.M.A., & Leng, T. S. (2011). Effects of Co nanoparticle addition to Sn–3.8 Ag–0.7 Cu solder on interfacial structure after reflow and ageing. Intermetallics, 19(5), 707-712.

Haseeb A.S.M.A., Leong, Y., & Arafat, M. (2014). In-situ alloying of Sn–3.5 Ag solder during reflow through Zn nanoparticle addition and its effects on interfacial intermetallic layers. Intermetallics, 54, 86-94.

Haseeb A.S.M.A, Gosh. S., Afifi ABM. (2013). A method of in-situ targeted interfacial alloying of lead-free solder joints. Patent Application No. PI 2013000584.

He, H., Xu, G., & Guo, F. (2010). Electromigration-enhanced intermetallic growth and phase evolution in Cu/Sn–58Bi/Cu solder joints. Journal of materials science, 45(4), 929-935.

Heinen, K. G., Schroen, W. H., Edwards, D. R., Wilson, A. M., Stierman, R. J., & Lamson, M. A. (1989). Multichip assembly with flipped integrated circuits. Components, Hybrids, and Manufacturing Technology, IEEE Transactions on, 12(4), 650-657.

Ho, C.-E., Yang, C.-H., Lee, P.-T., & Chen, C.-T. (2016). Real-time X-ray microscopy study of electromigration in microelectronic solder joints. Scripta Materialia, 114, 79-83.

Ho, C., Lin, Y., Yang, S., Kao, C., & Jiang, D. (2006). Effects of limited Cu supply on soldering reactions between SnAgCu and Ni. Journal of electronic materials, 35(5), 1017-1024.

Hong, J., Lee, H., & Wu, A. T. (2013). Massive spalling and morphological change of intermetallic compound affected by adding Pd in Co-based surface finishes. Journal of Alloys and Compounds, 580, 195-200.

Hongwen, H., Guangchen, X., & Fu, G. (2009). Electromigration-induced cracks in Cu/Sn3. 5Ag/Cu solder reaction couple at room temperature. Journal of Semiconductors, 30(3), 033006.

Hsu, C.-m., & Chen, S.-w. (2013). Interfacial reactions with and without current stressing at Sn–Co/Ag and Sn–Co/Cu solder joints. Journal of materials science, 48(19), 6640-6646.

Hu, S., Nozawa, J., Koizumi, H., Fujiwara, K., & Uda, S. (2015). Grain Boundary Segregation of Impurities During Polycrystalline Colloidal Crystallization. Crystal Growth & Design.

Hu, X., Chan, Y., Zhang, K., & Yung, K. (2013). Effect of graphene doping on microstructural and mechanical properties of Sn–8Zn–3Bi solder joints together with electromigration analysis. Journal of Alloys and Compounds, 580, 162-171.

Huang, M., Zhao, J., Zhang, Z., & Zhao, N. (2016). Dominant effect of high anisotropy in β-Sn grain on electromigration-induced failure mechanism in Sn-3.0 Ag-0.5 Cu interconnect. Journal of Alloys and Compounds, 678, 370-374.

Huang, M., Zhou, Q., Zhao, N., Liu, X., & Zhang, Z. (2014). Reverse polarity effect and cross-solder interaction in Cu/Sn–9Zn/Ni interconnect during liquid–solid electromigration. Journal of materials science, 49(4), 1755-1763.

Huang, M. L., Zhang, F., Yang, F., & Zhao, N. (2015). Size effect on tensile properties of Cu/Sn-9Zn/Cu solder interconnects under aging and current stressing. Journal of Materials Science-Materials in Electronics, 26(4), 2278-2285. doi:DOI 10.1007/s10854-015-2681-4.

Huang, T., Yang, T., Ke, J., Hsueh, C., & Kao, C. (2014). Effects of Sn grain orientation on substrate dissolution and intermetallic precipitation in solder joints under electron current stressing. Scripta Materialia, 80, 37-40.

Huang, T., Yang, T., Ke, J., Li, C., & Kao, C. (2013). Precipitation induced by diffusivity anisotropy in Sn grains under electron current stressing. Journal of Alloys and Compounds, 555, 237-240.

Igoshev, V., & Kleiman, J. (2000). Creep phenomena in lead-free solders. Journal of electronic materials, 29(2), 244-250.

Intel. (2004). Intel Research. www.intel.com.

Ismathullakhan, S., Lau, H., & Chan, Y.-c. (2013). Enhanced electromigration reliability via Ag nanoparticles modified eutectic Sn–58Bi solder joint. Microsystem technologies, 19(7), 1069-1080.

Jang, J. W., Ramanathan, L. N., Tang, J., & Frear, D. R. (2008). Secondary current crowding effect during electromigration of flip-chip solder joints. Journal of Electronic Materials, 37(2), 185-188. doi:DOI 10.1007/s11664-007-0330-2.

Jiang, M., Sato, J., Ohnuma, I., Kainuma, R., & Ishida, K. (2004). A thermodynamic assessment of the Co–Sn system. Calphad, 28(2), 213-220.

Kim, D. H., Cho, M. G., Seo, S.-K., & Lee, H. M. (2009). Effects of Co addition on bulk properties of Sn-3.5 Ag solder and interfacial reactions with Ni-P UBM. Journal of electronic materials, 38(1), 39-45.

Kim, P., Jang, J., Lee, T., & Tu, K. (1999). Interfacial reaction and wetting behavior in eutectic SnPb solder on Ni/Ti thin films and Ni foils. Journal of applied physics, 86(12), 6746-6751.

Kim, Y., Sugahara, T., Nagao, S., Suganuma, K., Ueshima, M., Albrecht, H., . . . Strogies, J. (2012). Effects of additional Ni and Co on microstructural evolution in Sn-Ag-Bi-In solder under current stressing. Paper presented at the CPMT Symposium Japan, 2012 2nd IEEE.

Koopman, N., Reiley, T., & Totta, P. (1989). Microelectronics packaging handbook. Van Reinhold, 361.

Kumar, A., Yang, Y., Wong, C. C., Kripesh, V., & Chen, Z. (2009). Effect of electromigration on the mechanical performance of Sn-3.5 Ag solder joints with Ni and Ni-P metallizations. Journal of electronic materials, 38(1), 78-87.

Kumar, S., & Jung, J. (2013). Mechanical and electronic properties of Ag 3 Sn intermetallic compound in lead free solders using ab initio atomistic calculation. Materials Science and Engineering: B, 178(1), 10-21.

Kwon, W.-S., & Paik, K.-W. (2002). High current induced failure of ACAs flip chip joint. Paper presented at the Electronic Components and Technology Conference, 2002. Proceedings. 52nd.

Lau, J. H. (1995). Ball grid array technology: McGraw-Hill Professional
.

Lau, J. H. (1996). Flip chip technologies: McGraw-Hill Professional.

Lau, J. H., Wong, C., Nakayama, W., & Prince, J. L. (1998). Electronic packaging: McGraw-Hill.

Laurila, T., Vuorinen, V., & Paulasto-Kröckel, M. (2010). Impurity and alloying effects on interfacial reaction layers in Pb-free soldering. Materials science and engineering: R: reports, 68(1), 1-38.

Lea, C. (1988). A scientific guide to surface mount technology (Vol. 319): Electrochemical Publications Ayr, Scotland.

Lee, K., Kim, K.-S., Tsukada, Y., Suganuma, K., Yamanaka, K., Kuritani, S., & Ueshima, M. (2011a). Effects of the crystallographic orientation of Sn on the electromigration of Cu/Sn–Ag–Cu/Cu ball joints. Journal of Materials Research, 26(03), 467-474.

Lee, K., Kim, K.-S., Tsukada, Y., Suganuma, K., Yamanaka, K., Kuritani, S., & Ueshima, M. (2011b). Influence of crystallographic orientation of Sn–Ag–Cu on electromigration in flip-chip joint. Microelectronics Reliability, 51(12), 2290-2297.

Li, M., Chang, H., Pang, X., Wang, L., & Fu, Y. (2011). Abnormal accumulation of intermetallic compound at cathode in a SnAg3. 0Cu0. 5 lap joint during electromigration. Journal of Physics D: Applied Physics, 44(11), 115501.

Lin, K.-L., & Lin, G.-P. (2007). The Electromigration Investigation on the Newly Developed Pb-free Sn-Zn-Ag-Al-Ga Solder Ball Interconnect. Paper presented at the Electronic Components and Technology Conference, 2007. ECTC'07. Proceedings. 57th.

Lin, M., & Basaran, C. (2005). Electromigration induced stress analysis using fully coupled mechanical–diffusion equations with nonlinear material properties. Computational Materials Science, 34(1), 82-98.

Lin, Y., Chang, C., Tsai, C., Lee, C., & Kao, C. (2006). Electromigration-induced UBM consumption and the resulting failure mechanisms in flip-chip solder joints. Journal of electronic materials, 35(5), 1010-1016.

Lin, Y., Tsai, C., Hu, Y., Lin, Y., & Kao, C. (2005). Electromigration-induced failure in flip-chip solder joints. Journal of electronic materials, 34(1), 27-33.

Lis, A., Park, M. S., Arroyave, R., & Leinenbach, C. (2014). Early stage growth characteristics of Ag 3 Sn intermetallic compounds during solid–solid and solid–liquid reactions in the Ag–Sn interlayer system: Experiments and simulations. Journal of Alloys and Compounds, 617, 763-773.

Liu, C., Chen, C., Mal, A., & Tu, K. (1999). Direct correlation between mechanical failure and metallurgical reaction in flip chip solder joints. Journal of applied physics, 85(7), 3882-3886.

Liu, L., Zhou, W., Zhang, H., Li, B., & Wu, P. (2010). Electromigration behavior in Cu/Sn–8Zn–3Bi/Cu solder joint. Microelectronics Reliability, 50(2), 251-257.

Liu, P., Wang, S., Li, D., Li, Y., & Chen, X.-Q. (2015). Fast and Huge Anisotropic Diffusion of Cu (Ag) and Its Resistance on the Sn Self-diffusivity in Solid β–Sn. Journal of Materials Science & Technology.

Lu, Y.-D., He, X.-Q., En, Y.-F., Wang, X., & Zhuang, Z.-Q. (2009). Polarity effect of electromigration on intermetallic compound formation in SnPb solder joints. Acta Materialia, 57(8), 2560-2566.

Ma, C., & Swalin, R. (1960). A study of solute diffusion in liquid tin. Acta metallurgica, 8(6), 388-395.

Ma, L., Xu, G., Guo, F., & Wang, X. (2011). Retarding electromigration on the Sn-Ag-Cu solder joints by micro-sized metal-particle reinforcement. Paper presented at the Electronic Packaging Technology and High Density Packaging (ICEPT-HDP), 2011 12th International Conference on.

Ma, L., Xu, G., Sun, J., Guo, F., & Wang, X. (2011). Effects of Co additions on electromigration behaviors in Sn–3.0 Ag–0.5 Cu-based solder joint. Journal of materials science, 46(14), 4896-4905.

Ma, Z., Belyakov, S., & Gourlay, C. (2016). Effects of cobalt on the nucleation and grain refinement of Sn-3Ag-0.5 Cu solders. Journal of Alloys and Compounds, 682, 326-337.

Maeshima, T., Ikehata, H., Terui, K., & Sakamoto, Y. (2016). Effect of Ni to the Cu substrate on the interfacial reaction with Sn-Cu solder. Materials & Design, 103, 106-113.

Massalski, T. B., & International, A. (1996). Binary alloy phase diagrams: plus updates, version 1.0: na.

Mattila, T., Laurila, T., & Kivilahti, J. (2005). Reliability of high-density lead-free interconnections. Preprinted from E. Suhir, CP Wong, and YC Lee,“Micro-and

Opto-Electronic Materials and Structures: Physics, Mechanics, Design, Reliability, Packaging", Springer Science+ Business Media, 313-349.

Mohanty, U. S., & Lin, K.-L. (2013). Corrosion Behavior of Pb-Free Sn-1Ag-0.5 Cu-XNi Solder Alloys in 3.5% NaCl Solution. Journal of electronic materials, 42(4), 628-638.

Moon, K.-W., Boettinger, W., Kattner, U., Biancaniello, F., & Handwerker, C. (2000). Experimental and thermodynamic assessment of Sn-Ag-Cu solder alloys. Journal of electronic materials, 29(10), 1122-1136.

Myers, T. (1969). Flip-Chip Microcircuit Bonding Systems. Paper presented at the Proc. ECC.

Nadia, A., & Haseeb A.S.M.A. (2012a). Effects of addition of copper particles of different size to Sn-3.5 Ag solder. Journal of Materials Science: Materials in Electronics, 23(1), 86-93.

Nadia, A., & Haseeb A.S.M.A. (2012b). Fabrication and properties of Sn-3.5 Ag-XCu solder by ball milling and paste Mixing. Paper presented at the Defect and Diffusion Forum.

Nah, J. W., Buchwalter, S. L., Gruber, P. A., Shih, D. Y., & Furman, B. K. (2008). C4NPCu-cored Pb-free flip chip interconnections. 58th Electronic Components & Technology Conference, Proceedings, 1351-1356.

Nash, P., & Nash, A. (1985). The Ni− Sn (Nickel-Tin) system. Bulletin of Alloy Phase Diagrams, 6(4), 350-359.

NEMI. (2004). lead-free.org/legislation and www.nemi.org/PbFreepublic.

NIST. National Institute of Standards and Technology (NIST) database. http://www.nist.gov/.

Oppert, T., Teutsch, T., Zakel, E., & Tovar, D. (1999). A bumping process for 12" wafers. Paper presented at the Electronics Manufacturing Technology Symposium, 1999. Twenty-Fourth IEEE/CPMT.

Pecht, M., Fukuda, Y., & Rajagopal, S. (2004). The impact of lead-free legislation exemptions on the electronics industry. Electronics Packaging Manufacturing, IEEE Transactions on, 27(4), 221-232.

Rao, B. C., Weng, J., Shen, L., Lee, T., & Zeng, K. (2010). Morphology and mechanical properties of intermetallic compounds in SnAgCu solder joints. Microelectronic engineering, 87(11), 2416-2422.

Ren, F., Nah, J.-W., Tu, K., Xiong, B., Xu, L., & Pang, J. H. (2006). Electromigration induced ductile-to-brittle transition in lead-free solder joints. Applied physics letters, 89(14), 141914.

Rhee, H., Guo, F., Lee, J., Chen, K. C., & Subramanian, K. (2003). Effects of intermetallic morphology at the metallic particle/solder interface on mechanical properties of Sn-Ag-based solder joints. Journal of electronic materials, 32(11), 1257-1264.

Rungyusiri, V., Sa-ngiamsak, C., Harnsoongnoen, S., & Intarakul, P. (2009). Comparison of electromigration for lead-free solder joints of Cu vs. Ni UBM flip chip structure. Paper presented at the Electrical Engineering/Electronics, Computer, Telecommunications and Information Technology, 2009. ECTI-CON 2009. 6th International Conference on.

Schmetterer, C., Flandorfer, H., Richter, K. W., Saeed, U., Kauffman, M., Roussel, P., & Ipser, H. (2007). A new investigation of the system Ni–Sn. Intermetallics, 15(7), 869-884.

Selvaraj, M. K. (2007). An experimental study of electromigration in flip chip packages: ProQuest.

Sharif, A., & Chan, Y. (2007). Retardation of spalling by the addition of Ag in Sn–Zn–Bi solder with the Au/Ni metallization. Materials Science and Engineering: A, 445, 686-690.

Shen, J., Cao, Z., Zhai, D., Zhao, M., & He, P. (2014). Effect of isothermal aging and low density current on intermetallic compound growth rate in lead-free solder interface. Microelectronics Reliability, 54(1), 252-258.

Siewert, T. (2002). Properties of lead-free solders. Colorado School of Mines.

Silva, B. L., Garcia, A., & Spinelli, J. E. (2016). Cooling thermal parameters and microstructure features of directionally solidified ternary Sn–Bi–(Cu, Ag) solder alloys. Materials Characterization, 114, 30-42.

Silva, B. L., Reinhart, G., Nguyen-Thi, H., Mangelinck-Noël, N., Garcia, A., & Spinelli, J. E. (2015). Microstructural development and mechanical properties of a near-eutectic directionally solidified Sn–Bi solder alloy. Materials Characterization, 107, 43-53.

Sohn, Y.-C., Yu, J., Kang, S. K., Shih, D.-Y., & Lee, T.-Y. (2004). Study of spalling behavior of intermetallic compounds during the reaction between electroless Ni-P metallization and lead-free solders. Paper presented at the Electronic Components and Technology Conference, 2004. Proceedings. 54th.

Song, J.-M., Huang, C.-F., & Chuang, H.-Y. (2006). Microstructural characteristics and vibration fracture properties of Sn-Ag-Cu-TM (TM= Co, Ni, and Zn) alloys. Journal of electronic materials, 35(12), 2154-2163.

Sujan, G., Haseeb A.S.M.A, & Afifi, A. (2014). Effects of metallic nanoparticle doped flux on the interfacial intermetallic compounds between lead-free solder ball and copper substrate. Materials Characterization, 97, 199-209.

Sujan, G., Haseeb A.S.M.A., Nishikawa, H., & Amalina, M. (2017). Interfacial reaction, ball shear strength and fracture surface analysis of lead-free solder joints prepared using cobalt nanoparticle doped flux. Journal of Alloys and Compounds, 695, 981-990.

Sun, J., Xu, G., Guo, F., Xia, Z., Lei, Y., Shi, Y., . . . Wang, X. (2011). Effects of electromigration on resistance changes in eutectic SnBi solder joints. Journal of materials science, 46(10), 3544-3549.

Taguma, Y., Uda, T., Ishida, H., Kobayashi, T., & Nakada, K. (1991). Application of dc magnetron sputtered Cr–Cu–Au thin film for flip-chip solder terminal contacts. Paper presented at the Proceedings of the 1991 International Electronic Packaging Conference.

Tay, S., Haseeb A.S.M.A, & Johan, M. R. (2011). Addition of cobalt nanoparticles into Sn-3.8 Ag-0.7 Cu lead-free solder by paste mixing. Soldering & Surface Mount Technology, 23(1), 10-14.

Tay, S., Haseeb A.S.M.A., Johan, M. R., Munroe, P., & Quadir, M. (2013). Influence of Ni nanoparticle on the morphology and growth of interfacial intermetallic compounds between Sn–3.8 Ag–0.7 Cu lead-free solder and copper substrate. Intermetallics, 33, 8-15.

Tonapi, S., Gopakumar, S., Borgesen, P., & Srihari, K. (2002). Reliability of lead-free solder interconnects-a review. Paper presented at the Reliability and Maintainability Symposium, 2002. Proceedings. Annual.

Totta, P. A., & Sopher, R. P. (1969). SLT device metallurgy and its monolithic extension. IBM Journal of Research and Development, 13(3), 226-238.

Tu, K.-N. (2007). Solder joint technology: Springer.

Tu, K. (2003). Recent advances on electromigration in very-large-scale-integration of interconnects. Journal of applied physics, 94(9), 5451-5473.

Tu, K., Gusak, A., & Li, M. (2003). Physics and materials challenges for lead-free solders. Journal of applied physics, 93(3), 1335-1353.

Tu, K., Lee, T., Jang, J., Li, L., Frear, D., Zeng, K., & Kivilahti, J. (2001). Wetting reaction versus solid state aging of eutectic SnPb on Cu. Journal of applied physics, 89(9), 4843-4849.

Wang, K.-K., Chin, P.-J., Yeh, C.-F., & Gan, D. (2015). The orientation relationships and interfaces of Ag 3 Sn and Ag 4 Sn on Ag and a discussion of their formation sequence. Thin Solid Films, 589, 27-31.

Wang, X., Zeng, Q., Zhu, Q., Wang, Z., & Shang, J. (2010). Effects of Current Stressing on Shear Properties of Sn-3.8 Ag-0.7 Cu Solder Joints. Journal of Materials Science & Technology, 26(8), 737-742.

Wang, X. Y., Han, M. T., Ma, L. M., Xu, G. C., & Guo, F. (2011). Electromigration Behavior in In-situ Cu6Sn5 Reinforced Eutectic SnAg Composite Solder Joints. 2011 12th International Conference on Electronic Packaging Technology and High Density Packaging (Icept-Hdp), 211-215.

Wang, Y., Chang, C., & Kao, C. (2009). Minimum effective Ni addition to SnAgCu solders for retarding Cu< sub> 3</sub> Sn growth. Journal of Alloys and Compounds, 478(1), L1-L4.

Wang, Y., Lu, K. H., Gupta, V., Stiborek, L., Shirley, D., Chae, S.-H., . . . Ho, P. S. (2012). Effects of Sn grain structure on the electromigration of Sn–Ag solder joints. Journal of Materials Research, 27(08), 1131-1141.

Warrior, M. (1990). Reliability improvements in solder bump processing for flip chips. Paper presented at the Electronic Components and Technology Conference, 1990.., 40th.

Wei, G., Yao, J., & Shi, Y. (2011). The Influence of Electromigration and Aging on the Reliability of SnAgCu Lead-Free Solder Joint at 100° C. Paper presented at the Electronic Packaging Technology and High Density Packaging (ICEPT-HDP), 2011 12th International Conference on.Westbrook, J. (1964). Segregation at grain boundaries. Metallurgical Reviews, 9(1), 415-471.

Wu, C., Yu, D., Law, C., & Wang, L. (2004). Properties of lead-free solder alloys with rare earth element additions. Materials Science and Engineering: R: Reports, 44(1), 1-44.

Xie, H., Friedman, D., Mirpuri, K., & Chawla, N. (2014). Electromigration Damage Characterization in Sn-3.9 Ag-0.7 Cu and Sn-3.9 Ag-0.7 Cu-0.5 Ce Solder Joints by Three-Dimensional X-ray Tomography and Scanning Electron Microscopy. Journal of electronic materials, 43(1), 33-42.

Xu, L., Pang, J. H., Ren, F., & Tu, K. (2006). Electromigration effect on intermetallic growth and Young's modulus in SAC solder joint. Journal of electronic materials, 35(12), 2116-2125.

Xu, S., Chan, Y. C., Zhang, K., & Yung, K. (2014). Interfacial intermetallic growth and mechanical properties of carbon nanotubes reinforced Sn3. 5Ag0. 5Cu solder joint under current stressing. Journal of Alloys and Compounds, 595, 92-102.

Yakymovych, A., Mudry, S., Shtablavyi, I., & Ipser, H. (2016). Effect of nano Co reinforcements on the structure of the Sn-3.0 Ag-0.5 Cu solder in liquid and after reflow solid states. Materials Chemistry and Physics, 181, 470-475.

Yang, T., Yu, J., Li, C., Lin, Y., & Kao, C. (2015). Dominant effects of Sn orientation on serrated cathode dissolution and resulting failure in actual solder joints under electromigration. Journal of Alloys and Compounds, 627, 281-286.

Yang, Z., Zhou, W., & Wu, P. (2013). Effects of Ni-coated Carbon Nanotubes addition on the electromigration of Sn–Ag–Cu solder joints. Journal of Alloys and Compounds, 581, 202-205.

Yano, H., Kataoka, M., Yamashita, H., Uchida, H., & Watanabe, M. (2007). Oxygen reduction activity of carbon-supported Pt− M (M= V, Ni, Cr, Co, and Fe) alloys prepared by nanocapsule method. Langmuir, 23(11), 6438-6445.

Yeh, E. C., Choi, W., Tu, K., Elenius, P., & Balkan, H. (2002). Current-crowding-induced electromigration failure in flip chip solder joints. Applied physics letters, 80(4), 580-582.

Zeng, K., Stierman, R., Chiu, T.-C., Edwards, D., Ano, K., & Tu, K. (2005). Kirkendall void formation in eutectic SnPb solder joints on bare Cu and its effect on joint reliability. Journal of applied physics, 97(2), 024508-024508-024508.

Zeng, K., & Tu, K.-N. (2002). Six cases of reliability study of Pb-free solder joints in electronic packaging technology. Materials science and engineering: R: reports, 38(2), 55-105.

Zhang, J., Chan, Y. C., Wu, Y., Xi, H., & Wu, F. (2008). Electromigration of Pb-free solder under a low level of current density. Journal of Alloys and Compounds, 458(1), 492-499.

Zhang, L., Ou, S., Huang, J., Tu, K., Gee, S., & Nguyen, L. (2006). Effect of current crowding on void propagation at the interface between intermetallic compound and solder in flip chip solder joints. Applied physics letters, 88(1), 012106.

Zhang, L., Wang, Z., & Shang, J. (2007). Current-induced weakening of Sn3. 5Ag0. 7Cu Pb-free solder joints. Scripta Materialia, 56(5), 381-384.

Zhang, L., Xue, S.-b., Gao, L.-l., Sheng, Z., Ye, H., Xiao, Z.-x., . . . Yu, S.-l. (2010). Development of Sn–Zn lead-free solders bearing alloying elements. Journal of Materials Science: Materials in Electronics, 21(1), 1-15.

Zhang, R., Xu, G., Wang, X., Guo, F., Lee, A., & Subramanian, K. (2010). Electromigration in Sn-Bi Modified with polyhedral oligomeric silsesquioxane. Journal of electronic materials, 39(12), 2513-2521.

Zhang, Y., Yuan, D.-W., Chen, J.-H., Zeng, G., Fan, T.-W., Liu, Z.-R., . . . Liu, L.-H. (2016). Alloying Effects on the Phase Stability and Mechanical Properties of Doped Cu-Sn IMCs: A First-Principle Study. Journal of electronic materials, 1-10.

Zhang, Z., Luo, S., & Wong, C. (2013). Flip chip underfill: Materials, process, and reliability Advanced Flip Chip Packaging (pp. 155-199): Springer.

Zhao, R., Ma, L., Zuo, Y., Liu, S., & Guo, F. (2013). Retarding Electromigration in Lead-Free Solder Joints by Alloying and Composite Approaches. Journal of electronic materials, 42(2), 280-287.

Ziegler, J. F. (1996). Terrestrial cosmic rays. IBM Journal of Research and Development, 40(1), 19-39.

Zuo, Y., Ma, L., Liu, S., Wang, T., Guo, F., & Wang, X. (2013). The coupling effects of thermal cycling and high current density on Sn58Bi solder joints. Journal of materials science, 48(6), 2318-2325.

LIST OF PUBLICATIONS AND PAPERS PRESENTED

ISI indexed Journal Papers

1. **Bashir, M. N.,** Haseeb, A.S.M.A., Rahman, A. Z. M. S., Fazal, M., & Kao, C. (2015). Reduction of electromigration damage in SAC305 solder joints by adding Ni nanoparticle through flux doping. Journal of materials science, 50(20), 6748-6756 (Published).

2. **Bashir, M. N.,** Haseeb, A.S.M.A., Rahman, A. Z. M. S., & Fazal, M., (2015). Effect of cobalt doping on the microstructure and tensile properties of lead-free solder subject to electromigration. Journal of materials science and technology, 32, 1129–1136 (Published).

3. **Bashir, M. N.,** Haseeb, A.S.M.A., Improving mechanical strength of Cu/SAC305/Cu solder joint by the addition of Ni nanoparticles doped flux under electromigration. Journal of Materials Science: Materials in Electronics (Under revision).
4. **Bashir, M. N.,** Haseeb, A.S.M.A., Effects of Ni and Co nanoparticle doped flux on interfacial IMC structure of SAC305 solder joint under electromigration. (Under initial review)
5. **Bashir, M. N.,** Haseeb, A.S.M.A., Improving structure of SAC305 solder matrix by addition of Ni and Co nanoparticle doped flux. (Under initial review)

Conference papers

1. **Bashir, M. N.,** Haseeb, A.S.M.A., Rahman, S., Zayed, A., & Fazal, M. (2014). Effect of Ni nanoparticles on intermetallic compounds formation in SAC305

solder joint under high current density. Paper presented at the Electronics Manufacturing Technology Conference (IEMT), 2014 IEEE 36th International.

2. **Bashir, M. N.,** Haseeb, A.S.M.A. The effect of Ni and Co nanoparticles doped flux on crystallographic structure of interfacial IMC of SAC305 solder joint under electromigration, AMPT2016 conference University of Malaya KL Malaysia.

3. **Bashir, M. N.,** Haseeb, A.S.M.A. Effect of Ni and Co nanoparticle doped flux on properties of Cu/SAC305/Cu solder joints. CAM Postgraduate Symposium 2017 19 April 2017 Faculty of Engineering.